# Novel microbial guilds implicated in $N_2O$ reduction

**A Dissertation Presented for the**

**Doctor of Philosophy**

**Degree**

**The University of Tennessee, Knoxville**

**Guang He**

**December 2023**

## ACKNOWLEDGEMENTS

I would like to take this opportunity to express my deep gratitude and appreciation to all those who have contributed to the completion of my Ph.D. dissertation. This journey has been both challenging and rewarding, and I am truly thankful for the support, guidance, and encouragement I have received along the way. First and foremost, I extend my heartfelt thanks to my dissertation advisor, Dr. Frank E. Löffler and Dr. Mark Radosevich, for their unwavering support, mentorship, and dedication to my academic and research pursuits. Their invaluable insights, patience, and guidance have been instrumental in shaping my research and academic growth. I am grateful to the members of my dissertation committee, Jie (Joe) Zhuang and Karen Lloyd, for their expertise and constructive feedback, which significantly enriched the quality of my research. Their thoughtful guidance and scholarly contributions have been invaluable throughout this process. I would like to acknowledge the support and resources provided by University of Tennessee, which have been indispensable in the execution of my research. I extend my appreciation to my fellow Ph.D. candidates, lab mates, and colleagues who have shared their knowledge, ideas, and camaraderie throughout my graduate studies. Your collaboration and friendship have made this journey enjoyable and intellectually stimulating. I also wish to express my gratitude to my family for their unwavering belief in my abilities and their constant encouragement. Your love and support have been my pillars of strength. Lastly, I acknowledge the countless individuals who have participated in my research studies and surveys, as well as the research funding agencies, including U.S. National Science Funding and China Scholarship Council, for their financial support. To everyone who has been a part of my Ph.D. journey, whether mentioned here or not, your contributions, no matter how big or small, have played a crucial role in the successful completion of this dissertation.

Thank you all for being a part of this incredible journey.

## ABSTRACT

$N_2O$ is a long-recognized greenhouse gas (GHG) with potential in global warming and ozone depletion. Terrestrial ecosystems are a major source of $N_2O$ due to imbalanced $N_2O$ production and consumption. Soil pH is a chief modulating factor controlling net $N_2O$ emissions, and $N_2O$ consumption has been considered negligible under acidic conditions (pH <6). In this dissertation, we obtained solids-free cultures reducing $N_2O$ at pH 4.5. Furthermore, a co-culture (designated culture EV) comprising two interacting bacterial population was acquired via consecutive transfer in mineral salt medium. Integrated phenotypic, metagenomic and metabolomic analysis dictated that the *Serratia* population excreted certain amino acid to support *Desulfosporosinus* population growth. Characterization of co-culture EV demonstrated that organisms synthesizing functional NosZ exist in acidic soils. To further close the knowledge gap of low pH $N_2O$ reduction, we conducted enrichment experiments on two contrasting soils representing natural and agricultural soils, respectively. With varying combination of carbon sources and $H_2$, $N_2O$ reduction activity was observed in a total of six solids-free cultures at pH 4.5. Comparative growth experiments documented that $N_2O$ was essential for $N_2O$-reducing organisms' growth. Reconstruction of the communities suggested the cultures were highly enriched following consecutive transfer efforts. Surprisingly, $N_2O$-reducing organisms recovered from the cultures were all identified as clade II lineage or a novel clade lineage. These results together suggested that clade II and the putative novel clade $N_2O$-reducing organisms are closely associated with low pH $N_2O$ reduction. The observation of low pH $N_2O$ reduction in current research was inconsistent to field observation, where the abiotic-biotic interaction occurs frequently. To simulate potential abiotic-biotic interaction of low pH $N_2O$ reduction, we tested the impact of geochemistry factors on $N_2O$ reduction by culture EV. The impeded $N_2O$ reduction of co-culture EV in the presence of trace amount (as low as 0.01 mM for nitrate and 0.001 mM for nitrite) of nitrogen oxyanions was unexpected, which may explain the weak $N_2O$ reduction activity under field conditions. These observations indicated $N_2O$ reduction in acidic soils may be limited by interacting abiotic factors, instead of pH itself.

## TABLE OF CONTENTS

**Chapter 1 Introduction** ..... 1

**1.1 Sources and sinks of $N_2O$** ..... 1

**1.2 Acidic soils are mainly $N_2O$ source** ..... 3

**1.3 Research objectives** ..... 5

**Chapter 2 Sustained bacterial $N_2O$ reduction at acidic pH** ..... 7

**Abstract** ..... 8

**2.1 Introduction** ..... 9

**2.2 Materials and methods** ..... 10
- **Soil sampling locations and microcosms** ..... 10
- **Enrichment cultures** ..... 10
- **Microbial community analysis** ..... 11
- **Isolation and classfication** ..... 12
- **Quantitative PCR (qPCR)** ..... 13
- **Nutritional interactions in the co-culture** ..... 14
- **Metagenome sequencing** ..... 14
- **Comparative analysis of nos gene clusters** ..... 15
- **Phylogenomic analysis** ..... 16
- **NosZ phylogenetic analysis** ..... 16
- **Metabolome analysis** ..... 16
- **Phenotypic characterization of co-culture EV** ..... 17
- **Analytical procedures** ..... 18

**2.3 Results** ..... 19
- **A consortium consisting of two populations reduces $N_2O$ at pH 4.5** ..... 19
- **Isolation efforts** ..... 23
- **Identification of auxotrophies** ..... 24
- **pH range of acidophilic $N_2O$ reduction by the Desulfosporosinus sp** ..... 25
- **Phylogenomic analysis** ..... 26
- **Genetic underpinning of $N_2O$ reduction in 'Ca. Desulfosporosinus nitrousreducens' strain PR** ..... 26
- **Genomic insights for a commensalistic relationship** ..... 27
- **Distribution of the novel $N_2O$ reducer in soil metagenomes** ..... 28

**2.4 Discussion** ..... 29

**Appendix** ..... 35

**Chapter 3 Clade III $N_2O$-respiring microbes implicated in $N_2O$ reduction.** ..... 65

**Abstract** ..... 66

**3.1 Introduction** ..... 67

**3.2 Materials and Methods** ..... 69
**Soil sampling, microcosms and enrichment cultures** ..... 69
**Comparative genomic analysis** ..... 70
**Phylogenomic analysis** ..... 71
**Computational analysis of nos operon cluster and NosZ structure modeling** .. 71
**Comparative growth assays with enrichment cultures harboring clade III $N_2O$ reducers** ..... 72
**Quantitative PCR** ..... 72

**3.3 Results** ..... 73
**Low pH $N_2O$ reducers enriched from circumneutral and acidic soils** ..... 73
**Novel species involved in low pH $N_2O$ reduction** ..... 74
**Identification of clade III nosZ** ..... 76
**Structural and functional validation of clade III nosZ in enrichment cultures** 78

**3.4 Discussion** ..... 79

**Appendix** ..... 85

**Chapter 4 Geochemical factors control $N_2O$ reduction under low pH conditions** . 108

**Abstract** ..... 109

**4.1 Introduction** ..... 110

**4.2 Materials and Methods** ..... 112
**Microorganisms and cultivation.** ..... 112
**Abiotic controls of $N_2O$ reduction at low pH.** ..... 113
**Analytical procedures.** ..... 113

**4.3 Results** ..... 114
**$N_2O$ reduction by culture EV and D. aromatica strain RCB require copper** . 114
**Effects of copper and $Na_2S$ on $N_2O$ reduction** ..... 115
**Effects of nitrogen oxyanion on low pH $N_2O$ reduction.** ..... 115

**4.4 Discussion** ..... 116

**Appendix** ..... 119

**Summary and Conclusion** ..... 123

**References** ..... 125

**Vita** ..... 138

# LIST OF TABLES

**Table 2-1. qPCR primers and probe designed for the enumeration of *Serratia* sp. strain MF and '*Ca.* Desulfosporosinus nitrousreducens' strain PR 16S rRNA genes. ....56**
**Table 2-2. Sequence information submitted to the NCBI database. ....57**
**Table 2-3. Organismal and genomic information of microorganisms with reported $N_2O$ reduction capacity under different pH. ....58**
**Table 2-4. Genomes used in phylogenomic analysis and classification of '*Ca.* Desulfosporosinus nitrousreducens'. ....59**
**Table 2-5. Amino acids and concentrations used to augment the growth medium for cultivation of '*Ca.* Desulfosporosinus nitrousreducens'. [a] ....61**
**Table 2-6. Genome features of '*Ca.* Desulfosporosinus nitrousreducens' strain PR and *Serratia* sp. strain MF, and comparison to closest relatives. ....63**
**Table 2-7. Genome features of '*Ca.* Desulfosporosinus nitrousreducens' strain PR and *Serratia* sp. strain MF, and close relatives. ....64**
**Table 3-1. Metadata associated with soils used for enrichment procedure. ....99**
**Table 3-2. Substrates provided to the $N_2O$-reducing cultures during the enrichment process. ....100**
**Table 3-3. Analyses of high-quality MAGs using the Microbial Genome Atlas (MiGA) [a]. ....101**
**Table 3-4. Statistics of the high-quality *nosZ*-carrying MAGs. ....106**
**Table 3-5. Growth of clade III $N_2O$ reducers is $N_2O$- and pH- dependent. [a] ....107**

## LIST OF FIGURES

**Figure 2-1. Establishment of $N_2O$-reducing microcosms and enrichment cultures yielding co-culture EV. (A) Schematic of the workflow leading from a soil sample to a solids-free enrichment, and to a co-culture. (B) Community structure profiling based on 16S rRNA gene sequence analysis documents the enrichment process. Soil microbial community structure was profiled with 16S rRNA genes extracted from shotgun metagenomic reads. Community profiling of 6$^{th}$ and 9$^{th}$ transfers was based on 16S rRNA gene amplicon sequencing. Sequences with abundances <2% were grouped as "Others". (C) Percent of the metagenomic short read fragments obtained from El Verde soil and the 15$^{th}$ transfer culture that recruited to the genomes of *Serratia* sp. or *Desulfosporosinus* sp. A representative graph showing the high identity (> 95%) of reads mapping evenly across *Desulfosporosinus* sp. genome is presented in Supplementary Figure 2-3. The *Serratia* sp. or *Desulfosporosinus* sp. genomes were not detected in the soil metagenome dataset, with less than 0.01% of the metagenomic reads mapping to the two genomes (white bar). (D) Pyruvate fermentation (Phase I, white circles) and $N_2O$ consumption (Phase II, black circles) in co-culture EV. *Serratia* (blue diamonds) and *Desulfosporosinus* (red diamonds) cell numbers were determined with specific, 16S rRNA gene-targeted qPCR. (E) Amplicon sequencing illustrates the population shifts in co-culture EV following pyruvate consumption (day 7) and following $N_2O$ consumption (day 18). Relative abundance of *Serratia* (blue bars) and *Desulfosporosinus* (red bars) in co-culture EV following Phase I (day 7) and Phase II (day 18) in vessels with pyruvate plus $N_2O$ (left) and pyruvate only (right). Sequencing was performed on single representative cultures. All other data represent the averages of triplicate incubations and error bars represent standard deviations (n=3). Error bars are not shown if smaller than the symbol.....35**

**Figure 2-2. Interspecies cross-feeding supports low pH $N_2O$ reduction in co-culture EV. (A) Pyruvate fermentation (Phase I, light blue background) in vessels inoculated with axenic *Serratia* sp. strain MF and $N_2O$ consumption (Phase II, red background) following inoculation with co-culture EV comprising the *Serratia* sp. and the $N_2O$-reducing *Desulfosporosinus* sp. (indicated by the arrow). The bottom part of Panel A shows the amino acid profile in the supernatant immediately after inoculation with the *Serratia* sp. (green background), during Phase I, and during Phase II following inoculation with co-culture EV (day 7; 3% inoculum). Samples for untargeted metabolome analysis were collected immediately after inoculation with *Serratia* sp. (light green), during Phase I (light blue, pyruvate fermentation) and Phase II (light red, $N_2O$ reduction). The stacked bars show the ratio (%) of areas under the curve (AUC) of the respective amino acids and amino acid derivatives. Metabolites not assigned to structures representing amino acids or its derivatives are not shown. (B) Principal coordinate analysis (PCoA) of amino acid profiles. The enclosing ellipses were estimated using the Khachiyan algorithm with the ggforce package. Permanova analysis was conducted with the vegan Community Ecology package. Black, blue, and red circles represent samples collected at day 0, during Phase I, and during Phase II, respectively. (C) $N_2O$ consumption in co-culture EV in medium amended with mixtures comprising 5 (blue), 6 (orange), or 15 (black) amino acids (see SI for composition of mixtures), $H_2$, and $N_2O$. The *Desulfosporosinus* sp. cell numbers (red diamonds) were determined with 16S rRNA gene-targeted qPCR and show growth in medium receiving the 15-amino acid mixture. Various other amino acid mixtures tested resulted in no or negligible $N_2O$ consumption. All growth assays with amino acid mixture supplementation were performed in triplicates and repeated in independent experiments.....37**

**Figure 2-3. Phylogenomic and Average Amino acid Identity (AAI) analyses indicate that the $N_2O$-reducing strain PR in co-culture EV represents a new species of the genus *Desulfosporosinus*. Phylogenomic analysis was based on 120 conserved marker genes and included *Peptococcaceae* genomes available from NCBI. Bootstrap values higher than 90 are not displayed. The scale bar indicates 0.05 nucleotide acid substitution per site. Bar plots display the genome-wide AAI (%) between the $N_2O$-reducing '*Ca*. Desulfosporosinus nitrousreducens' and related isolates with sequenced genomes. .....39**

**Figure 2-4. Relatedness and similarity of the clade II NosZ of '*Ca.* Desulfosporosinus nitrousreducens' strain PR to representative clade II NosZ. The tree represents a phylogenetic reconstruction of select clade II NosZ protein sequences. The clade II NosZ of *Gemmatimonas aurantiaca* was used to root the tree. The scale bar indicates 0.2 amino acid substitution per site. Numbers at nodes are bootstrap values smaller than 90. The two-column heatmap shows the AAI values between the NosZ of strain PR (PR) and *Desulfosporosinus meridiei* (DM) to other clade II NosZ sequences, with the darker shades of blue indicating higher percent AAI values.....40**

**Figure 2-5. Comparison of representative *nos* clusters. Included are clade II *nos* clusters encoding select NosZ. and select clade I *nos* clusters of bacteria with confirmed $N_2O$ reduction activity at circumneutral pH. The colored arrows represent genes with different functions and indicate orientation and approximate length. Green, *nosZ*; gray, *nos* accessory genes (i.e., *nosD*, *nosF*, *nosY*, *nosL*, *nosX* and *nosR*); yellow, genes encoding iron-sulfur (Fe-S) proteins; purple, genes encoding Rieske iron-sulfur proteins (S); orange (cy-b) and red (cy-c), genes encoding b-type and c-type cytochromes, respectively; cyan, *nosB* genes encoding transmembrane proteins characteristic for clade II *nos* operons; black, genes of unknown function. *Desulfosporosinus* and *Desulfitobacterium* spp., *Nitratiruptor* and *Nitratifractor* spp., and *Paracoccus* and *Bradyrhizobium* spp. share similar *nos* cluster architectures, respectively. .....41**

**Figure 2-6. Proposed interspecies cross-feeding interactions in co-culture EV. Genes involved in mixed acid fermentation are only found on the *Serratia* sp. strain MF genome, and genes involved in periplasmic $N_2O$ reduction are exclusive to '*Ca.* Desulfosporosinus nitrousreducens' strain PR. External substrates (i.e., pyruvate or the 15-amino acid mixture, $H_2$, $N_2O$) provided to co-culture EV are shown in red font, and metabolites produced by *Serratia* are shown in blue font. Fifteen versus two complete amino acid biosynthesis pathways are present on the *Serratia* sp. strain MF and '*Ca.* Desulfosporosinus nitrousreducens' strain PR genomes, respectively. Strain PR has an incomplete TCA cycle, and the red dashed arrows indicate the absence of the corresponding genes. TCA cycle: tricarboxylic acid cycle; AA: amino acids; FDH: formate dehydrogenase complex; NosZ: nitrous oxide reductase; OM: outer membrane; IM: inner membrane. .....42**

**Figure 3-1. Novel microbial guilds implicated in $N_2O$ reduction. (A) Distribution of putative $N_2O$-reducing population in transfer cultures with (+) or without (-) $N_2O$ amendment. The relative abundance (% of the total metagenome fragments) of MAGs was calculated using CoverM (https://github.com/wwood/CoverM). Taxonomy was assigned to MAGs using GTDB-TK (91). Displayed are MAGs predicted to have at least one *nosZ* gene based on Prokka annotation (137). The comprehensive microbial community profiled with the 43 high-quality MAGs are summarized in Fig. S4. (B). Phylogenomic analyses of *nosZ*-carrying MAGs recovered from low pH $N_2O$-reducing cultures. The tree topology was obtained from the Maximum Likelihood (ML) tree by using RAxML-NG (92), inferred from a 120 conserved marker genes alignment of 20 complete genomes (selected based on GTDB-TK results) (91) and 7 MAGs. The top scale bar indicates 0.2 amino acid substitution rates per site. Sizes of open circles alongside the branches of each sublineage indicate bootstrap percentages obtained by RAxML-NG. The pairwise genome-wide AAI calculated for each MAGs are shown on the right, with the scale displayed on the bottom. Values for each comparison for a given MAGs are connected by lines, and the comparison to self is indicated as 100%. Pair-wise AAI values of 65-95% (i.e., data points fall between the dashed lines) are indicative of species boundary (179). The color legend corresponds to the bar and line colors in panel (A) and (B).....85**

**Figure 3-2. Phylogenetic trees showing the placement of acidic cultures derived NosZ (green) among the reference NosZ (black) and putative NosZ (red). (A) Unrooted phylogenetic tree of NosZ showing three independent clades (i.e., I, II and III). The tree topology was inferred from RAxML-NG. Bootstrap values are displayed as white (> 90%), grey (70 < BP < 90) and black circles (< 70%). (B) Phylogenetic tree showing clade I NosZ with branches belonging to clade II and clade III collapsed. (C) Phylogenetic tree showing clade II NosZ with branches belonging to clade I and clade III collapsed. (D) Phylogenetic tree showing clade III NosZ with branches**

**belonging to clade I and clade II collapsed. Of note, the MAG4 *nos* gene cluster is identical to '*Ca.* Desulfosporosinus nitrousreducens' in a co-culture reported in a prior study (Guang, et al., 2023). Accessory genes associated with *nosZ* are displayed as oriented arrows and gene designation is represented by color legend in panel D. .....87**

**Figure 3-3. Structural and functional validation of clade III NosZ. (A). The NosZ enzyme is a homodimer in head-to-tail orientation with the tetranuclear $Cu_Z$ active site located in the N-terminal, seven-bladed β-propeller domain and the binuclear $Cu_A$ site in the C-terminal cupredoxin domain. The $Cu_A$–$Cu_Z$ distance within one monomer is around 42.5 Å (i.e., $Cu_A$-A to $Cu_Z$-A) and thus too large for efficient electron transfer. Instead, the $Cu_A$ site of one monomer is at a distance of only 10.5 Å from $Cu_Z$ in the other monomer ($Cu_A$-A to $Cu_Z$-B) (B). Conserved residues associated with $Cu_A$ and $Cu_Z$ sites. Two histidine and cysteine residues are conserved in $Cu_A$ site, and seven histidine residues are conserved in $Cu_Z$ site. The Y163 residue enclosed in red is an unexpected (lacking in clade I and clade II NosZ) tyrosine associated with $Cu_Z$ site. (C) Comparative growth assays performed with 27$^{th}$ Sabana and (D) 15$^{th}$ WS2 transfers cultures. Green and red lines indicate $N_2O$ reduction performance in different pH (4.5 and 7) medium. Green bars represent the cells (pH 4.5) enumerated with specific primers targeting the clade III *Desulftobacterium nosZ*. Fold changes of *nosZ* transcripts (orange bars) and assembled NosZ protein (yellow bars) are calculated based on corresponding cultures grown in pH 4.5 medium with (+) and without (-) $N_2O$ amendment. Of note, growth of clade III $N_2O$ reducers was not substantial in cultures without $N_2O$. Data represent averages of triplicate incubations and error bars represent standard deviations (n=3). Error bars are not shown when smaller than the symbol.....89**

**Figure 4-1. Effects of copper on $N_2O$ reduction. Nitrous oxide transformation of culture EV (a) and *D. aromatica* strain RCB (b). $N_2O$ reduction in culture EV (c) and *D. aromatica* strain RCB (d) amended with varying concentrations of $CuCl_2$. Cultures received 0.2 mM $Na_2S$ sequestering residual copper were referred as 0 mM $CuCl_2$. The data represent the averages of triplicate incubations and error bars represent the standard deviations (n=3). Error bars are not shown if smaller than the symbol. .....119**

**Figure 4-2. Effect of $Na_2S$ on $N_2O$ reduction. Mean $N_2O$ reduction rates of culture EV (a) and *D. aromatica* strain RCB (b) in the presence or absence of $Na_2S$. $N_2O$ reduction in culture EV (c) and *D. aromatica* strain RCB (d) received either $CuCl_2$ or $Na_2S$ and cultures amended with excess $CuCl_2$ and $Na_2S$. The data represent the averages of triplicate incubations and error bars represent the standard deviations (n=3). Error bars are not shown if smaller than the symbol. .....120**

**Figure 4-3. Reversible and irreversible inhibition of $Na_2S$ on $N_2O$ reduction. $N_2O$ reduction of culture EV following $CuCl_2$ (a) or $Na_2S$ dosing (c). $N_2O$ reduction by *D. aromatica* strain RCB following $CuCl_2$ (c) or $Na_2S$ dosing (d). Arrows indicate $CuCl_2$ or $Na_2S$ dosing. The data represent the averages of triplicate incubations and error bars represent the standard deviations (n=3). Error bars are not shown if smaller than the symbol. .....121**

**Figure 4-4. Inhibition of nitrogen oxyanions on $N_2O$ reduction by culture EV. $N_2O$ reduction in culture EV received varying concentrations of $NO_2^-$ (a) or $NO_3^-$ (b). $N_2O$ reduction in culture EV (c) and *Dechlromonas aromatica* strain RCB (d) following nitrogen oxyanion dosing. The data represent the averages of triplicate incubations and error bars represent the standard deviations (n=3). Error bars are not shown if smaller than the symbol. .....122**

**Supplementary Figure 2-1. Phenotypic characterization of co-culture EV. Cultures were grown in 160 mL glass serum bottles containing 100 mL of medium amended with pyruvate (50 or 250 µmol), $H_2$ (416 µmol) and $N_2O$ (416 µmol) (A and B), pyruvate and $H_2$ (C and D), or pyruvate and $N_2O$ (E and F). The arrows in panels D and F indicate additional doses of $N_2O$ or $H_2$ to corresponding culture vessels lack $N_2O$ (D) or $H_2$ (F) to resume $N_2O$ reduction activity. Pyruvate consumption and associated product formation are documented in panels A, C, and E. $N_2O$ and $H_2$ consumption are documented in panels B, D, F. Panel G shows the performance of co-culture EV grown with a lower amount of pyruvate. Panel H depicts pyruvate, $H_2$ and**

**$N_2O$ amounts over time in vessels without inoculum. Autotrophic activity in cultures with $CO_2$, but lacking pyruvate, was not observed (I). The light blue shaded areas represent the pyruvate fermentation phase (Phase I) and the light red areas represent the $N_2O$ reduction phase (Phase II). The data represent the averages of triplicate incubations and error bars represent the standard deviations (n=3). Error bars are not shown when smaller than the symbol. .....43**

**Supplementary Figure 2-2. Medium pH over the course of the incubation. pH profiles were measured in replicate co-culture EV incubation vessels that received 0, 0.5, and 2.5 mM pyruvate. pH changes (Δ pH) were calculated by subtracting the pH values measured immediately following inoculation from pH values measured at the end of incubation period. Pyruvate was not consumed in vessels that were not inoculated with co-culture EV. The data shown are the averages of triplicate incubations and error bars represent the standard deviations (n=3). Error bars are not shown when smaller than the symbol. .....45**

**Supplementary Figure 2-3. Fragment recruitment plot of the '*Ca*. Desulfosporosinus nitrousreducens' strain PR genome to the metagenome dataset derived from the 15th generation co-culture EV. The recruitment was performed via processing a BLAST search of the metagenome fragments against the '*Ca*. Desulfosporosinus nitrousreducens' strain PR genome. The tabular BLAST result was parsed using BLASTab.catsbj.pl, and graphical representation was generated with the BlasTab.recplot2.R embedded in Enveomics collection (88). (A) The bar on the left shows the number of fragments with different identity recruited to each position on the genome. (B) indicates the sequencing depth across the '*Ca*. Desulfosporosinus nitrousreducens' strain PR genome on a logarithmic scale. (C) Sequencing depth histogram with peaks from values above 95% identity automatically identified as skewed normal distribution. (D) Metagenome fragments recruited to the '*Ca*. Desulfosporosinus nitrousreducens' strain PR genome, placed by location (x-axis) and identity (y-axis). (E) Identity histogram of mapping fragments (light gray) and smoothed spline (black). The backgrounds in panels D and E, and the line colors in panels B and C, correspond to identity matches above (dark blue) and below (light blue) 95 %. A recruitment plot of the '*Ca*. Desulfosporosinus nitrousreducens' strain PR genome to the metagenome datasets derived from El Verde soil is not shown as the covered fraction of the 5.6 Mbp genome was below 10% (i.e., 0.56 Mbp). .....46**

**Supplementary Figure 2-4. Comparison of '*Ca.* Desulfosporosinus nitrousreducens' strain PR and *Serratia* sp. strain MF 16S rRNA gene sequences derived from cloned 16S rRNA gene fragments (Sanger sequencing) and co-culture EV (metagenome sequencing). DNA extracted from co-culture EV following $N_2O$ consumption served as template for the amplification of 16S rRNA gene fragments with general primer pair 8F-1541R. 16S rRNA gene fragments were cloned in *E. coli* and two uniform clone populations were obtained, represented by Cloned_Desulfosporosinus_16S and Cloned_Serratia_16S. .....48**

**Supplementary Figure 2-5. Formation of gas bubbles in soft agar shake tubes. (A) Visible gas bubbles (presumably $N_2$) following $N_2O$ consumption. The vials were incubated with the stoppers down for 28 days. (B) The formation of gas bubbles was strictly dependent on $N_2O$, and no bubbles formed in replicate vials without $N_2O$. No gas bubbles formed in control incubations without inoculum. .....49**

**Supplementary Figure 2-6. Dynamic changes of amino acids in the supernatants of cultures following inoculation with *Serratia* sp. and with '*Ca.* Desulfosporosinus nitrousreducens' strain PR (as co-culture EV). Axenic *Serratia* sp. cultures amended with pyruvate, $N_2O$, and $H_2$ were inoculated with co-culture EV on day 7. Orange lines represent amino acids in cultures inoculated with axenic *Serratia* sp. on day 0. Red lines represent amino acids in cultures inoculated with the axenic *Serratia* sp. on day 0 and subsequently inoculated with co-culture EV on day 7. Note that axenic *Serratia* sp. cultures without co-culture EV inoculum cannot reduce $N_2O$. Shown are representative data obtained from a single culture in medium reduced with l-cysteine. Cystine was detected in cultures reduced with l-cysteine; however, in samples from replicates from an independent experiment where DTT served as reductant, cystine was not detected, suggesting *Serratia* sp. does not release cystine into the medium. .....50**

**Supplementary Figure 2-7. Performance of co-culture EV at different medium pH values. (A) $N_2O$ reduction was measured in triplicate 160 mL serum bottles containing 100 mL of medium (pH 3.5, 4.5, 5, 6, 7, 8) and inoculated with co-culture EV. $N_2O$ reduction was observed between pH 4.5 and 6, but not at pH 3.5 and at or above pH 7. (B) Pyruvate consumption rates by *Serratia* sp. in cultures adjusted to pH 4.5, 5, 6, 7, and 8. Pyruvate was consumed in all incubation vessels except for those at pH 3.5. (C) $N_2O$ consumption rates of '*Ca.* Desulfosporosinus nitrousreducens' at pH 4.5, 5, and 6. No $N_2O$ consumption was observed in pH 3.5, 7.0, and 8.0 cultures. Consumption rates of pyruvate and $N_2O$ were calculated using data that fell within the linear ranges of consumption. Each black dot in the box plots represent the consumption rates calculated from a single experiment. The data from three and six replicate cultures were used for the calculations of pyruvate and $N_2O$ consumption rates, respectively. .....51**

**Supplementary Figure 2-8. Gene clusters found on the '*Ca.* Desulfosporosinus nitrousreducens' strain PR genome. Displayed are formate dehydrogenase (*fdh* gene cluster), b-type Ni/Fe hydrogenase (*hyp* gene cluster), group 1 Ni/Fe hydrogenase (*hya* gene cluster), FeFe type Nitrogenase (*anf* gene cluster), Mo-Fe Nitrogenase (*nif* gene cluster), Nitric-oxide reductase (*nor* gene cluster), High-affinity amino acid transport system (*ilv* gene cluster). The arrows indicate operon length and orientations. Preliminary annotation of coding genes was done with Prokka (137), MicrobeAnnotator (138), and the RAST server (87), and genes of interests were curated via blasting to the NCBI nr database. Cy-b: b-type cytochrome; ABC: ATP-binding cassette. The black arrow in the *fdh* gene cluster represents a gene encoding a small protein of unknown function. .....52**

**Supplementary Figure 2-9. Comparative growth studies with 'Ca. Desulfosporosinus nitrousreducens' strain PR (as co-culture EV) and *Desulfosporosinus acididurans* strain D. Panel A shows growth of '*Ca.* Desulfosporosinus nitrousreducens' strain PR with 4.16 mM (nominal) $N_2O$ (blue) or 5 mM $SO_4^{2-}$ (red) as electron acceptor in pH 4.5 medium amended with the 15-amino acid mixture and 4.16 mM (nominal) $H_2$. Over the 9-day incubation period, strain PR completely consumed the initial dose of $N_2O$, whereas cultures amended with 5 mM $SO_4^{2-}$ showed no growth or $SO_4^{2-}$ consumption (4.97 ± 0.23 mM sulfate remained). OD values below 0.01 were measured in replicate cultures that did not receive $N_2O$ as electron acceptor or $H_2$ as electron donor. Panel B compares growth of *Desulfosporosinus acididurans* strain D with 4.16 mM (nominal) $N_2O$ (blue) or 5 mM $SO_4^{2-}$ (red) as electron acceptors in pH 5.5 medium with 10 mM glycerol as electron donor. Over a 9-day incubation period, *Desulfosporosinus acididurans* strain D reduced 5 mM $SO_4^{2-}$, but $N_2O$ was not consumed (4.10 ± 0.59 mM $N_2O$ remained) in replicate cultures, even after an extended 20-day incubation period. Growth was monitored by measuring the optical density at 600 nm ($OD_{600}$). .....53**

**Supplementary Figure 2-10. Distribution of '*Ca.* Desulfosporosinus nitrousreducens' strain PR and *Serratia* sp. strain MF in select publicly available soil metagenomes. Metagenome datasets were downloaded from the European Nucleotide Archive (accession number PRJEB44414) with associated metadata available in a Supplemental Information/Source Data file (https://doi.org/10.1038/s41467-022-29161-3). (A) Geographical distribution of the soil metagenomes included in the analysis. Blue dots indicate a soil pH >7, red dots indicate a soil pH <7. (B) The partial importance (%) of different parameters, including the presence of *Serratia* sp. (based on short reads that align to the *Serratia* sp. strain MF genome), organic matter (OM content), $NO_3^-$ content, $NH_4^+$ content, C/N ratio, and pH for the relative abundance of '*Ca.* Desulfosporosinus nitrousreducens' strain PR based on Random Forest models (139). (C) Correlation between percentages of short read fragments aligned to the *Serratia* sp. strain MF and the '*Ca.* Desulfosporosinus nitrousreducens' strain PR genomes. The significance values for the correlations were calculated with the Pearson test (140) implemented in the ggpubr package (https://github.com/kassambara/ggpubr). .....54**

**Supplementary Figure 3-1. Low pH $N_2O$ reduction of transfer cultures derived from farm and tropical soils. Numbers inside parenthesis indicate the transfer generations. For example, panel labeled as WS1 ($4^{th}$) showed $N_2O$ data collected from $4^{th}$ WS1 transfer culture. Data were collected from single experiment. .....91**

**Supplementary Figure 3-2. Schematic of establishing low pH $N_2O$ reducing cultures. Shotgun metagenomic sequencing was applied to original Caney Fork Farm and Puerto Rico Soils to study the baseline microbiota. Soil samples from Caney Fork Farm and Puerto Rico Forest were subsequently used to establish pH 4.5 and 7 soil microcosms. Consecutive transfers were performed in pH 4.5 and 7 basal salt medium and derived solids-free cultures. Comparative shotgun metagenomic analyses were conducted with corresponding pH 4.5 cultures with or without $N_2O$ substrate. Amplicon sequencing targeting 16S V3-V4 regions was performed on cultures transferred in pH 7 basal salt medium. .....92**
**Supplementary Figure 3-3. Nonpareil analysis of soil- and enrichment cultures' metagenomes. (A) Nonpareil curves of PR soil- and derived enrichment cultures. (B) Nonpareil curves of CFF soil- and derived enrichment cultures. Open circles represent the estimated average coverage of the datasets obtained and projections based on model fitting to reach 95% and 99% coverage are indicated (horizontal dashed lines). The arrows at the bottom represent sequencing effort required to achieve 50% coverage. .....93**
**Supplementary Figure 3-4. Microbial community constructed with high-quality MAGs. Relative abundance of MAGs in each metagenome was calculated with CoverM. Taxonomy was assigned to MAGs using GTDB-TK. Microbial community was displayed at class level with ggplot package. T axa highlighted with text are population selectively growing in the presence of $N_2O$. .....95**
**Supplementary Figure 3-5. Preliminary phylogenetic analyses allude to the clade III *nosZ* genes recovered from acidic $N_2O$-reducing cultures. (A) clade I and (B) clade II *nosZ* are shown separately for readers' convenience. The branch labels in black indicate the 80 referecen *nosZ* genes, whereas branch labels in red indicate the *nosZ* genes recovered from acidic $N_2O$-reducing cultures. Bifurcation with bootstrap values over 75% are indicated with closed circle symbols. Tree scales indicate amino acid substitution rates. The *nosZ* genes (MAG6 and 7) not cluster with either clade I or clade II are enclosed in red. .....96**
**Supplementary Figure 3-6. Heatmap showing amino acid identity between the NosZ recovered from high-quality MAGs. Numbers inside cells represent the pairwise sequence identity (%) between two NosZ. Four and two different NosZ are found on MAG1 and MAG5, respectively. The MAG6 and MAG7 NosZ share no more than 30% to reference NosZ shown as black labels in Fig. S5. .....97**
**Supplementary Figure 3-7. AlfphaFold2 predicted structures of proteins located closely to NosZ. Signalp 6.0 was used to identify and remove signal peptides prior to structure prediction. The corresponding membrane orientations of proteins were predicted using MembraneFold. .....98**

# Chapter 1 Introduction

## 1.1 Sources and sinks of $N_2O$

Nitrous oxide ($N_2O$), an odorless gas, is the dominant ozone-depleting substance emitted in the 21st century (1). Soils and industrial processes have contributed considerably to the increased $N_2O$ emissions over the last decades (2, 3). Agricultural and natural soils are the major contributors of the current global annual $N_2O$ budget as high as 17.0 Tg N $yr^{-1}$ (3). However, the $N_2O$ uptake of soils was as low as 0.01 Tg N $yr^{-1}$, which was much lower than that produced from soils (9.4 Tg N $yr^{-1}$ in total). The imbalance may be related to the multiple $N_2O$ sources ($N_2O$-producing process) versus the single $N_2O$ sink ($N_2O$-consuming process) (4).

Coupled abiotic-biotic processes are the predominant $N_2O$ sources in terrestrial ecosystems (5). During the Great Oxidation Event (GOE), nitrite ($NO_2^-$) and nitrate ($NO_3^-$) were produced as a result of oxidization of inorganic nitrogen (6). In the $Fe^{2+}$-rich environments, Fe minerals could have mediated the formation of nitric oxide (NO) and $N_2O$ via chemical reaction with $NO_2^-$ (7). In addition, the chemical process is also coupled to biotic process when $Fe^{3+}$ and $NO_3^-$ reduction occur simultaneously. For example, *Anaeromyxobacter dehalogenans* reduced both $Fe^{3+}$ and $NO_3^-$ under anoxic conditions, the resulting $Fe^{2+}$ and $NO_2^-$ subsequently react to form $N_2O$ chemically ($4Fe^{2+} + 2NO_2^- + 5H_2O \rightarrow 2Fe^{3+} + N_2O + 6H^+$) (8). In this specific chemical reaction, $Mn^{2+}$ could substitute $Fe^{2+}$ as the oxidant ($2Mn^{2+} + 2NO_2^- + 6H^+ \rightarrow 2Mn^{4+} + N_2O + 3H_2O$) (9). These metal minerals could also react with hydroxylamine, an important intermediate product in nitrification, yielding $N_2O$ as the end product ($4Fe^{3+}/2Mn^{4+} + 2NH_2OH \rightarrow 4Fe^{2+}/2Mn^{2+} + N_2O + H_2O + 4H^+$) (10, 11). Thus, abiotic processes could have been the major contributor to $N_2O$ production when microbial processes yielding $N_2O$ were not available in the Archaean.

In modern terrestrial ecosystems, microbial transformations of nitrogen, coupled to abiotic processes, have become the major $N_2O$ source (12). Following the start-up

reaction of nitrogen fixation, the resulting ammonia ($NH_4^+$) become available to microorganisms and ready for microbial conversions. Microorganisms convert $NH_4^+$ to $NO_3^-$ via nitrification with $NH_2OH$ and $NO_2^-$ is formed as an intermediate product, which could further react with metal minerals to formulate $N_2O$. In contrast, modular microbial denitrification processes produce $N_2O$ as the intermediate product from the reverse reaction ($NO_3^- \rightarrow NO_2^- \rightarrow N_2O \rightarrow N_2$) (4). Denitrifying organisms such as fungi that lack the gene coding NosZ would produce $N_2O$ as end product (13).

To date, transformation of $N_2O$ has been achieved with three enzymes (14), though two of them are not physiology relevant to $N_2O$ reduction. The nitrogenase was demonstrated to utilize $N_2O$ as alternative substrate, with the end-product being $N_2$ and $NH_3$ ($N_2O \rightarrow N_2 \rightarrow NH_3$). However, the conversion of $N_2O$ by nitrogenase was documented to be biologically irrelevant, as in vivo $N_2O$ reduction mainly occurred with NosZ (15). Another enzyme that putatively consumed $N_2O$ is a multicopper oxidase from the archaeon *Pyrobaculum aerophilum* while the end-product remains unknown (16). The most widely studied enzyme catalyzing $N_2O$ reduction is the NosZ comprising two copper centers (17), constituting the last step of microbial denitrification pathway (12).

$N_2O$ reduction is associated with energy conservation, disposal of excess electrons, and detoxification in organisms expressing NosZ (18). $N_2O$ respiring bacteria grow and build up biomass with $N_2O$ as the sole electron acceptor (i.e., energy conservation) (19). In contrast, obligate aerobic organisms that only reproduce under oxic conditions utilize $N_2O$ as a temporary substitute for oxygen, allowing them to survive under hypoxia conditions (20). For corrinoid-dependent organisms, consumption of $N_2O$ serves as a detoxification mechanisms due to its inhibitory effect on corrinoid-dependent processes (21). Therefore, organisms have acquired $N_2O$ reduction capacity in response to divergent environmental stress.

Study of NosZ has long been focused on denitrifying organisms until the novel NosZ (hereafter referred as clade II NosZ) was identified recently (12). The conventional NosZ (hereafter referred as clade I NosZ) is comprised entirely of *Proteobacteria* and *Archaea*

and was distinguished with the Tat signal translocation pathway and likelihood of dentification (22). In contrast, a broader organismic distribution was observed for clade II NosZ (e.g., *Chloroflexi*, *Bacteroidetes* and *Firmicutes*) with a Sec signal peptide conserved in the genes. In addition to the gene diversification, the structures of Nos operon clusters comprising accessory genes of NosZ also differentiate clade I and II NosZ. For example, a membrane-bounding protein harboring at least four transmembrane helixes were exclusively identified immediately following clade II NosZ (12). Despite extensive efforts applied to investigate NosZ, the growing diversity suggests it is underexplored. For example, *nosZ* was conspicuously absent in the genomes of *Acidobacteria*, which suggested a lower frequency of *nosZ* in associated acidic conditions (23). However, a recent study implicated organisms affiliated with *Acidobacteria* were the predominant $N_2O$ reducers in tundra soil ecosystems (24).

### 1.2 Acidic soils are the main $N_2O$ source

Global soil ecosystems are experiencing acidification due to intensive application of nitrogen fertilizer. Biotic reactions of nitrogen are the main cause of soil acidification. A notable example is the nitrification process generating acidity: $NH_4^+ + 2O_2 \rightarrow 2H^+ + NO_3^- + H_2O$ (25). In the case of a meta-analysis, soil pH has declined by 0.26 on average as a result of N fertilizer application over the past decades (26). Global excessive nitrogen use (27) would exacerbate soil acidification in the future and cause environmental problems (28) such as increasing net $N_2O$ emissions (29).

Soil pH is a chief modulating factor affecting the magnitude of $N_2O$ production and consumption, consequently controlling net $N_2O$ emissions (30). The mechanisms behind this are the organisms/enzymes involved in the N-cycling network have different pH preferences. For instance, acidification led to increased $N_2O$ production from both ammonia oxidizing microbes via nitrifier-denitrification process ($NH_4^+ \rightarrow NO_2^- \rightarrow N_2O$) (31). Furthermore, pH is a control of competing metabolisms within individual organisms: acidic and circumneutral pH favored *Shewanella loihica* strain PV-4 to carry out denitrification and respiratory ammonification (32), with the former conditions

yielding $N_2O$ as major product. Therefore, the effects of pH on $N_2O$ production are multidimensional at organismic level.

The physiological pH optima of enzymes are a determining factor controlling $N_2O$ production of individual organisms, consequently affecting the soil $N_2O$ emissions. In contrast to the circumneutral pH (~7.3) optima of $N_2O$ consumption, the preferred pH of $N_2O$ production was reported to be more acidic (pH 5 to 6) (30). Thus, acidic soils are hypothesized to be the main $N_2O$ emitters. However, laboratory incubations of acidic solids-containing microcosms arguing the hypothesis showed $N_2O$ reduction activity (33, 34). The observed $N_2O$ reduction activity in acidic microcosms may occur in the microsites associated with solids (i.e., soils) where the pH is different from bulk medium (35). For example, a *Cloacibacterium* isolate greatly reduced net $N_2O$ emission in acidic solids-containing microcosm (pH 5.5) but showed no $N_2O$ reduction activity in pH 5.5 liquid medium (36). The observed $N_2O$ sink effect in acidic microcosms could be that *Cloacibacterium* cells were embedded in solid phase, protected against acidic bulk medium pH.

In contrast to the microcosm-based observation, solid-free laboratory incubations and field measurements of $N_2O$ showed weak or no $N_2O$ sink capacity under acidic conditions compared to that under circumneutral pH conditions. For example, net $N_2O$ emissions were negatively correlated to soil pH (37). Furthermore, the $N_2O$ emission factors were higher in acidic soils than that in circumneutral pH soils, indicating more N fertilizer applied to acidic soils were lost in the form of $N_2O$. Phenotypic studies of clade I $N_2O$ reducers showed that $N_2O$ reduction was completely blocked at pH values lower than 6 (38, 39), suggesting the weak $N_2O$ reduction capacity is the main cause of higher $N_2O$ emissions from acidic soils. Transcriptional analysis and resting cell assays documented that NosZ assembly is impaired under acidic conditions, while the expression of *nosZ* genes was not affected (40, 41). Consistent to these observations, mechanistic study unraveled a conformational change of clade I NosZ under acidic conditions, which explains its incapability in consuming $N_2O$ (42). However, the impact

of acidic pH on clade II NosZ remains unclear though extensive studies have been conducted to explore clade I NosZ at organismic, genetic, enzymatic level.

### 1.3 Research objectives

The proposed work will elucidate the microbiology of low pH $N_2O$ reduction and address the following hypotheses.

**Hypothesis 1:** $N_2O$-reducing microbes in soils have adapted to acidic pH conditions (<5) and can be enriched from acidic soils.

**Rationale**: A metagenomic study focused on Luquillo Experimental Forest soils identified diverse *nosZ* gene sequences, suggesting genomic potential for $N_2O$ reduction in low pH soils (43). A subsequent microcosm study demonstrated $N_2O$ reduction activity at a pH of 4.5 (44). These microcosms are available for studying the microbiology involved in low pH $N_2O$ reduction.

**Hypothesis 2:** Acidophilic $N_2O$-reducing microbes also exist in acidic microsites in soils with circumneutral pH values.

**Rationale**: The naturally acidic sites on the Earth are known to thrive a variety of acidophilic microorganisms (45), whereas the circumneutral soil are overlooked source of acidophiles. Soils are complex matrixes with high pH heterogeneity, and pH varies by as much as 1.3 pH among samples less than 50 cm apart (46). The microbial metabolism could have led to more contrasting pH at finer scale: the microscale varied by 2 pH in spots localized closely (less than 5 mm) following straw patch amendment (47). Obviously, acidic microsites could occur in circumneutral CFF soils and harbor the acidophilic $N_2O$-reducing microorganisms.

**Hypothesis 3:** Geochemical factors are controlling $N_2O$ reduction in acidic soils.

**Rationale**: Growth of most acidophilic $N_2O$-reducing microbes acquired in this study requires amendment of complex substrates (e.g., amino acids and peptides). In microbial

network, the reliance on external growth factors would render the acidophilic $N_2O$-reducing microbes weak competitors for nutrients and energy.

# Chapter 2 Sustained bacterial $N_2O$ reduction at acidic pH

A version of this chapter was submitted to the preprint server Biorxiv, available under DOI: https://doi.org/10.1101/2023.10.06.560748.


## Abstract

Nitrous oxide ($N_2O$) is a climate-active gas and emissions from terrestrial ecosystems are concerning. Microbial reduction of $N_2O$ to dinitrogen ($N_2$) is the only known consumption process and has been studied extensively at circumneutral pH; however, $N_2O$ reduction under acidic conditions is thought to be limited. Global soil acidification, accelerated by anthropogenic practices, introduces high uncertainty into $N_2O$ emission budgets. We obtained an enrichment culture from an acidic tropical forest soil that robustly reduces $N_2O$ to $N_2$ at pH 4.5 with the addition of pyruvate and hydrogen. Consecutive transfers at pH 4.5 yielded a co-culture and temporal analyses revealed a bimodal growth pattern with a *Serratia* sp. growing during the initial pyruvate fermentation phase followed by growth of a novel *Desulfosporosinus* sp. via hydrogenotrophic $N_2O$ reduction. The *Desulfosporosinus* sp. produced $(3.1 \pm 0.11) \times 10^8$ cells per mmol of $N_2O$ consumed, on par with growth yields reported for clade II $N_2O$ reducers at circumneutral pH. Genome analysis identified a clade II *nos* gene cluster, but an incomplete pathway for sulfate reduction, a hallmark feature of the genus *Desulfosporosinus*. Physiological and metabogenomic characterization revealed interspecies nutritional interactions, with the pyruvate fermenting *Serratia* sp. supplying amino acids as essential growth factors to the *Desulfosporosinus* sp. The co-culture reduced $N_2O$ between pH 4.5 and 6 but not at or above pH 7, contradicting the paradigm that sustained microbial $N_2O$ reduction ceases under acidic pH conditions, thus confirming a previously unrecognized $N_2O$ reduction potential in acidic soils.

## 2.1 Introduction

Exploitation, mismanagement, and unsustainable practices deteriorate soil health across the globe (48). pH is a key soil health parameter, but soil acidification, a natural process accelerated by the reliance of synthetic nitrogen fertilizer, the growth of legumes, and acidic precipitation/deposition, plagues regions around the world (49, 50). In addition to pH change, N fertilizer input substantially increases the formation of $N_2O$, a compound linked to ozone depletion and climate warming (1, 51-54), and interference with biogeochemical processes such as methanogenesis, mercury methylation, and reductive dechlorination (55, 56). The rise in global $N_2O$ emissions indicates an imbalance between $N_2O$ formation versus consumption, which has been explained by the contrasting pH optima of processes involved in $N_2O$ formation (pH 5-6) versus consumption (circumneutral pH) (30). A few studies reported $N_2O$ consumption in acidic soil laboratory microcosms (57, 58); however, soil heterogeneity and associated (microscale) patchiness of pH conditions make generalized conclusions untenable (35, 36). Attempts with denitrifying enrichment and axenic cultures have thus far failed to demonstrate growth-linked $N_2O$ reduction and sustainability of such a process under acidic pH conditions (34, 36, 59).

The only known sink for $N_2O$ are microorganisms expressing $N_2O$ reductase (NosZ), a periplasmic enzyme that catalyzes the conversion of $N_2O$ to environmentally benign dinitrogen ($N_2$). NosZ expression and proteomics studies with the model denitrifier *Paracoccus denitrificans* demonstrated that acidic pH interferes with NosZ maturation (38, 60), a phenomenon also observed in enrichment cultures harboring diverse $N_2O$-reducing bacteria (40). Studies with *Marinobacter hydrocarbonoclasticus* found active NosZ with a $Cu_Z$ center in the 4Cu2S form in cells grown at pH 7.5, but observed a catalytically inactive NosZ with the $Cu_Z$ center in the form 4Cu1S when the bacterium was grown at pH 6.5 (42). These observations support the paradigm that microbial $N_2O$ reduction is limited to circumneutral pH environments. A metagenome-based analysis of soil microbial communities in the Luquillo Experimental Forest (Puerto Rico) provided evidence that $N_2O$-reducing soil microorganisms are not limited to circumneutral pH

soils and exist in acidic tropical forest soils (43). Microcosms established with acidic Luquillo Experimental Forest soil demonstrated the $N_2O$ reduction activity, and suggested that the microbial communities in pH 4.5 and pH 7 microcosms differed (44). To shed light on the microorganisms performing $N_2O$ reduction at pH 4.5, a two-population co-culture was derived from $N_2O$-reducing soil microcosms established with acidic tropical forest soil collected in the Luquillo Experimental Forest (El Yunque National Forest) in Puerto Rico. Characterization of the co-culture demonstrated the activity of an acidophilic *Desulfosporosinus* sp. that utilizes $N_2O$ as electron acceptor at pH 4.5.

## 2.2 Materials and methods

### Soil sampling locations and microcosms

Soil samples were collected in August 2018 at the El Verde research station in the El Yunque Natural Forest in Puerto Rico (43). The measured soil pH was 4.45 and characteristic for the region. Vertical distance of the El Verde research station to mean sea level is 434 meters. Fresh soil materials from 9 to 18 cm depth were used to establish pH 4.5 laboratory microcosm that were amended with $N_2O$ and lactate (44).

### Enrichment cultures

Transfer cultures were established in 160-mL glass serum bottles containing 100 mL of anoxic, completely synthetic, defined basal salt medium prepared as described (61) with the following modifications. $NaHCO_3$ and $Na_2S$ were omitted and the total $KH_2PO_4$ concentration was increased to 7.0 g $L^{-1}$. l-cysteine (0.2 mM) was the sole reductant unless indicated otherwise. The medium pH was 4.27 to 4.35. The bottles with $N_2$ headspace were sealed with butyl rubber stoppers (Bellco Glass, Vineland, NJ, USA) held in place with aluminum crimp caps and autoclaved. All subsequent amendments to the medium bottles used sterile plastic syringes and needles to augment the medium with

aqueous filter-sterilized (0.2 µm polyethersulfone membrane filter, Thermo Scientific, Waltham, MA, USA) stock solutions and undiluted gases (62). Ten mL of $N_2O$ gas (416 µmol, 4.16 mM nominal; 99.5%) was added 24 hours prior to inoculation from an El Verde microcosm showing $N_2O$ reduction activity. The microcosm was manually shaken before 1 mL aliquots were transferred with a 3-mL plastic syringe and a 2-gauge needle. Initial attempts to obtain solids-free enrichment cultures with 5 mM lactate as carbon source and electron donor showed no $N_2O$ reduction. As such, the following substrates were subsequently tested in the transfer cultures: 5 mM propionate, 20 mM pyruvate, 20 mM pyruvate plus 10 mL (416 µmol, 4.16 mM nominal) hydrogen ($H_2$), 1 mM formate plus 1 mM acetate and 5 mL (208 µmol, 2.08 mM nominal) $CO_2$, and 0.1 or 10 g $L^{-1}$ yeast extract. Subsequent transfers (3%, v/v) used medium supplemented with 0.5 or 2.5 mM pyruvate and 10 mL $H_2$, and occurred when the initial dose of 10 mL $N_2O$ had been consumed. All culture vessels were incubated in upright position at 30ºC in the dark without agitation.

**Microbial community analysis**

16S rRNA gene amplicon sequencing was performed with samples collected from 6$^{th}$-generation transfer culture following complete $N_2O$ consumption, and 9$^{th}$-generation transfer cultures following complete pyruvate consumption (Phase I) and complete $N_2O$ consumption (Phase II). Biomass from 1 mL of culture suspension samples were collected by centrifugation (10,000 x g, 20 min, 4 ºC), and genomic DNA was isolated from the cell pellets using the DNeasy PowerSoil Kit (Qiagen, Hilden, Germany). 16S rRNA gene-based amplicon sequencing was conducted at the University of Tennessee Genomics Core following published procedures (63). Primer sets used in amplicon sequencing of 6$^{th}$ and 9$^{th}$ transfer cultures are 341F-785R and 515F-805R, respectively (64).

Analysis of amplicon reads was conducted with nf-core/ampliseq v2.3.1 using Nextflow (65). Software used in nf-core/ampliseq was containerized with Singularity v3.8.6 (66). Amplicon read quality was evaluated with FastQC v0.11.9 (67) and primer removal used

Cutadapt v3.4 (68). Quality control including removal of sequences with poor quality, denoising, and chimera removal was performed, and amplicon sequence variants (ASVs) were inferred using DADA2 (69). Barrnap v0.9 was used to discriminate rRNA sequences as potential contamination (70). ASVs were taxonomically classified based on the Silva v138.1 database (71). Relative and absolute abundances of ASVs were calculated using Qiime2 v2021.8.0 (72). Short read fragments of the El Verde soil metagenome representing 16S rRNA genes were identified and extracted using Parallel-Meta Suite v3.7 (73).

**Isolation and classfication**

Following 15 consecutive transfers, 100 µL cell suspension aliquots were serially diluted and plated on tryptic soy agar (TSA, MilliporeSigma, Maryland, US) medium. Colonies with uniform morphology were observed, and a single colony was transferred to a new TSA plate. This process was repeated three times before a single colony was transferred to liquid basal salt medium (pH 4.5) amended with 2.5 mM pyruvate, 416 µmol $N_2O$, and 416 µmol $H_2$. Following growth, DNA was extracted for PCR amplification with general bacterial 16S rRNA gene-targeted primer pair 8F-1541R (74), and Sanger sequencing of both strands yielded a 1,471-bp long 16S rRNA gene fragment.

Efforts to isolate the $N_2O$ reducer applied the dilution-to-extinction principle (61). Ten-fold dilution-to-extinction series used 20 mL glass vials containing 9 mL of basal salt medium and 0.6% (w/v) low melting agarose (MP Biomedicals, LLC., Solon, OH) with a gelling temperature below 30º were established as described (61). Each glass vial received 2.5 mM pyruvate, 1 mL (41.6 µmol, 4.16 mM nominal) $H_2$ and 1 mL (41.6 µmol, 4.16 mM nominal) $N_2O$ following heat sterilization. Parallel $10^{-1}$ to $10^{-10}$ dilution-to-extinction series were established in liquid basal salt medium without low melting agarose, which were used to inoculate the respective soft agar dilution vials. Additional attempts to isolate the $N_2O$ reducer used solidified (1.5% agar, w/v) basal salt medium. A 1-mL sample of a 15$^{th}$-generation transfer culture that actively reduced $N_2O$ was 10-fold serially diluted in liquid basal salt medium, and 100 µL of cell suspension aliquots were

evenly distributed on the agar surface. The plates were incubated under an atmosphere of $N_2/H_2/N_2O$ (8/1/1, v/v/v), and colony formation was monitored every 2 weeks over a 6-month period.

**Quantitative PCR (qPCR)**

SYBR Green qPCR assays targeting the 16S rRNA gene of the *Serratia* sp., and TaqMan qPCR assays targeting the 16S rRNA gene of the *Desulfosporosinus* sp. were designed using Geneious Prime (Table 2-1). Probe and primer specificities were examined by *in silico* analysis using the Primer-BLAST tool (75), and experimentally confirmed using 1,538 bp- and 1,467 bp-long synthesized linear DNA of the respective complete 16S rRNA genes of the *Serratia* sp. and the *Desulfosporosinus* sp., respectively (Integrated DNA Technologies, USA). For enumeration of *Serratia* 16S rRNA genes, 25 µL qPCR tubes received 10 µL 1X Power SYBR Green, 9.88 µL UltraPure nuclease-free water (Invitrogen, Carlsbad, CA, USA), 300 nM of each primer, and 2 µL template DNA. For enumeration of *Desulfosporosinus* 16S rRNA genes, the qPCR tubes received 10 µL TaqMan Universal PCR Master Mix (Life Technologies, Carlsbad, CA, USA), 300 nM of TaqMan probe (5'-6FAM-AAGCTGTGAAGTGGAGCCAATC-MGB-3'), 300 nM of each primer, and 2 µL template DNA (76). All qPCR assays were performed using an Applied Biosystems ViiA 7 system (Applied Biosystems, Waltham, MA, USA) with the following amplification conditions: 2 min at 50ºC and 10 min at 95ºC, followed by 40 cycles of 15 s at 95ºC and 1 min at 60ºC. The standard curves were generated using 10-fold serial dilutions of the linear DNA fragments carrying a complete sequence of the *Serratia* sp. (1,538 bp) or the *Desulfosporosinus* sp. (1,467 bp) 16S rRNA gene, covering the 70- and 72-bp qPCR target regions, respectively.

The qPCR standard curves established with the linear DNA fragments carrying complete *Serratia* sp. or *Desulfosporosinus* sp. 16S rRNA genes had slopes of -3.82 and -3.404, y-intercepts of 37.408 and 34.181, $R^2$ values of 0.999 and 1, and qPCR amplification efficiencies of 82.7% and 96.7%, respectively. The linear range spanned 1.09 to 1.09 x $10^8$ gene copies per reaction with a calculated detection limit of 10.9 gene copies per

reaction. The genome analysis indicated that both the *Serratia* sp. and the *Desulfosporosinus* sp. genomes carry a single 16S rRNA gene, indicating that the enumeration of 16S rRNA gene allows estimates of cell abundances. The 16S rRNA gene sequences of the *Serratia* sp. and the *Desulfosporosinus* sp. are available under NCBI accession numbers OR076433 and OR076434, respectively.

**Nutritional interactions in the co-culture**

To explore the nutritional requirements of the *Desulfosporosinus* sp., a time series metabolome analysis of culture supernatant was conducted. Briefly, the axenic *Serratia* sp. culture was grown in basal salt medium amended with 2.5 mM pyruvate, 4.16 mM (nominal) $H_2$, and 4.16 mM (nominal) $N_2O$. Following a 7-day incubation period, during which pyruvate was completely consumed, the bottles received 1% (v/v) co-culture EV inoculum. Cell suspension aliquots (1.5 mL) were collected and centrifuged, and the resulting cell-free supernatants were transferred to 2 mL plastic tubes and immediately stored at –80 ºC for metabolome analysis. Additional samples assessed the metabolome associated with supernatant of axenic *Serratia* sp. cultures that received 1 mM DTT instead of l-cysteine as reductant. The results of the metabolome analysis guided additional cultivation experiments with amino acid mixtures replacing pyruvate. The 100-fold concentrated, aqueous 15-amino acid stock solution contained (g $L^{-1}$): alanine (0.5); aspartic acid (1); proline (1); tyrosine (0.3); histidine (0.3); tryptophan (0.2); arginine (0.5); isoleucine (0.5); methionine (0.4); glycine (0.3); threonine (0.5); valine (0.9); lysine (1); glutamate (1); serine (0.8). The aqueous stock solution was filter-sterilized and stored in the dark.

**Metagenome sequencing**

DNA was isolated from the axenic *Serratia* sp. culture grown with 2.5 mM pyruvate, and the $N_2O$-reducing 15$^{th}$ generation co-culture EV grown on $H_2$, $N_2O$, and the amino acid mixture. Metagenome sequencing was performed at the University of Tennessee Genomics Core using the Illumina NovaSeq 6000 platform. Shotgun sequencing

generated a total of 494 and 387 Gbp of raw sequences from the axenic *Serratia* sp. culture and co-culture EV. Metagenomic short reads were processed using the nf-core/mag pipeline (77). Short read quality was evaluated with FastQC v0.11.9, followed by quality filtering and Illumina adapter removal using fastp v0.20.1 (78). Short reads mapped to the PhiX genome (GCA_002596845.1, ASM259684v1) with Bowtie2 v2.4.2 were removed (79). Assembly of processed short reads used Megahit2 v1.2.9 (80). Binning of assembled contigs was conducted with MetaBAT2 v2.15 based on the sequencing depth (81), and metagenome-assembled genomes (MAGs) that passed CheckM (82) were selected for further analysis. Protein-coding sequences on MAGs were predicted using MetaGeneMark-2 (83) and functional annotation used Blastp (84) against the Swiss-Prot database (85), KEGG (86) and the RAST server (87). Amino acid biosynthesis completeness was evaluated using KofamKOALA (86).

Metagenomic datasets of El Verde soil and a 15$^{th}$ transfer culture were searched against the '*Ca*. Desulfosporosinus nitrousreducens' strain PR MAG using blastn (84). The best hits were extracted using an in-house script embedded in Enveomics Collection tools (88). Graphical representation showing short reads recruited to the '*Ca.* Desulfosporosinus nitrousreducens' strain PR MAG was generated with BlasTab.recplot2.R. The coverage evenness was assessed based on distribution of high nucleotide identity reads across the reference genome sequences. Nonpareil v3.4.1 using the weighted NL2SOL algorithm was used to estimate the average coverage level of the metagenomic datasets (89). Metagenome data of the original El Verde soil was downloaded from NCBI (accession number PRJEB26500). Metagenomic datasets of co-culture EV and axenic *Serratia* isolate were deposited at NCBI under accession numbers SRR24709127 and SRR24709126, respectively (Table 2-2).

**Comparative analysis of nos gene clusters**

Available genomes of select $N_2O$ reducers were downloaded from NCBI (Table 2-3). Functional annotation of the genomes was conducted using the RAST server. Transmembrane topology of the protein encoded by *nosB*, a gene located immediately

adjacent to *nosZ* was confirmed using DeepTMHMM (90). Accessory genes associated with NosZ functionality were selected from a set of seven genomes and used as PSI-BLAST database to query accessory genes on contigs predicted to harbor *nosZ* on the '*Ca.* Desulfosporosinus nitrousreducens' strain PR genome. The *nos* gene clusters were visualized using the gggenes package (https://wilkox.org/gggenes/index.html).

**Phylogenomic analysis**

Phylogenomic reconstruction was performed with genomes of the *Desulfitobacteriaceae* family available in the NCBI database (Table 2-4). Conserved marker genes of the 20 genomes were identified and aligned with GTDB-TK (91). Phylogenetic relationships were inferred based on the alignment of 120 concatenated bacterial marker genes using RAxML-NG (92) with 1,000 bootstrap replicates. A best fit evolutionary model was selected based on the result of Modeltest-NG (93). Calculation of average amino acid identity (AAI) and hierarchical clustering of taxa based on AAI values were conducted with EzAAI (94). Tree annotation and visualization were performed with the ggtree package (95).

**NosZ phylogenetic analysis**

NosZ reference sequences were downloaded from pre-compiled models of ROCker (96). The NosZ sequence of 'Ca. Desulfosporosinus nitrousreducens' strain PR was aligned to the NosZ reference sequences using MAFFT (97), and a maximum likelihood tree was created with RAxML-NG based on the best model from Modeltest-NG. The inferred tree and amino acid identity between '*Ca.* Desulfosporosinus nitrousreducens' strain PR, *Desulfosporosinus meridiei* and the NosZ reference sequences were visualized using ggtree package.

**Metabolome analysis**

Cell-free samples were prepared as described (98). Briefly, 1.5 mL of 0.1 M formic acid in 4:4:2 (v:v:v) acetonitrile:water:methanol was added to 100 µL aliquots of supernatant

samples. The tubes were shaken at 4°C for 20 minutes and centrifuged at 16,200 x g for 5 minutes. The supernatant was collected and dried under a steady stream of $N_2$. The dried extracts were suspended in 300 µL of water prior to analysis. For water soluble metabolites, the mass analysis was performed in untargeted mode (99). The chromatographic separations utilized a Synergi 2.6 µm Hydro RP column (100 Å, 100 mm x 2.1 mm; Phenomenex, Torrance, CA) with tributylamine as an ion pairing reagent, an UltiMate 3000 binary pump (Thermo Scientific, San Jose, CA), and previously described elution conditions (98). The mass analysis was carried out using an Exactive Plus Orbitrap MS (Thermo Scientific) using negative electrospray ionization and full scan mode. Following the analysis, metabolites were identified using exact masses and retention times, and the areas under the curves (AUC) for each chromatographic peak were integrated using the open-source software package Metabolomic Analysis and Visualization Engine (99, 100). Dynamic changes of metabolites over time were assessed by comparative analysis of AUC values.

**Phenotypic characterization of co-culture EV**

To test for autotrophic growth of co-culture EV, pyruvate was replaced by 5 mL (2.08 mM nominal) of $CO_2$ (99.5% purity). All experiments used triplicate cultures, and vessels without pyruvate, without $H_2$, without $N_2O$, or without inoculum served as controls. Growth experiments were conducted to determine the responses of the *Serratia* sp. and the *Desulfosporosinus* sp. to pH. Desired medium pH values of 3.5, 4.5, 5, 6, 7 and 8 were achieved by adjusting the mixing ratios of $KH_2PO_4$ and $K_2HPO_4$. To achieve pH 3.5, the pH 4.5 medium was adjusted with 5 M hydrochloric acid. The medium with different pH, 3.5, 4.5, 5, 6, 7 and 8, was achieved by adjusting the mix ratios of $KH_2PO_4$ and $K_2HPO_4$. Replicate incubation vessels received 4.16 mM (nominal) $N_2O$ and 4.16 mM $H_2$ (nominal), and 2.5 mM pyruvate, following an overnight equilibration period, 1% inocula from the axenic *Serratia* sp. culture or the $N_2O$-reducing co-culture EV, both pregrown in pH 4.5 medium. The replicate cultures inoculated with the *Serratia* sp. were incubated for 14-days, after which three vessels received an inoculum of co-culture EV (1%) to initiate $N_2O$ consumption. Three *Serratia* sp. cultures not receiving a co-culture

EV inoculum served as controls. Consumption rates of pyruvate and $N_2O$ were calculated based on data points representing linear ranges of consumption according to

$$V = \frac{N}{T_1 - T_0}$$

Equation 1

where V represent the consumption rate; N represent the initial amounts of pyruvate or $N_2O$. $T_1$ refers to timepoints when pyruvate or $N_2O$ were completely consumed. $T_0$ for pyruvate consumption refers to day zero (i.e., after inoculation with axenic *Serratia* sp.). $T_0$ for $N_2O$ consumption refers to day 14 (i.e., after inoculation with co-culture EV), following which a linear $N_2O$ consumption was observed.

**Analytical procedures**

$N_2O$, $CO_2$, and $H_2$ were analyzed by manually injecting 100 µL headspace samples manually injected into an Agilent 3000A Micro-Gas Chromatograph (Palo Alto, CA, USA) equipped with Plot Q and molecular sieve columns coupled with a thermal conductivity detector as described (101). Aqueous concentrations (µM) were calculated from the headspace partial pressures based on reported dimensionless Henry's law constants for $N_2O$ ($2.4\times10^{-4}$), $H_2$ ($7.8\times10^{-6}$) and $CO_2$ ($3.3\times10^{-4}$) (102) according to

$$HRT = \frac{C_g}{C_{aq}}$$

Equation 2

Where $H$ = Henry's law constants, $R$ = universal gas constant, $T$ = temperature, $C_g$ = headspace gas-phase concentration and $C_{aq}$ = liquid-phase (dissolved) concentration. Five-point standard curves for $N_2O$, $CO_2$ and $H_2$ spanned concentration ranges of 8,333 to 133,333 ppmv. Pyruvate, acetate and formate were measured with an Agilent 1200 Series high-performance liquid chromatography (HPLC) system (Palo Alto, CA, USA) as described (101). pH was measured in 0.4 mL samples of culture supernatant following removal of cells by centrifugation with a pH electrode.

## 2.3 Results

### A consortium consisting of two populations reduces $N_2O$ at pH 4.5

Microcosms established with El Verde tropical soil amended with lactate consumed $N_2O$ at pH 4.5; however, this activity was lost in transfer cultures amended with the same electron donor. The addition of acetate, formate (1 or 5 mM each), and $CO_2$ (208 µmol, 2.08 mM nominal), propionate (5 mM), or yeast extract (0.10 – 10 g $L^{-1}$) did not stimulate $N_2O$ reduction in pH 4.5 transfer cultures. Limited $N_2O$ consumption was observed in transfer cultures amended with 2.5 mM pyruvate, but complete removal of $N_2O$ required the addition of $H_2$ or formate. In transfer cultures with $H_2$ or formate, but lacking pyruvate, $N_2O$ was not consumed. Subsequent transfers in completely synthetic basal salt medium amended with both pyruvate and $H_2$ yielded a robust enrichment culture, which consumes $N_2O$ at pH 4.5 (Figure 2-1 A). Phenotypic characterization illustrated that pyruvate utilization was independent of $N_2O$, while $N_2O$ reduction only commenced following complete consumption of pyruvate.

Cultivation experiments were performed in 160 mL glass serum bottles containing 100 mL of defined basal salt medium. The consortium consumed 239 ± 1.16 µmol pyruvate within 7 days (Phase I) in the presence or absence of $N_2O$, and acetate (136 ± 6.05 µmol), formate (58.5 ± 3.33 µmol) and $CO_2$ (201 ± 5.53 µmol) were produced (Supplementary Figure 2-1 A). In cultures without $N_2O$, formate was stable but was readily consumed when cultures were supplemented with $N_2O$ (Supplementary Figure 2-1 A, C, E). Measurable acetate consumption did not occur in any of the vessels indicating that acetate is not an electron donor for $N_2O$ reduction (Supplementary Figure 2-1 A, C, E).

In vessels that received pyruvate, $H_2$, and $N_2O$, $H_2$ and $N_2O$ were simultaneously consumed following the depletion of pyruvate (day 10, Supplementary Figure 2-1 B). $N_2O$ consumption (Phase II) continued until $H_2$ became limiting but resumed when additional $H_2$ was provided (day 33, Supplementary Figure 2-1 B). In cultures lacking $N_2O$, $H_2$ was stable, but consumption commenced immediately following the addition of

$N_2O$ (Supplementary Figure 2-1 D). In replicate vessels without $H_2$, $N_2O$ was consumed after day 10, apparently coupled to the oxidation of formate, a product of pyruvate fermentation (Supplementary Figure 2-1 E, F). Pyruvate consumption (Phase I) and the production of formate, acetate and $CO_2$ as fermentation products preceded measurable consumption of $N_2O$ and $H_2$ (or formate) (Phase II), suggesting that pyruvate was not a direct electron donor for $N_2O$ reduction (Supplementary Figure 2-1 A-F). Following an 18-day incubation period, triplicate cultures that received pyruvate (239 ± 1.16 µmol), $H_2$ (390 ± 1.66 µmol), and $N_2O$ (378 ± 11.7 µmol) had completely consumed $N_2O$ and nearly half of the exogenously added $H_2$ (143 ± 8.96 µmol) (Supplementary Figure 2-1 B). Reduction of one molecule $N_2O$ requires two electrons derived from the oxidation of one molecule of $H_2$ (i.e., $H_2 + N_2O \rightarrow H_2O + N_2$). The amount of $H_2$ oxidized did not reach the expected 1:1 stoichiometry, indicating that products from pyruvate fermentation (e.g., formate) serve as electron donors for $N_2O$ reduction. Consistently, in cultures that received a low amount of pyruvate (i.e., 50 µmol), $H_2$ oxidation (361.2 ± 5.68 µmol) closely matched the amount of $N_2O$ reduced (377 ± 3.53 µmol) (Supplementary Figure 2-1 G). Pyruvate, $H_2$, and $N_2O$ consumption were not apparent in vessels without inoculum (Supplementary Figure 2-1 H). No growth occurred in cultures where $CO_2$ replaced pyruvate, suggesting no autotrophic activity (Supplementary Figure 2-1 I).

The fermentation of pyruvate resulted in pH increases, with the magnitude of the medium pH change proportional to the initial pyruvate concentration. The amount of pyruvate did not exceed 250 µmol per 100 mL of medium (i.e., 2.5 mM), which limited the pH increase following complete pyruvate fermentation to 0.53 ± 0.03 pH units (Supplementary Figure 2-2). $N_2O$ reduction was also observed in cultures that received 5 mM glucose. $N_2O$ reduction was oxygen sensitive and $N_2O$ was not consumed in medium without reductant (i.e., cysteine, dithiothreitol).

Microbial profiling of El Verde soil and solids-free transfer cultures documented effective enrichment in defined pH 4.5 medium amended with pyruvate, $H_2$, and $N_2O$ (Figure 2-1 B). Shotgun metagenome sequencing performed on the original El Verde soil recovered 2,718 short read fragments (150 bp) representing 16S rRNA genes, which

could be assigned to 187 bacterial genera (43). 16S rRNA gene fragments representing uncultured microbes, or not assigned to known genera in the El Verde soil sequence pools, accounted for 33.1% and 27.3% of the total 16S rRNA gene fragments, respectively. The remaining 16S rRNA gene fragments were assigned to *Acidothermus* (3.1%), '*Ca.* Solibacter' (2.0%) and '*Ca.* Udaeobacter' (7.4%). Taxa with less than 2% representation in the sequence pools are grouped as 'Others' and accounted for 27% of the 16S rRNA gene fragments. Following six consecutive transfers (3%, v/v) of the El Verde soil microcosm in defined basal salt medium amended with pyruvate, $H_2$, and $N_2O$, all 16S rRNA amplicon sequences could be assigned to *Serratia* (68.0%), *Desulfosporosinus* (24.3%), *Desufitobacterium* (7.5%), *Caproiciproducens* (0.19%), *Peptoclostridium* (<0.05%) and *Lachnoclostridium* (<0.05%). Following nine consecutive transfers, *Serratia* and *Desulfosporosinus* each contributed about half of the 16S rRNA amplicon sequences (49.7% and 50.2%, respectively), and less than 0.05% of the sequences represented *Planctomycetota*, *Lachnoclostridium*, *Caproiciproducens*.

Following fifteen sequential transfers in the same medium reduced the microbial diversity to two populations, a *Serratia* sp. and *Desulfosporosinus* sp. In 16S rRNA gene clone libraries generated with DNA collected during Phase II from a 15$^{th}$ generation transfer culture, Sanger sequencing revealed 16S rRNA genes matching those of the *Serratia* sp. and *Desulfosporosinus* sp., and no other sequences were found. Deep metagenome sequencing (total of 387 Gbp obtained) yielded a 2,865-fold coverage of the *Serratia* sp. genome and 15,103-fold coverage of the *Desulfosporosinus* sp. genome (Supplementary Figure 2-3), and 99.48% of the short read sequences could be mapped to the contigs representing these two genomes. Of note, the *Serratia* genomes constructed from co-culture EV and the axenic *Serratia* culture were nearly identical (ANI 99.9%), suggesting the sequencing depth was sufficient to study the genomic characteristics in the co-culture. The assembly of 16S rRNA gene fragments generated eight partial and two complete 16S rRNA genes, which shared between 91.1 to 99.5% sequence identity to the respective *Serratia* sp. and *Desulfosporosinus* sp. 16S rRNA gene sequences determined by Sanger sequencing (Supplementary Figure 2-4). Both genomes possess a single 16S

rRNA gene, and the observed differences in 16S rRNA sequences were attributed to errors associated with short read assembly and sequencing. Phase contrast microscopy performed with co-culture EV suspension samples collected during Phase I and Phase II revealed the presence of the reported *Serratia* sp. (103) and the *Desulfosporosinus* sp. cell morphologies (104). Taken together, these observations support that 15 consecutive transfers yielded a consortium (i.e., a co-culture) comprising two bacterial populations, a *Serratia* sp. and a *Desulfosporosinus* sp. Deep shotgun metagenome sequencing performed on a $15^{th}$ transfer culture recovered two draft genomes representing the *Serratia* sp. and the *Desulfosporosinus* sp., accounting for more than 95% of the total short read fragments. All 16S rRNA genes associated with assembled contigs could be assigned to *Serratia* or *Desulfosporosinus* (Supplementary Figure 2-4), indicating that the enrichment process yielded a consortium consisting of a *Serratia* sp. and a *Desulfosporosinus* sp., designated co-culture EV. Efforts to recover the *Serratia* and *Desulfosporosinus* genomes from the original soil metagenome data sets via recruiting the soil metagenome fragments to the two genomes (Figure 2-1 C) were not successful, highlighting the effectiveness of the enrichment strategy. Redundancy-based analysis with Nonpareil (89) revealed that the average covered species richness in the metagenome data set obtained from the $15^{th}$ transfer culture was 99.9%, much higher than what was achieved for the El Verde soil (39.5%), suggesting the metagenome analysis of the original soil did not fully capture the resident microbial diversity.

The application of 16S rRNA gene-targeted qPCR assays to DNA extracted from $9^{th}$ transfer $N_2O$-reducing cultures revealed a bimodal growth pattern. During pyruvate fermentation (Phase I), the *Serratia* cell numbers increased nearly 1,000-fold from $(2.3 \pm 0.8) \times 10^2$ to $(1.8 \pm 0.2) \times 10^5$ cells $mL^{-1}$, followed by a 40-fold increase from $(3.5 \pm 1.5) \times 10^4$ to $(1.2 \pm 0.4) \times 10^6$ cells $mL^{-1}$ of *Desulfosporosinus* cells during $N_2O$ reduction (Phase II) (Figure 2-1 D). In vessels without $N_2O$, *Desulfosporosinus* cell numbers did not increase, indicating that growth of this population depended on the presence of $N_2O$. Growth yields of $(3.1 \pm 0.11) \times 10^8$ cells $mmol^{-1}$ of $N_2O$ and $(7.0 \pm 0.72) \times 10^7$ cells $mmol^{-1}$ of pyruvate were determined for the *Desulfosporosinus* and the *Serratia*

populations, respectively. 16S rRNA gene amplicon sequencing performed on representative samples collected at the end of Phase I (day 7) and Phase II (day 18) confirmed a bimodal growth pattern. Sequences representing *Serratia* increased during Phase I and *Desulfosporosinus* sequences increased during Phase II (Figure 2-1 E). Taken together, the physiological characterization, qPCR, genomic, and amplicon sequencing results indicate that co-culture EV performs low pH $N_2O$ reduction, with a *Serratia* sp. fermenting pyruvate and a *Desulfosporosinus* sp. reducing $N_2O$. Isolation efforts yielded an axenic *Serratia* sp., designated strain MF, capable of pyruvate fermentation. Despite extensive efforts, the *Desulfosporosinus* sp. resisted isolation, presumably due to auxotrophic interactions with strain MF (Supplementary Figure 2-5).

**Isolation efforts**

Numerous attempts were made to isolate the $N_2O$-reducing *Desulfosporosinus* sp. from co-culture EV. Serial 10-fold dilution-to-extinction series in pH 4.5 basal salt liquid medium amended with 2.5 mM pyruvate, 4.16 mM (nominal) $N_2O$, and 4.16 mM (nominal) $H_2$ recovered $N_2O$ reduction activity from $10^{-6}$ dilution vials; however, the *Serratia* sp. was also present. The omission of pyruvate prevented growth of the *Serratia* sp. but without pyruvate, $N_2O$ consumption did not commence. Plating of serially diluted culture suspension aliquots on solid Tryptic Soy Agar (TSA) medium yielded uniform colonies. Sanger sequencing of PCR-amplified 16S rRNA genes of four isolated colonies from a $10^{-6}$ dilution plate yielded identical sequences with 100% sequence identity to the *Serratia* sp. Microscopic analysis revealed motile, short rods about 2 µm long representing *Serratia* cells that grew readily in Tryptic Soy Broth medium. Growth also occurred in defined basal salt pH 4.5 medium amended with pyruvate, but the *Serratia* sp. did not consume $H_2$ or $N_2O$. Following complete $N_2O$ consumption in co-cultures grown with 2.4 ± 0.01 mM pyruvate, 4.06 ± 1.16 mM (nominal) of $H_2$, and 3.96 ± 1.08 mM (nominal) of $N_2O$, *Desulfosporosinus* cells outnumbered *Serratia* cells approximately 5-fold. Microscopic observations also documented this population shift and *Desulfosporosinus* cells (motile rods about 6 µm in length) dominated the cell suspensions following $N_2O$ consumption. Attempts to obtain isolated colonies of the

*Desulfosporosinus* sp. in soft agar (0.8% low melting agarose, w/v) shake tubes were not productive because the reduction of $N_2O$ generated $N_2$ gas bubbles preventing the recovery of isolated colonies (Supplementary Figure 2-5). Despite extensive efforts, the *Desulfosporosinus* sp. could not be separated from the *Serratia* sp.

**Identification of auxotrophies**

To investigate the specific nutritional requirements of the *Desulfosporosinus* sp. in co-culture EV, untargeted metabolome analysis was conducted on supernatant collected from axenic *Serratia* sp. cultures growing with pyruvate and during $N_2O$ consumption (Phase II) following inoculation with co-culture EV (Figure 2-2 A). Peaks representing potential metabolites were searched against a custom library and 33 features were assigned to known structures, including seven amino acids (alanine, glutamate, methionine, valine, leucine, aspartate, and tyrosine). Cystine, the oxidized derivative of the amino acid cysteine, was also detected; however, cystine or cysteine were not found in cultures where dithiothreitol (DTT) replaced cysteine as the reductant, suggesting that *Serratia* did not excrete either compound into the culture supernatant. Time series metabolome analysis of culture supernatant demonstrated dynamic changes to the amino acid profile following inoculation with the *Serratia* sp. and the *Desulfosporosinus* sp. (as co-culture EV) (Figure 2-2 A, B). Alanine, valine, leucine, and aspartate increased during pyruvate fermentation (Phase I) and were not consumed by the *Serratia* sp. (Supplementary Figure 2-6). Consumption of alanine, valine, leucine, and aspartate did occur following the inoculation of the *Desulfosporosinus* sp. (as co-culture EV) (Figure 2-2 A). These findings suggest that the $N_2O$-reducing *Desulfosporosinus* sp. is an amino acid auxotroph, and a series of growth experiments explored if amino acid supplementation (Table 2-5) can replace the requirement for pyruvate fermentation by the *Serratia* sp. for enabling subsequent $N_2O$ consumption by the *Desulfosporosinus* sp. The addition of individual amino acids (n=20) was not sufficient to initiate $N_2O$ reduction in pH 4.5 medium, as was the combination of alanine, valine, leucine, aspartate, and tyrosine. Incomplete $N_2O$ consumption (<20% of initial dose) was observed in cultures supplemented with the aforementioned amino acid combination plus methionine. $N_2O$

reduction and growth of the *Desulfosporosinus* sp. occurred without delay in cultures supplied with a 15-amino acid mixture (Figure 2-2 C). Omission of single amino acids from the 15-amino acid mixture led to incomplete $N_2O$ reduction, similar to what was observed with the 6-amino acid combination. Efforts to isolate the *Desulfosporosinus* sp. in medium without pyruvate but amended with amino acids were unsuccessful because of concomitant growth of the *Serratia* sp., as verified with qPCR.

**pH range of acidophilic $N_2O$ reduction by the *Desulfosporosinus* sp**

Growth assays with co-culture EV were performed to determine the pH range for $N_2O$ reduction. Co-culture EV reduced $N_2O$ at pH 4.5, 5.0 and 6.0, but not at pH 3.5, 7.0 and 8.0. Cultures at pH 4.5 exhibited about two times longer (i.e., 10 versus 5 days) lag periods prior to the onset of $N_2O$ consumption than cultures incubated at pH 5.0 or 6.0 (Supplementary Figure 2-7 A). In medium without amino acid supplementation, pyruvate fermentation is required for the initiation of $N_2O$ consumption, raising the question if pH impacts pyruvate fermentation by the *Serratia* sp., $N_2O$ reduction by the *Desulfosporosinus* sp., or both processes. Axenic *Serratia* sp. cultures fermented pyruvate over a pH range of 4.5 to 8.0, with the highest pyruvate consumption rates observed at pH 6.0 and 7.0 ($1.47 \pm 0.04$ mmol $L^{-1}$ $day^{-1}$), and the lowest rates measured at pH 4.5 ($0.43 \pm 0.05$ mmol $L^{-1}$ $day^{-1}$) (Supplementary Figure 2-7 B). The $N_2O$ consumption rates in co-culture EV between pH 4.5 to 6.0 ranged from $0.24 \pm 0.01$ to $0.26 \pm 0.01$ mmol $L^{-1}$ $day^{-1}$ (Supplementary Figure 2-7 C). Since $N_2O$ reduction in the absence of amino acids only commenced following pyruvate consumption (Figure 2-1 C), pyruvate fermentation by *Serratia* sp., not $N_2O$ reduction by *Desulfosporosinus* sp., explains the extended lag periods observed at pH 4.5 (Supplementary Figure 2-7 A). Consistently, shorter lag phase for both $N_2O$ reduction and *Desulfosporosinus* growth were observed in co-culture EV amended with the amino acid mixture (Figure 2-2 C).

## Phylogenomic analysis

Phylogenomic reconstruction based on concatenated alignment of 120 bacterial marker genes corroborated the affiliation of the $N_2O$-reducing bacterium with the genus *Desulfosporosinus* (Figure 2-3). The genus *Desulfosporosinus* comprises strictly anaerobic, sulfate-reducing bacteria, and *Desulfosporosinus acididurans* strain SJ4 and *Desulfosporosinus acidiphilus* strain M1 were characterized as acidophilic sulfate reducers. The $N_2O$-reducing *Desulfosporosinsus* sp. in co-culture EV possesses the *aprAB* and *dsrAB* genes encoding adenylyl sulfate reductase and dissimilatory sulfate reductase, respectively, but lacks the *sat* gene encoding sulfate adenylyl transferase sulfurylase (Supplementary Figure 2-8).

To provide experimental evidence that the $N_2O$-reducing *Desulfosporosinus* sp. in co-culture EV lacks the ability to reduce sulfate, a hallmark feature of the genus *Desulfosporosinus*, comparative growth studies were performed. The $N_2O$-reducing *Desulfosporosinsus* sp. in co-culture EV did not grow with sulfate as sole electron acceptor, consistent with an incomplete dissimilatory sulfate reduction pathway (Supplementary Figure 2-9 A). *Desulfosporosinus acididurans* strain D (104), a close relative of the $N_2O$-reducing *Desulfosporosinus* sp. in co-culture EV, grew with sulfate in pH 5.5 medium, but did not grow with $N_2O$ under the same incubation conditions (Supplementary Figure 2-9 B). These observations corroborate that the $N_2O$-reducing *Desulfosporosinus* sp. lacks the ability to perform dissimilatory sulfate reduction. Based on phylogenetic and physiologic features, the $N_2O$-reducer in culture EV represents a novel *Desulfosporosinus* sp., for which the name '*Candidatus* Desulfosporosinus nitrousreducens' strain PR is proposed.

## Genetic underpinning of $N_2O$ reduction in 'Ca. Desulfosporosinus nitrousreducens' strain PR

The strain PR genome harbors a single *nosZ* gene affiliated with clade II *nosZ* sequences (Figure 2-3). Independent branch placement of the strain PR NosZ on the clade II NosZ tree suggests an ancient divergence; a finding supported by amino acid identity (AI) value comparisons between the NosZ sequences versus their homologs in the genomes of

‘*Ca.* Desulfosporosinus nitrousreducens’ strain PR and *Desulfosporosinus meridiei* (AI: 44% versus 73.83%) (Figure 2-3 and

Figure 2-4 B). The NosZ of ‘*Ca.* Desulfosporosinus nitrousreducens’ strain PR is more similar (AI: 45%) to the taxonomically distant relative *Desulfotomaculum ruminis*.

Comparative analysis of the strain PR *nos* operon with bacterial and archaeal counterparts corroborated characteristic clade II features, including a Sec translocation system, genes encoding cytochromes and an iron-sulfur protein, and a *nosB* gene located immediately downstream of *nosZ* (Figure 2-5). *nosB* encodes a transmembrane protein of unknown function and has been exclusively found on clade II *nos* operons. The *nos* gene clusters found in closely related taxa (e.g., *Desulfosporosinus meridiei*, *Desulfitobacterium dichloroeliminans*, *Desulfitobacterium hafniense*) show similar organization; however, differences were observed in the *nos* gene cluster of ‘Ca. Desulfosporosinus nitrousreducens’ strain PR. Specifically, the genes encoding an iron-sulfur cluster protein and cytochromes precede *nosZ* in *Desulfosporosinus meridiei*, but are located downstream of two genes encoding proteins of unknown functions in strain PR (Figure 2-5). Of note, among the microbes with *nos* operons and included in the analyses, only ‘*Ca.* Desulfosporosinus nitrousreducens’ and *Nitratiruptor labii* (105), both with a clade II *nos* operon, were experimentally validated to grow with $N_2O$ below pH 6 (Table 2-3).

**Genomic insights for a commensalistic relationship**

Functional annotation of the *Serratia* sp. and the ‘*Ca*. Desulfosporosinus nitrousreducens’ strain PR genomes was conducted to investigate the interspecies interactions (Figure 2-6). A *ptsT* gene encoding a specific, high-affinity pyruvate/proton symporter (106) and genes implicated in pyruvate fermentation (i.e., *pflAB*, *poxB*) are present on the *Serratia* genome, but are missing on the strain PR genome, consistent with the physiological characterization results. *fdhC* genes encoding a formate transporter are present on both genomes, but only the strain PR genome harbors the *fdh* gene cluster encoding a formate dehydrogenase complex (Supplementary Figure 2-8), consistent with the observation that the *Serratia* sp. excretes formate, which strain PR utilizes as electron donor for $N_2O$

reduction (Supplementary Figure 2-1). Gene clusters encoding two different Ni/Fe-type hydrogenases (i.e., *hyp* and hya gene *clusters*) (Supplementary Figure 2-8) and a complete *nos* gene cluster (Figure 2-5) are present on the strain PR genome, but not on the *Serratia* sp. genome.

Based on the KEGG (86) and Uni-Prot databases (85), the *Serratia* genome contains the biosynthesis pathways (100% completeness) for aspartate, lysine, threonine, tryptophan, isoleucine, serine, leucine, valine, glutamate, arginine, proline, methionine, tyrosine, cysteine, and histidine. In contrast, only aspartate and glutamate biosynthesis are predicted to be complete on the strain PR genome, whereas the completeness level for biosynthesis pathways of other amino acids was below 80%. The *Serratia* genome encodes a complete set of TCA cycle enzymes, indicating the potential for forming aspartate and glutamate via transamination of oxaloacetate and α-ketoglutarate. In contrast, the strain PR genome lacks genes encoding malate dehydrogenase, citrate synthase, and aconitate hydratase, indicative of an incomplete TCA cycle. Therefore, strain PR is deficient of *de novo* formation of precursors for glutamate, aspartate, alanine, and related amino acids (107). A high-affinity amino acid transport system was found on the strain PR genome (Supplementary Figure 2-8), suggesting this bacterium can efficiently acquire extracellular amino acids to meet its nutritional requirements.

**Distribution of the novel $N_2O$ reducer in soil metagenomes**

For estimating the distribution of the *Serratia* sp. and '*Ca*. Desulfosporosinus nitrousreducens' strain PR in acidic and some circumneutral pH soils, fragments of soil metagenomes (n=195) from a prior study (29) were aligned to the *Serratia* sp. strain MF and the '*Ca*. Desulfosporosinus nitrousreducens' strain PR genomes (Supplementary Figure 2-10 A). The percentage of metagenome fragments that aligned to strain MF and strain PR ranged between 0.11-1.15% and 0.039-0.094%, respectively. RandomForest analysis revealed weak relationships between the presence of '*Ca*. Desulfosporosinus nitrousreducens' strain PR and soil C/N ratio, pH, and $NH_4^+$ content. In contrast, *Serratia* sp. strain MF showed the strongest relationship to '*Ca*. Desulfosporosinus

nitrousreducens' strain PR, explaining 32.6% of the variability of strain PR abundance in the metagenomes included in the analysis (Supplementary Figure 2-10 B). Furthermore, the relative abundances of the two populations showed a positive correlation (Supplementary Figure 2-10 C), suggesting the observed commensalistic relationship may not have coincidentally developed in co-culture EV, and possibly occurs in soil habitats. Soil organic matter ($r = -0.35$, $p < 0.01$) and $NO_3^-$ ($r = -0.31$, $p < 0.01$) content strongly correlated with the presence of '*Ca*. Desulfosporosinus nitrousreducens' strain PR.

## 2.4 Discussion

Biological processes fix about 180 Tg N per year (108) and conventional agriculture introduces more than 100 Tg N of chemically fixed N each year (109). Biogeochemical cycling converts a substantial fraction of fixed N to $N_2O$, and rising atmospheric $N_2O$ concentrations indicate that $N_2O$ sources outpace microbial $N_2O$ sinks. Soil acidification is a major concern relevant to N cycling and $N_2O$ emissions. Microbial processes (e.g., nitrification and denitrification) involved in $N_2O$ production have been reported to cause greater $N_2O$ emissions at pH < 6 than at circumneutral pH (31, 41). In contrast, characterized $N_2O$ reducers from soil habitats consume $N_2O$ within a narrow pH window ranging from 6 to 8 with generally weak activity approaching pH 6.0 and no activity at lower pH (38, 39, 110, 111). Interestingly, metagenomic studies revealed that acidic Luquillo Experimental Forest (Puerto Rico) tropical soils and temperate circumneutral pH soils harbor a comparable diversity of *nosZ* genes (43), and that pH selects for different $N_2O$ reducers in Luquillo tropical soil microcosms (44).

A few studies reported limited $N_2O$ reduction activity in acidic microcosms, but enrichment cultures for detailed experimentation were not obtained (41, 57, 112). Possible explanations for the observed $N_2O$ consumption in acidic microcosms include residual activity of existing $N_2O$-reducing biomass, or the presence of microsites on soil particles where solid phase properties influence local pH, generating pH conditions not captured by bulk aqueous phase pH measurements (113, 114). Soil microcosms providing

microsites with favorable (i.e., higher) pH conditions can give the false impression of low pH $N_2O$ consumption; however, removal of solids during transfers eliminates this niche and microorganisms experience bulk phase pH conditions, resulting in the cessation of $N_2O$ reduction activity. Our work with acidic tropical soils alludes to another crucial issue, explicitly the choice of carbon source for the successful transition from microcosms to soil-free enrichment cultures. Lactate sustained $N_2O$ reduction in pH 4.5 Luquillo tropical soil microcosms, but transfer cultures commenced $N_2O$ reduction only when pyruvate substituted lactate. Lactate has a higher p$K_a$ value than pyruvate (3.8 versus 2.45), indicating that a larger fraction of protonated, and potentially toxic, lactic acid exists at pH 4.5 (115). As discussed above, in soil microcosms, particles with ion exchange capacity (i.e., microsites) can suppress inhibitory effects of protonated organic acids, a possible explanation why lactate supported $N_2O$ reduction in the microcosms but not in the enrichment cultures.

Fifteen repeated transfers with $N_2O$, pyruvate, and $H_2$ yielded a co-culture comprising a *Serratia* sp. and a *Desulfosporosinus* sp. The rapid enrichment of a co-culture may be surprising considering that pyruvate and $H_2$ are excellent substrates for many soil microbes. $N_2O$ was the sole electron acceptor provided to the defined basal salt medium, with some $CO_2$ being formed during pyruvate fermentation (Phase I); however, no evidence was obtained for $H_2$-driven $CO_2$ reduction to acetate or to methane. $N_2O$ has been recognized as potent inhibitor of corrinoid-dependent enzyme systems (55, 56), and both $CO_2/H_2$ reductive acetogenesis and hydrogenotrophic methanogenesis would not be expected to occur in the enrichment cultures, a prediction supported by the analytical measurements.

Available axenic and mixed cultures obtained from circumneutral pH soils reduce $N_2O$ at circumneutral pH, but not below pH 6.0 (36, 39, 116). The discovery and cultivation of co-culture EV comprising '*Ca.* Desulfosporosinus nitrousreducens' strain PR extends the pH range for microbial growth with $N_2O$ as electron acceptor to pH 4.5. Metagenomic studies routinely detect *nosZ* in acidic soils providing evidence that bacteria capable of low pH $N_2O$ reduction exists and are likely more widely distributed in acidic soil habitats

(43, 117, 118). The distribution of bacteria capable of low pH $N_2O$ reduction may extend to the deep marine biosphere, a hypothesis supported by the recent discovery of the thermophile *Nitratiruptor labii* strain HRV44 with the capacity to reduce $N_2O$ over a pH range of 5.4 to 6.4 (105).

'*Ca.* Desulfosporosinus nitrousreducens' strain PR reduces $N_2O$ between pH 4.5 and 6.0, with no $N_2O$ reduction observed at or above pH 7. This finding implies that '*Ca.* Desulfosporosinus nitrousreducens' cannot be enriched with $N_2O$ as electron acceptor at or above pH 6.5, suggesting the maintenance of acidic pH conditions during enrichment is crucial to cultivate new microorganisms capable of low pH $N_2O$ reduction. Available $N_2O$-reducing soil isolates enriched and isolated at circumneutral pH cannot grow with $N_2O$ as electron acceptor below pH 6.0. Apparently, pH selects for distinct groups of $N_2O$ reducers, with prior research mostly focused on soil isolates obtained at circumneutral pH. The discovery of '*Ca.* Desulfosporosinus nitrousreducens' strain PR lends credibility to the hypothesis that the diverse *nosZ* genes found in metagenomes of acidic soils (43) may indeed be functional. Further, the cultivation of strain PR provides a blueprint for unraveling the unknown microbiology of low pH $N_2O$ reduction and exploring the geochemical parameters that govern this process in acidic soils.

'*Ca.* Desulfosporosinus nitrousreducens' strain PR possesses a clade II *nos* operon similar to those found in clade II neutrophilic $N_2O$ reducers without distinguishing features based on gene content and *nos* operon structure (Figure 2-5). Experimental work with *Paracoccus denitrificans*, a model organism harboring a clade I *nosZ* and used for studying denitrification, has shown that acidic pH impairs $N_2O$ reductase assembly and maturation (38). NosZ is a periplasmic enzyme with a distinguishing feature of clade I versus clade II NosZ being the mechanism of protein transport across the cytoplasmic membrane. Clade II NosZ follows the general Secretion route known as Sec-pathway, which translocates unfolded proteins. In contrast, clade I NosZ are translocated in a folded state via the Twin-arginine pathway (Tat-pathway) (119). Differences exist between clade I and cade II *nos* operons, and *nosB*, encoding a transmembrane protein of unknown function, has been exclusively found associated with clade II *nos* clusters

(Figure 2-5) (12, 23). To what extent gene content and the secretion pathway influence the pH range of $N_2O$ reduction is unclear and warrants further genetic/biochemical studies. Other factors that can impact $N_2O$ reduction at acidic pH include an organism's ability to cope with the potential toxicity of protonated organic acids and maintain pH homeostasis (120, 121). The '*Ca.* Desulfosporosinus nitrousreducens' strain PR genome harbors multiple genes associated with DNA repair and potassium transport, suggesting this bacterium can respond to pH stress.

Soils harbor diverse microbiomes with intricate interaction networks that govern soil biogeochemical processes, including $N_2O$ turnover (122), and define the functional dynamics of microbiomes (123-125). Interspecies cooperation between bacteria can enhance $N_2O$ reduction via promoting electron transfer (126), the provision of essential nutrients (as demonstrated in co-culture EV), or limit $N_2O$ reduction due to competition for electron donor(s) or metal cofactors (i.e., copper) (127, 128). Metabolomic workflows unraveled that *Serratia* sp. strain MF excretes amino acids during growth with pyruvate, which '*Ca.* Desulfosporosinus nitrousreducens' strain PR requires to initiate $N_2O$ reduction, a finding supported by genome functional predictions (i.e., 15 complete AA biosynthesis pathways in strain MF versus only two complete AA biosynthesis pathways in strain PR). An amino acid mixture supported $N_2O$ reduction by strain PR in the absence of pyruvate; however, slight growth of *Serratia* sp. strain MF was observed, preventing the isolation of the $N_2O$ reducer Interspecies interactions based on amino acid auxotrophies have been implicated in shaping dynamic anaerobic microbial communities, bolster community resilience, and thus promote functional stability (123). Other microbes can potentially fulfill the nutritional demands of '*Ca.* Desulfosporosinus nitrousreducens', and the observed interrelationship between the *Serratia* sp. and strain PR might have developed coincidentally during the enrichment process; however, the co-occurrence pattern does imply some level of specificity and that the interactions may occur in situ.

Members of the genus *Desulfosporosinus* have been characterized as strictly anaerobic sulfate reducers with the capacity to grow autotrophically with $H_2$, $CO_2$, and sulfate, or,

in the absence of sulfate, with pyruvate (129). Most characterized *Desulfosporosinus* spp. show optimum growth at circumneutral pH (~7) conditions, except for the acidophilic isolates *Desulfosporosinus metallidurans*, *Desulfosporosinus acidiphilus*, *Desulfosporosinus acididurans*, and *Desulfosporosinus* sp. strain I2, which perform sulfate reduction at pH 4.0, 3.6, 3.8, and 2.6, respectively (104, 115, 130-132). Among the 10 *Desulfosporosinus* species with sequenced genomes, only *Desulfosporosinus meridiei* DSM 13257 carries a *nos* cluster (12). *Desulfosporosinus meridiei* DSM 13257 grows within a narrow range of pH 6-8 (129), and its ability to reduce $N_2O$ has not been demonstrated. '*Ca.* Desulfosporosinus nitrousreducens' strain PR lacks the hallmark feature of sulfate reduction and is the first acidophilic soil bacterium capable of growth with $N_2O$ as electron acceptor at pH 4.5, but not at pH 7 or above. Strain PR couples $N_2O$ reduction and growth at pH 4.5 with the oxidation of $H_2$ or formate, and our experimental efforts with co-culture EV could not demonstrate the utilization of other electron donors. The four characterized acidophilic representatives of the genus *Desulfosporosinus* show considerable versatility, and various organic acids, alcohols, and sugars, in addition to $H_2$, support sulfate reduction (104, 130, 131). The utilization of $H_2$ as electron donor appears to be a shared feature of *Desulfosporosinus* spp., and two or more gene clusters encoding hydrogenase complexes were found on available *Desulfosporosinus* spp. genomes (132-134).

Escalating usage of N fertilizers to meet societal demands for agricultural products increases $N_2O$ emissions due to accelerated N cycling and associated $N_2O$ formation and due to soil acidification, which presumably slows $N_2O$ consumption. Liming is commonly employed to ameliorate soil acidity, a practice considered beneficial for curbing $N_2O$ emissions based on the assumption that microbial $N_2O$ reduction is limited to circumneutral pH soils (39-41, 47). Our findings demonstrate that soils harbors microorganisms (e.g., '*Ca.* Desulfosporosinus nitrousreducens' strain PR) that utilize $N_2O$ as growth-supporting electron acceptor between pH 4.5 and 6.5. Apparently, $N_2O$ consumption is not limited to circumneutral pH conditions and acidophilic respiratory $N_2O$ reducers exist in acidic soils. Thus, increased $N_2O$ production due to fertilizer

application could potentially be mitigated, at least partially, by microbial $N_2O$ consumption in acidic soils. Recent efforts have shown substantial $N_2O$ emission reductions from soils treated with biofertilizers or augmented with mixed cultures harboring clade II $N_2O$ reducers (135, 136). Based on metagenomic surveys, bacteria capable of low pH $N_2O$ are not limited to acidic tropical soils, and are more broadly distributed in terrestrial ecosystems (44). The discovery of a naturally occurring soil bacterium that couples $N_2O$ consumption to growth under acidic pH conditions offers opportunities for the knowledge-based manipulation of agricultural soils to stimulate microbial $N_2O$ consumption. Curbing undesirable $N_2O$ emissions at the field scale would allow farmers to further reduce their greenhouse gas emissions footprint and potentially earn carbon credits.

## Appendix

**Figure 2-1. Establishment of $N_2O$-reducing microcosms and enrichment cultures yielding co-culture EV.** (A) Schematic of the workflow leading from a soil sample to a solids-free enrichment, and to a co-culture. (B) Community structure profiling based on 16S rRNA gene sequence analysis documents the enrichment process. Soil microbial community structure was profiled with 16S rRNA genes extracted from shotgun metagenomic reads. Community profiling of 6$^{th}$ and 9$^{th}$ transfers was based on 16S rRNA gene amplicon sequencing. Sequences with abundances <2% were grouped as "Others". (C) Percent of the metagenomic short read fragments obtained from El Verde soil and the 15$^{th}$ transfer culture that recruited to the genomes of *Serratia* sp. or *Desulfosporosinus* sp. A representative graph showing the high identity (> 95%) of reads mapping evenly across *Desulfosporosinus* sp. genome is presented in Supplementary Figure 2-3. The *Serratia* sp. or *Desulfosporosinus* sp. genomes were not detected in the soil metagenome dataset, with less than 0.01% of the metagenomic reads mapping to the two genomes (white bar). (D) Pyruvate fermentation (Phase I, white circles) and $N_2O$ consumption (Phase II, black circles) in co-culture EV. *Serratia* (blue diamonds) and *Desulfosporosinus* (red diamonds) cell numbers were determined with specific, 16S rRNA gene-targeted qPCR. (E) Amplicon sequencing illustrates the population shifts in co-culture EV following pyruvate consumption (day 7) and following $N_2O$ consumption (day 18). Relative abundance of *Serratia* (blue bars) and *Desulfosporosinus* (red bars) in co-culture EV following Phase I (day 7) and Phase II (day 18) in vessels with pyruvate plus $N_2O$ (left) and pyruvate only (right). Sequencing was performed on single representative cultures. All other data represent the averages of triplicate incubations and error bars represent standard deviations (n=3). Error bars are not shown if smaller than the symbol.

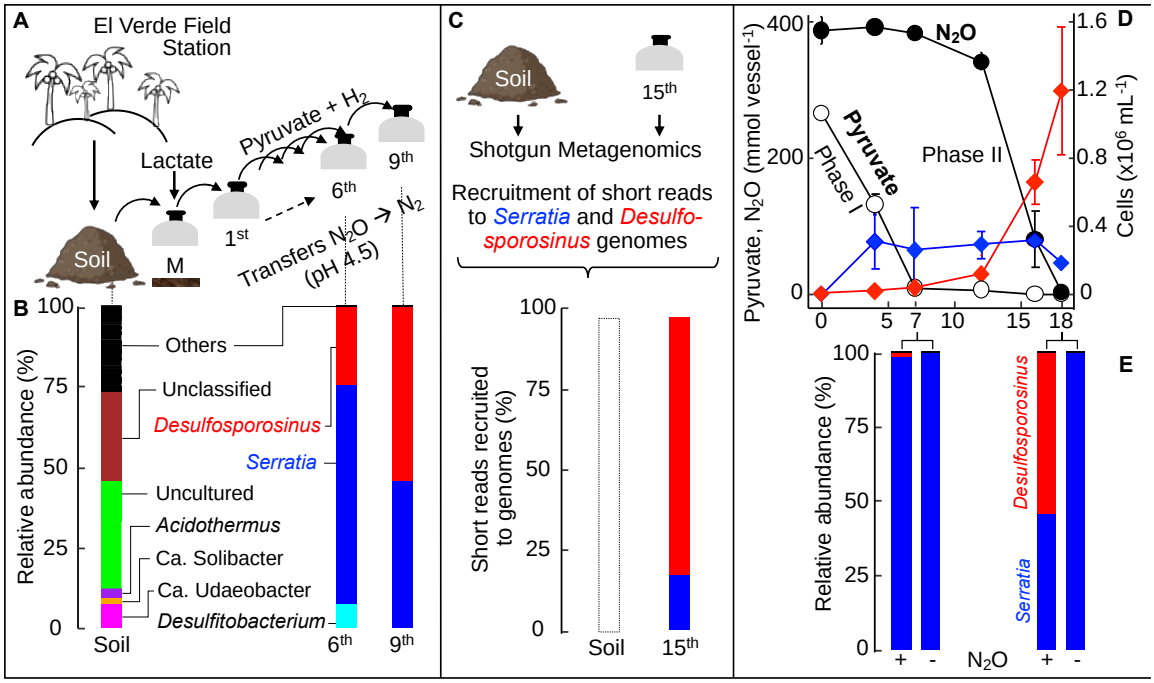
A
El Verde Field Station
Lactate
Pyruvate + H2
Soil
M
1st
6th
9th
Transfers N2O → N2 (pH 4.5)
B
Relative abundance (%)
Others
Unclassified
Desulfosporosinus
Serratia
Uncultured
Acidothermus
Ca. Solibacter
Ca. Udaeobacter
Desulfitobacterium
Soil
6th
9th
C
Soil
15th
Shotgun Metagenomics
Recruitment of short reads to Serratia and Desulfosporosinus genomes
Short reads recruited to genomes (%)
Soil
15th
D
Pyruvate, N2O (mmol vessel-1)
Cells (x10^6 mL-1)
N2O
Pyruvate
Phase I
Phase II
E
Relative abundance (%)
Desulfosporosinus
Serratia
+
-
N2O

**Figure 2-2. Interspecies cross-feeding supports low pH $N_2O$ reduction in co-culture EV.** (A) Pyruvate fermentation (Phase I, light blue background) in vessels inoculated with axenic *Serratia* sp. strain MF and $N_2O$ consumption (Phase II, red background) following inoculation with co-culture EV comprising the *Serratia* sp. and the $N_2O$-reducing *Desulfosporosinus* sp. (indicated by the arrow). The bottom part of Panel A shows the amino acid profile in the supernatant immediately after inoculation with the *Serratia* sp. (green background), during Phase I, and during Phase II following inoculation with co-culture EV (day 7; 3% inoculum). Samples for untargeted metabolome analysis were collected immediately after inoculation with *Serratia* sp. (light green), during Phase I (light blue, pyruvate fermentation) and Phase II (light red, $N_2O$ reduction). The stacked bars show the ratio (%) of areas under the curve (AUC) of the respective amino acids and amino acid derivatives. Metabolites not assigned to structures representing amino acids or its derivatives are not shown. (B) Principal coordinate analysis (PCoA) of amino acid profiles. The enclosing ellipses were estimated using the Khachiyan algorithm with the ggforce package. Permanova analysis was conducted with the vegan Community Ecology package. Black, blue, and red circles represent samples collected at day 0, during Phase I, and during Phase II, respectively. (C) $N_2O$ consumption in co-culture EV in medium amended with mixtures comprising 5 (blue), 6 (orange), or 15 (black) amino acids (see SI for composition of mixtures), $H_2$, and $N_2O$. The *Desulfosporosinus* sp. cell numbers (red diamonds) were determined with 16S rRNA gene-targeted qPCR and show growth in medium receiving the 15-amino acid mixture. Various other amino acid mixtures tested resulted in no or negligible $N_2O$ consumption. All growth assays with amino acid mixture supplementation were performed in triplicates and repeated in independent experiments.

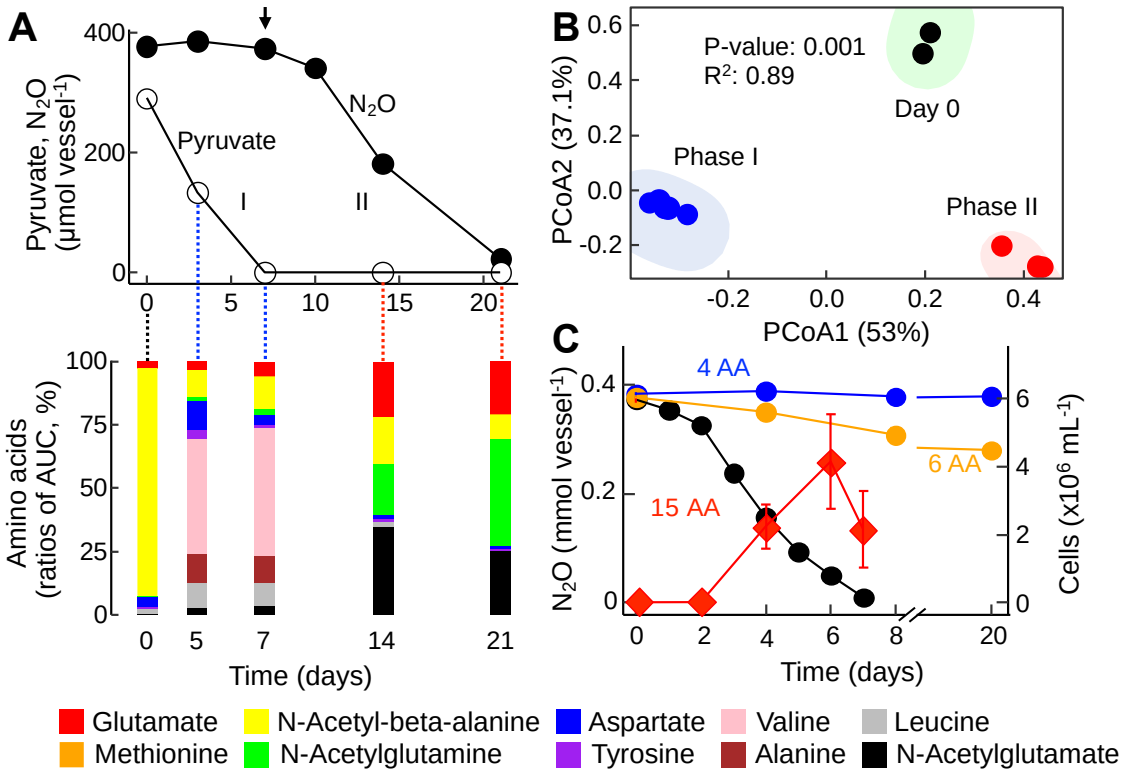
A
Pyruvate, N2O (µmol vessel-1)
400
200
0
Pyruvate
N2O
I
II
0
5
10
15
20
Amino acids (ratios of AUC, %)
100
75
50
25
0
0
5
7
14
21
Time (days)
B
PCoA2 (37.1%)
0.6
0.4
0.2
0.0
-0.2
P-value: 0.001
R2: 0.89
Day 0
Phase I
Phase II
-0.2
0.0
0.2
0.4
PCoA1 (53%)
C
N2O (mmol vessel-1)
0.4
0.2
0
4 AA
6 AA
15 AA
Cells (x10^6 mL-1)
6
4
2
0
0
2
4
6
8
20
Time (days)
Glutamate
N-Acetyl-beta-alanine
Aspartate
Valine
Leucine
Methionine
N-Acetylglutamine
Tyrosine
Alanine
N-Acetylglutamate

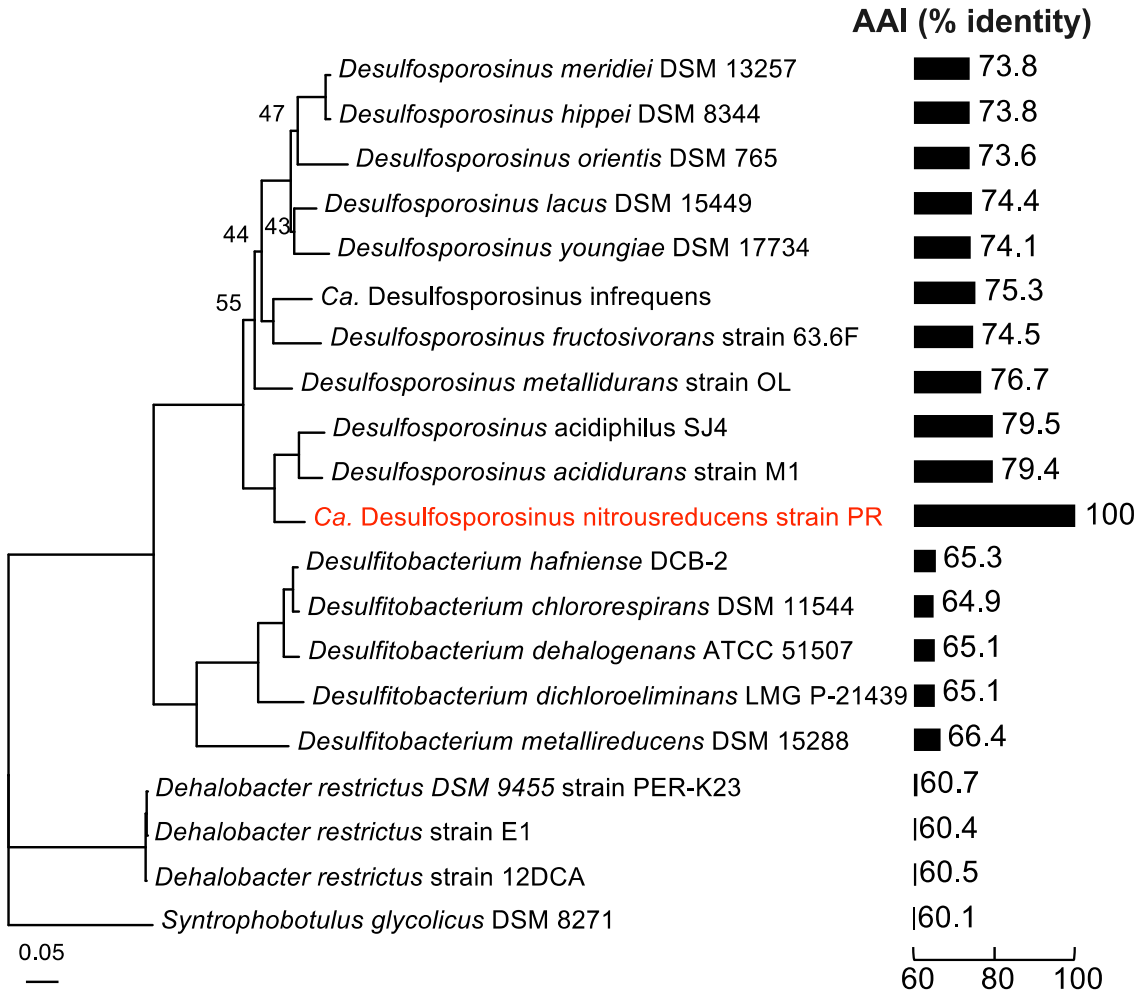


**Figure 2-3. Phylogenomic and Average Amino acid Identity (AAI) analyses indicate that the $N_2O$-reducing strain PR in co-culture EV represents a new species of the genus *Desulfosporosinus*.** Phylogenomic analysis was based on 120 conserved marker genes and included *Peptococcaceae* genomes available from NCBI. Bootstrap values higher than 90 are not displayed. The scale bar indicates 0.05 nucleotide acid substitution per site. Bar plots display the genome-wide AAI (%) between the $N_2O$-reducing '*Ca.* Desulfosporosinus nitrousreducens' and related isolates with sequenced genomes.

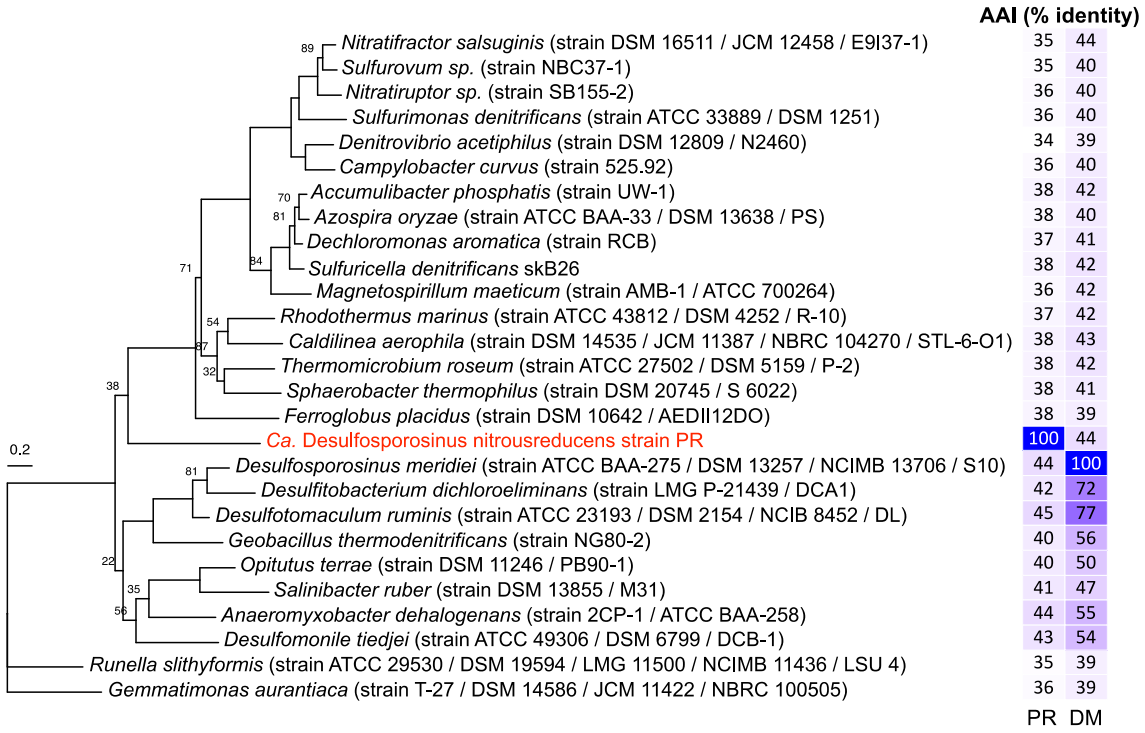


**Figure 2-4. Relatedness and similarity of the clade II NosZ of '*Ca.* Desulfosporosinus nitrousreducens' strain PR to representative clade II NosZ.** The tree represents a phylogenetic reconstruction of select clade II NosZ protein sequences. The clade II NosZ of *Gemmatimonas aurantiaca* was used to root the tree. The scale bar indicates 0.2 amino acid substitution per site. Numbers at nodes are bootstrap values smaller than 90. The two-column heatmap shows the AAI values between the NosZ of strain PR (PR) and *Desulfosporosinus meridiei* (DM) to other clade II NosZ sequences, with the darker shades of blue indicating higher percent AAI values.

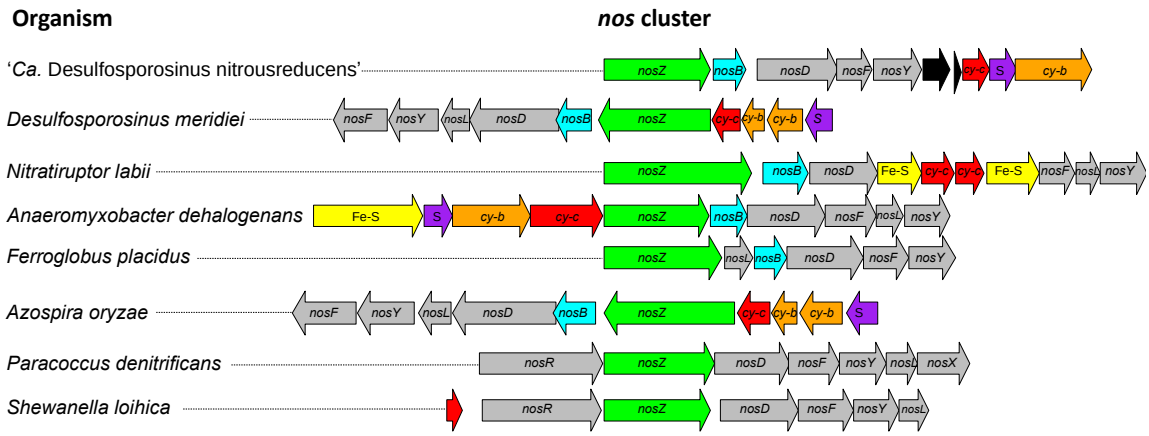


**Figure 2-5. Comparison of representative *nos* clusters.** Included are clade II *nos* clusters encoding select NosZ. and select clade I *nos* clusters of bacteria with confirmed $N_2O$ reduction activity at circumneutral pH. The colored arrows represent genes with different functions and indicate orientation and approximate length. Green, *nosZ*; gray, *nos* accessory genes (i.e., *nosD*, *nosF*, *nosY*, *nosL*, *nosX* and *nosR*); yellow, genes encoding iron-sulfur (Fe-S) proteins; purple, genes encoding Rieske iron-sulfur proteins (S); orange (cy-b) and red (cy-c), genes encoding b-type and c-type cytochromes, respectively; cyan, *nosB* genes encoding transmembrane proteins characteristic for clade II *nos* operons; black, genes of unknown function. *Desulfosporosinus* and *Desulfitobacterium* spp., *Nitratiruptor* and *Nitratifractor* spp., and *Paracoccus* and *Bradyrhizobium* spp. share similar *nos* cluster architectures, respectively.

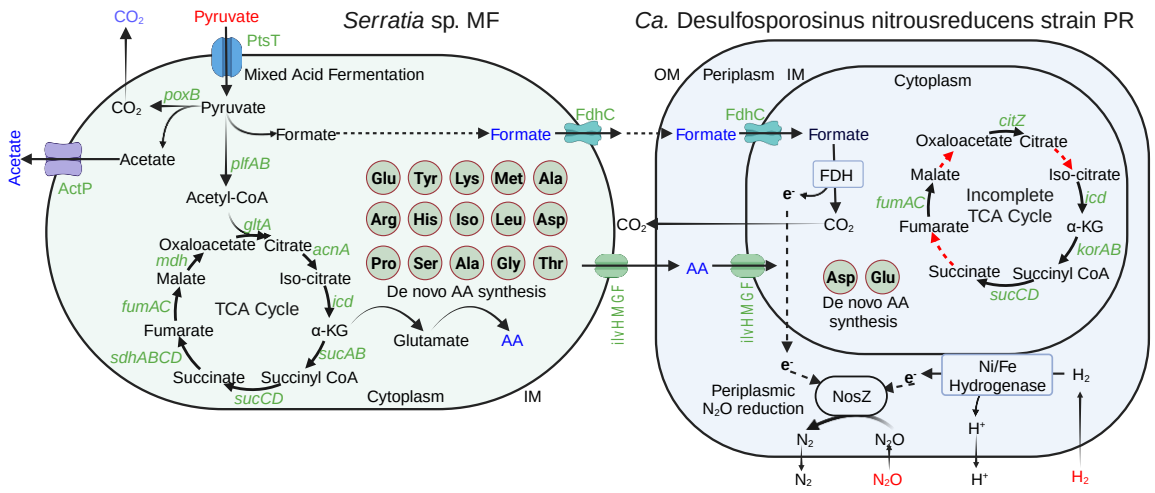


**Figure 2-6. Proposed interspecies cross-feeding interactions in co-culture EV.** Genes involved in mixed acid fermentation are only found on the *Serratia* sp. strain MF genome, and genes involved in periplasmic $N_2O$ reduction are exclusive to '*Ca.* Desulfosporosinus nitrousreducens' strain PR. External substrates (i.e., pyruvate or the 15-amino acid mixture, $H_2$, $N_2O$) provided to co-culture EV are shown in red font, and metabolites produced by *Serratia* are shown in blue font. Fifteen versus two complete amino acid biosynthesis pathways are present on the *Serratia* sp. strain MF and '*Ca.* Desulfosporosinus nitrousreducens' strain PR genomes, respectively. Strain PR has an incomplete TCA cycle, and the red dashed arrows indicate the absence of the corresponding genes. TCA cycle: tricarboxylic acid cycle; AA: amino acids; FDH: formate dehydrogenase complex; NosZ: nitrous oxide reductase; OM: outer membrane; IM: inner membrane.

**Supplementary Figure 2-1.** Phenotypic characterization of co-culture EV. Cultures were grown in 160 mL glass serum bottles containing 100 mL of medium amended with pyruvate (50 or 250 µmol), $H_2$ (416 µmol) and $N_2O$ (416 µmol) (A and B), pyruvate and $H_2$ (C and D), or pyruvate and $N_2O$ (E and F). The arrows in panels D and F indicate additional doses of $N_2O$ or $H_2$ to corresponding culture vessels lack $N_2O$ (D) or $H_2$ (F) to resume $N_2O$ reduction activity. Pyruvate consumption and associated product formation are documented in panels A, C, and E. $N_2O$ and $H_2$ consumption are documented in panels B, D, F. Panel G shows the performance of co-culture EV grown with a lower amount of pyruvate. Panel H depicts pyruvate, $H_2$ and $N_2O$ amounts over time in vessels without inoculum. Autotrophic activity in cultures with $CO_2$, but lacking pyruvate, was not observed (I). The light blue shaded areas represent the pyruvate fermentation phase (Phase I) and the light red areas represent the $N_2O$ reduction phase (Phase II). The data represent the averages of triplicate incubations and error bars represent the standard deviations (n=3). Error bars are not shown when smaller than the symbol.

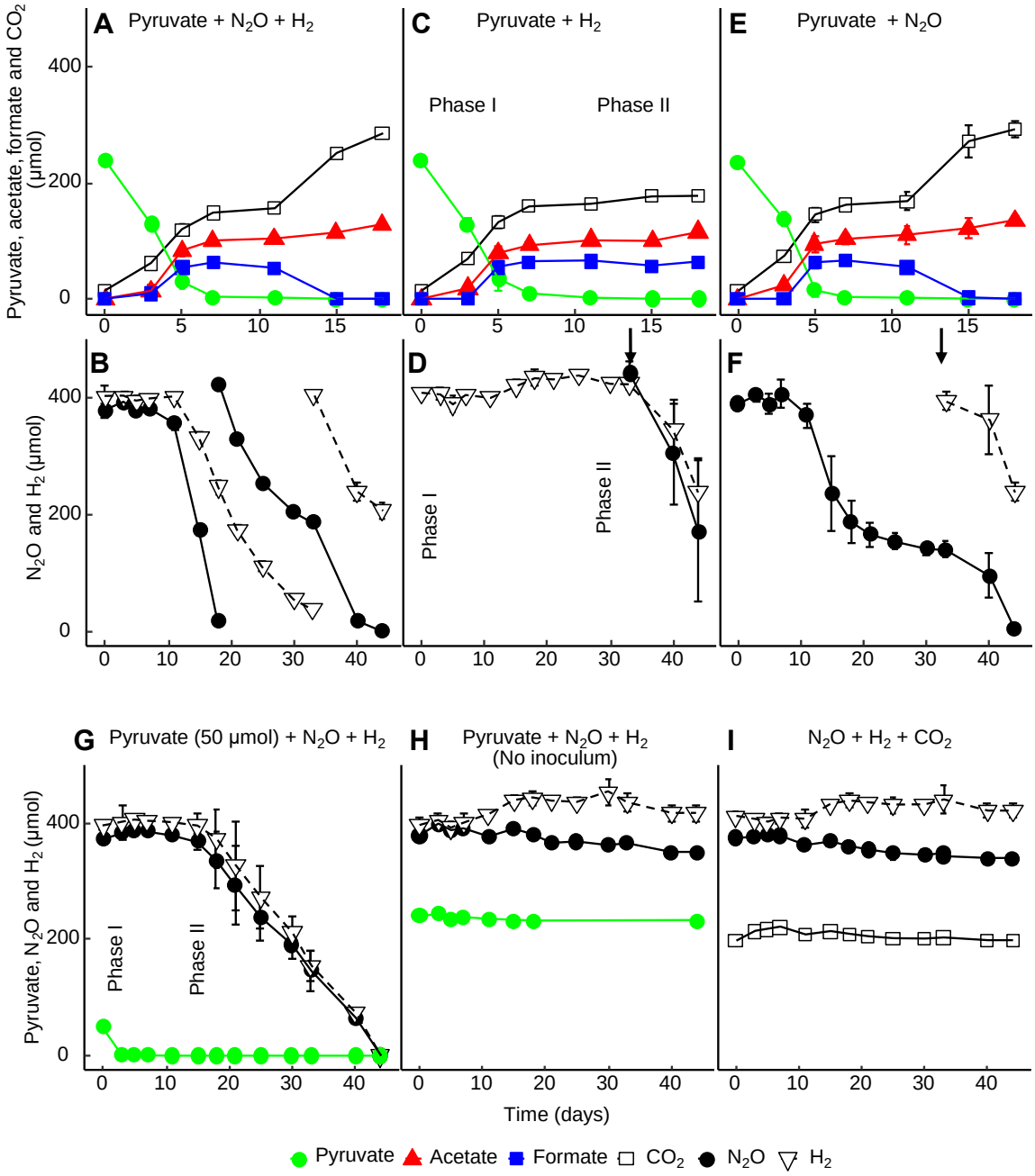
A Pyruvate + N2O + H2
C Pyruvate + H2
E Pyruvate + N2O
Phase I
Phase II
Pyruvate, acetate, formate and CO2 (µmol)
B
D
F
N2O and H2 (µmol)
G Pyruvate (50 µmol) + N2O + H2
H Pyruvate + N2O + H2 (No inoculum)
I N2O + H2 + CO2
Pyruvate, N2O and H2 (µmol)
Time (days)
Pyruvate
Acetate
Formate
CO2
N2O
H2

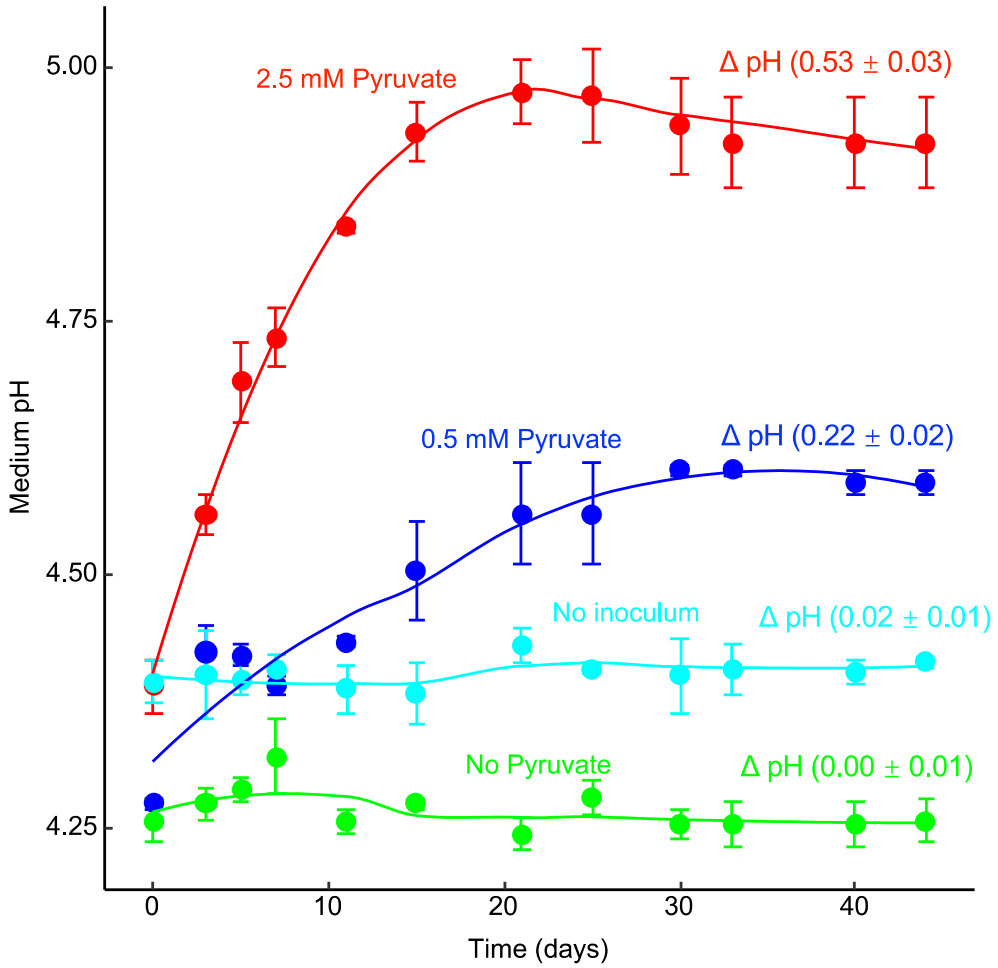


**Supplementary Figure 2-2. Medium pH over the course of the incubation. pH profiles were measured in replicate co-culture EV incubation vessels that received 0, 0.5, and 2.5 mM pyruvate.** pH changes (Δ pH) were calculated by subtracting the pH values measured immediately following inoculation from pH values measured at the end of incubation period. Pyruvate was not consumed in vessels that were not inoculated with co-culture EV. The data shown are the averages of triplicate incubations and error bars represent the standard deviations (n=3). Error bars are not shown when smaller than the symbol.

**Supplementary Figure 2-3. Fragment recruitment plot of the '*Ca*. Desulfosporosinus nitrousreducens' strain PR genome to the metagenome dataset derived from the 15$^{th}$ generation co-culture EV.** The recruitment was performed via processing a BLAST search of the metagenome fragments against the '*Ca*. Desulfosporosinus nitrousreducens' strain PR genome. The tabular BLAST result was parsed using BLASTab.catsbj.pl, and graphical representation was generated with the BlasTab.recplot2.R embedded in Enveomics collection (88). (A) The bar on the left shows the number of fragments with different identity recruited to each position on the genome. (B) indicates the sequencing depth across the '*Ca*. Desulfosporosinus nitrousreducens' strain PR genome on a logarithmic scale. (C) Sequencing depth histogram with peaks from values above 95% identity automatically identified as skewed normal distribution. (D) Metagenome fragments recruited to the '*Ca*. Desulfosporosinus nitrousreducens' strain PR genome, placed by location (x-axis) and identity (y-axis). (E) Identity histogram of mapping fragments (light gray) and smoothed spline (black). The backgrounds in panels D and E, and the line colors in panels B and C, correspond to identity matches above (dark blue) and below (light blue) 95 %. A recruitment plot of the '*Ca*. Desulfosporosinus nitrousreducens' strain PR genome to the metagenome datasets derived from El Verde soil is not shown as the covered fraction of the 5.6 Mbp genome was below 10% (i.e., 0.56 Mbp).

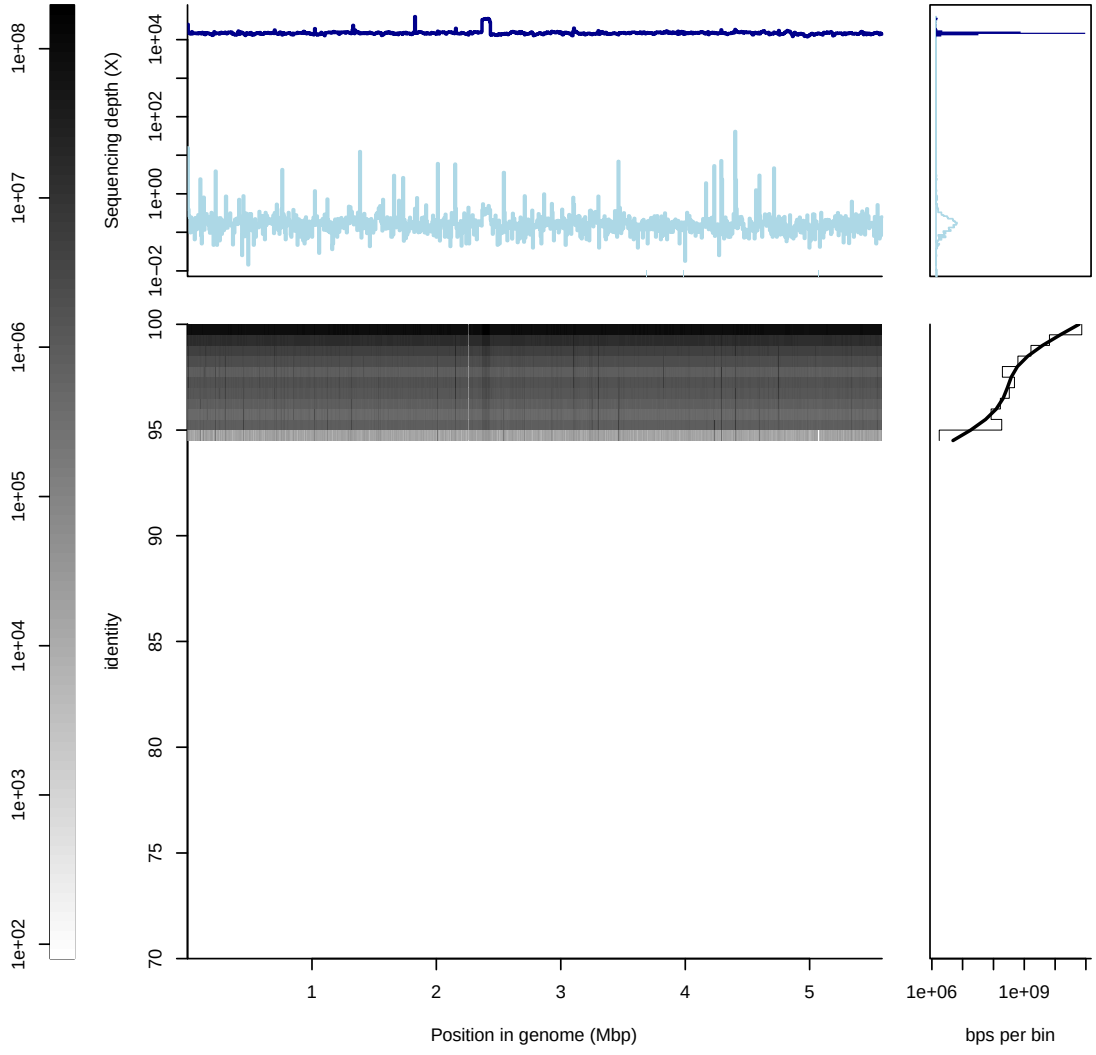
1e+08
1e+07
1e+06
1e+05
1e+04
1e+03
1e+02
Sequencing depth (X)
1e+04
1e+02
1e+00
1e−02
identity
100
95
90
85
80
75
70
1
2
3
4
5
Position in genome (Mbp)
1e+06
1e+09
bps per bin

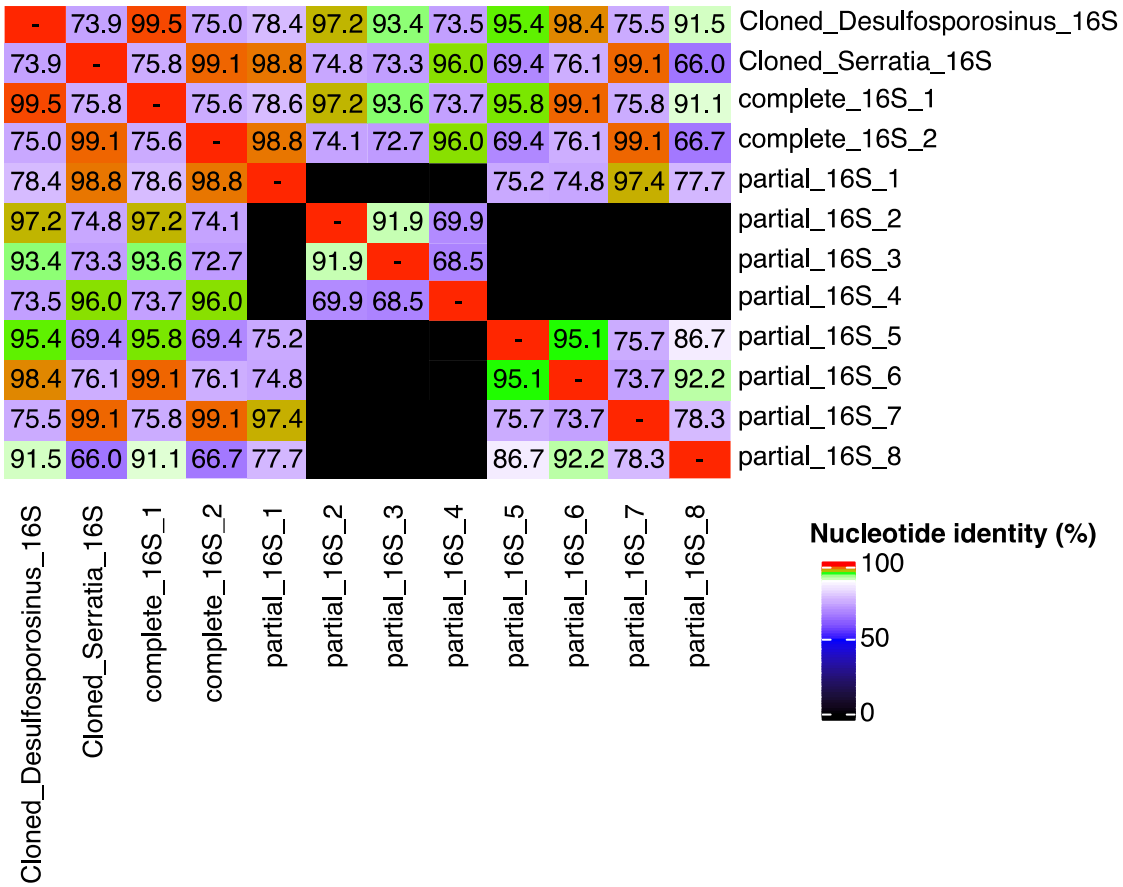


**Supplementary Figure 2-4. Comparison of '*Ca.* Desulfosporosinus nitrousreducens' strain PR and *Serratia* sp. strain MF 16S rRNA gene sequences derived from cloned 16S rRNA gene fragments (Sanger sequencing) and co-culture EV (metagenome sequencing).** DNA extracted from co-culture EV following $N_2O$ consumption served as template for the amplification of 16S rRNA gene fragments with general primer pair 8F-1541R. 16S rRNA gene fragments were cloned in *E. coli* and two uniform clone populations were obtained, represented by Cloned_Desulfosporosinus_16S and Cloned_Serratia_16S.

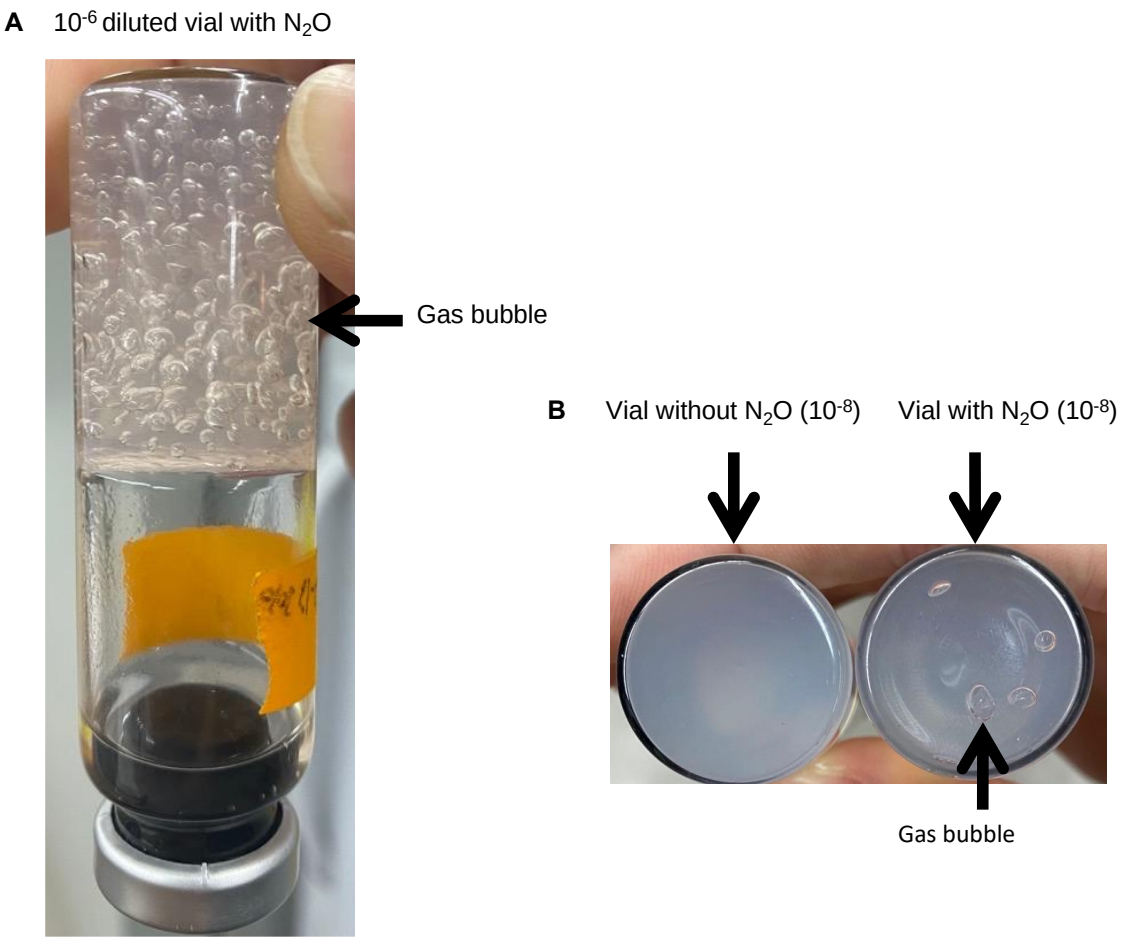


**Supplementary Figure 2-5. Formation of gas bubbles in soft agar shake tubes. (A) Visible gas bubbles (presumably $N_2$) following $N_2O$ consumption.** The vials were incubated with the stoppers down for 28 days. (B) The formation of gas bubbles was strictly dependent on $N_2O$, and no bubbles formed in replicate vials without $N_2O$. No gas bubbles formed in control incubations without inoculum.

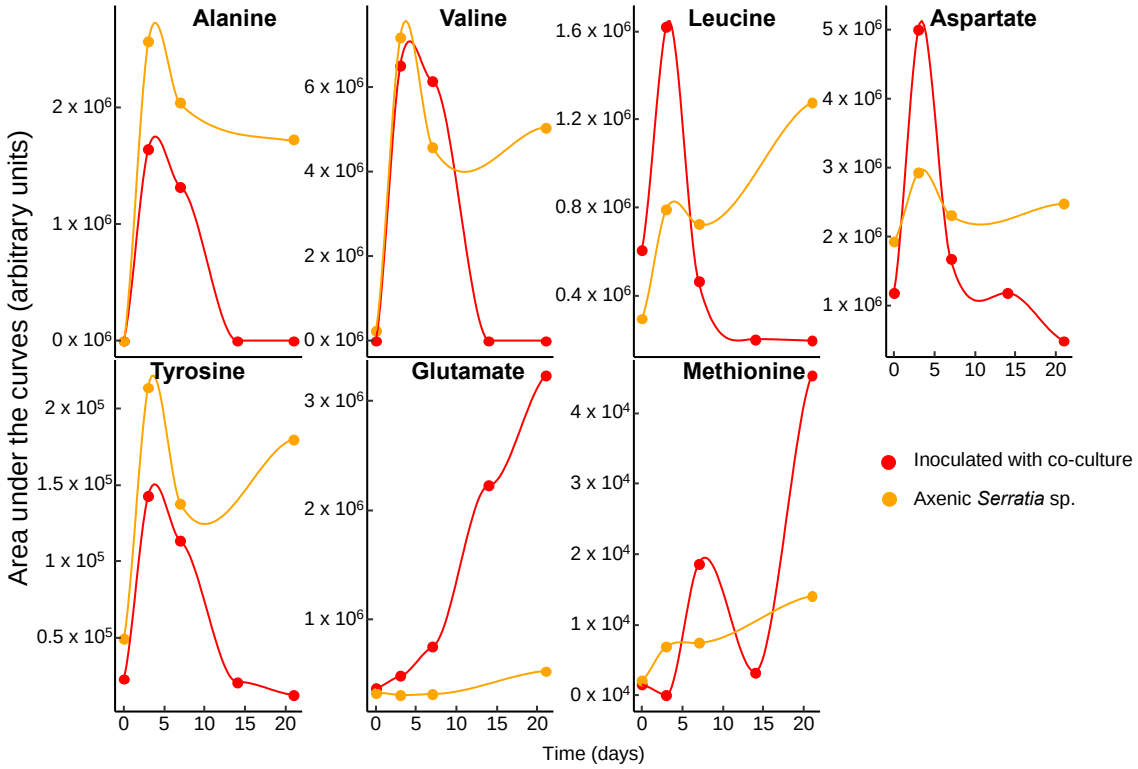


**Supplementary Figure 2-6. Dynamic changes of amino acids in the supernatants of cultures following inoculation with *Serratia* sp. and with '*Ca.* Desulfosporosinus nitrousreducens' strain PR (as co-culture EV).** Axenic *Serratia* sp. cultures amended with pyruvate, $N_2O$, and $H_2$ were inoculated with co-culture EV on day 7. Orange lines represent amino acids in cultures inoculated with axenic *Serratia* sp. on day 0. Red lines represent amino acids in cultures inoculated with the axenic *Serratia* sp. on day 0 and subsequently inoculated with co-culture EV on day 7. Note that axenic *Serratia* sp. cultures without co-culture EV inoculum cannot reduce $N_2O$. Shown are representative data obtained from a single culture in medium reduced with l-cysteine. Cystine was detected in cultures reduced with l-cysteine; however, in samples from replicates from an independent experiment where DTT served as reductant, cystine was not detected, suggesting *Serratia* sp. does not release cystine into the medium.

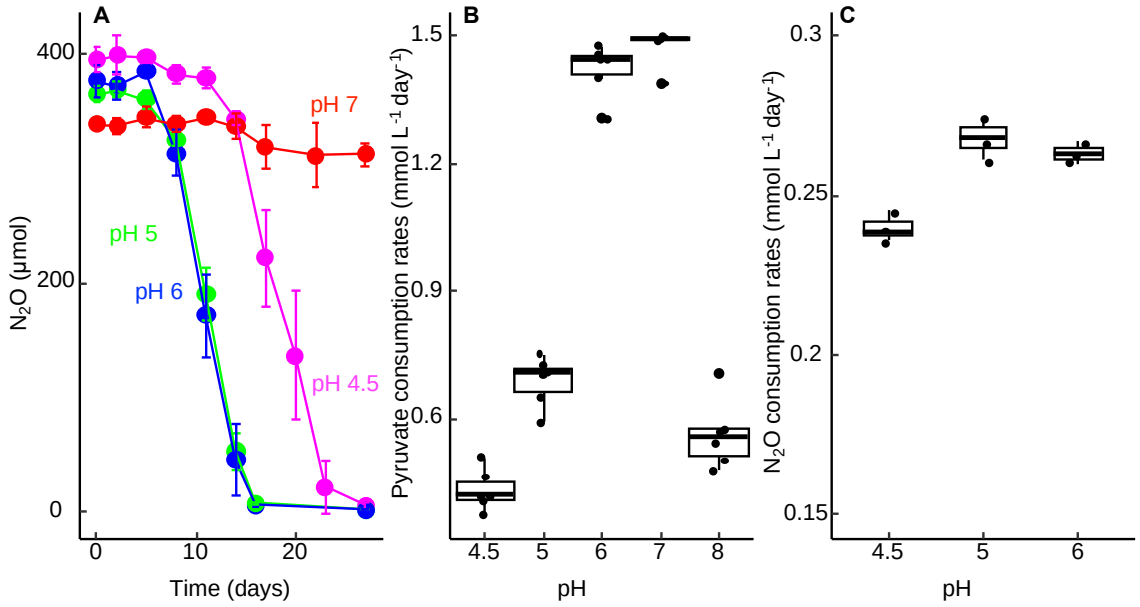


**Supplementary Figure 2-7. Performance of co-culture EV at different medium pH values.** (A) $N_2O$ reduction was measured in triplicate 160 mL serum bottles containing 100 mL of medium (pH 3.5, 4.5, 5, 6, 7, 8) and inoculated with co-culture EV. $N_2O$ reduction was observed between pH 4.5 and 6, but not at pH 3.5 and at or above pH 7. (B) Pyruvate consumption rates by *Serratia* sp. in cultures adjusted to pH 4.5, 5, 6, 7, and 8. Pyruvate was consumed in all incubation vessels except for those at pH 3.5. (C) $N_2O$ consumption rates of '*Ca.* Desulfosporosinus nitrousreducens' at pH 4.5, 5, and 6. No $N_2O$ consumption was observed in pH 3.5, 7.0, and 8.0 cultures. Consumption rates of pyruvate and $N_2O$ were calculated using data that fell within the linear ranges of consumption. Each black dot in the box plots represent the consumption rates calculated from a single experiment. The data from three and six replicate cultures were used for the calculations of pyruvate and $N_2O$ consumption rates, respectively.

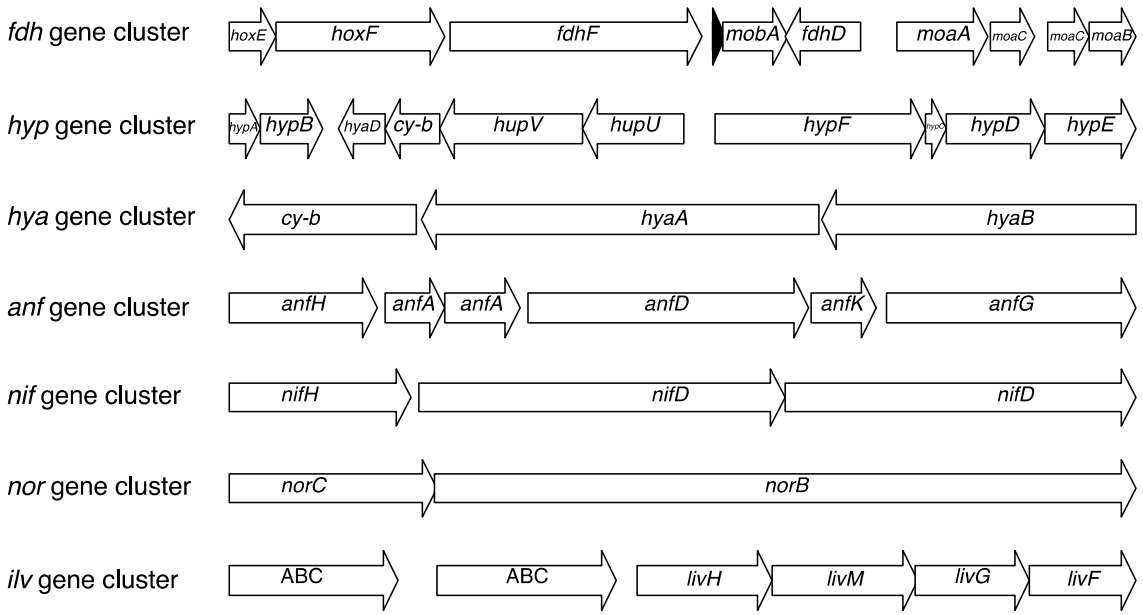


**Supplementary Figure 2-8. Gene clusters found on the '*Ca*. Desulfosporosinus nitrousreducens' strain PR genome.** Displayed are formate dehydrogenase (*fdh* gene cluster), b-type Ni/Fe hydrogenase (*hyp* gene cluster), group 1 Ni/Fe hydrogenase (*hya* gene cluster), FeFe type Nitrogenase (*anf* gene cluster), Mo-Fe Nitrogenase (*nif* gene cluster), Nitric-oxide reductase (*nor* gene cluster), High-affinity amino acid transport system (*ilv* gene cluster). The arrows indicate operon length and orientations. Preliminary annotation of coding genes was done with Prokka (137), MicrobeAnnotator (138), and the RAST server (87), and genes of interests were curated via blasting to the NCBI nr database. Cy-b: b-type cytochrome; ABC: ATP-binding cassette. The black arrow in the *fdh* gene cluster represents a gene encoding a small protein of unknown function.

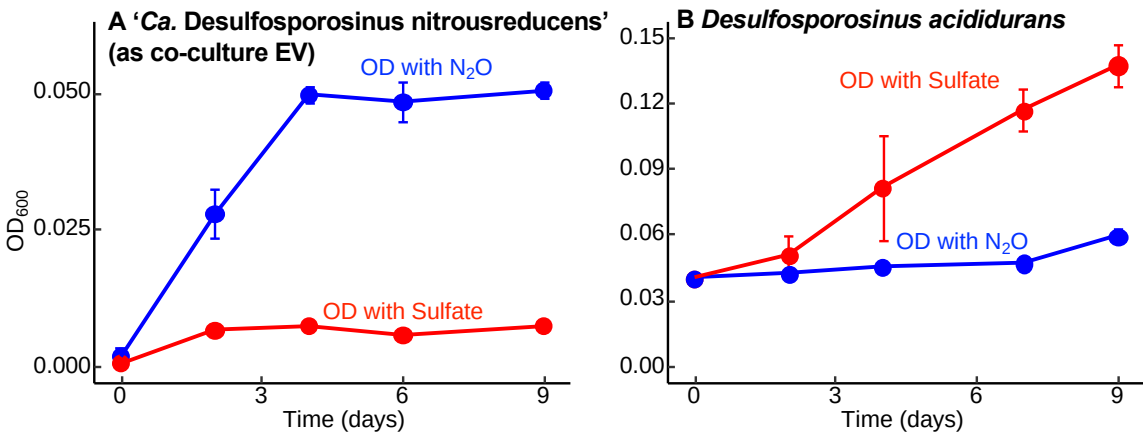


**Supplementary Figure 2-9. Comparative growth studies with 'Ca. Desulfosporosinus nitrousreducens' strain PR (as co-culture EV) and *Desulfosporosinus acididurans* strain D.** Panel A shows growth of '*Ca*. Desulfosporosinus nitrousreducens' strain PR with 4.16 mM (nominal) $N_2O$ (blue) or 5 mM $SO_4^{2-}$ (red) as electron acceptor in pH 4.5 medium amended with the 15-amino acid mixture and 4.16 mM (nominal) $H_2$. Over the 9-day incubation period, strain PR completely consumed the initial dose of $N_2O$, whereas cultures amended with 5 mM $SO_4^{2-}$ showed no growth or $SO_4^{2-}$ consumption (4.97 ± 0.23 mM sulfate remained). OD values below 0.01 were measured in replicate cultures that did not receive $N_2O$ as electron acceptor or $H_2$ as electron donor. Panel B compares growth of *Desulfosporosinus acididurans* strain D with 4.16 mM (nominal) $N_2O$ (blue) or 5 mM $SO_4^{2-}$ (red) as electron acceptors in pH 5.5 medium with 10 mM glycerol as electron donor. Over a 9-day incubation period, *Desulfosporosinus acididurans* strain D reduced 5 mM $SO_4^{2-}$, but $N_2O$ was not consumed (4.10 ± 0.59 mM $N_2O$ remained) in replicate cultures, even after an extended 20-day incubation period. Growth was monitored by measuring the optical density at 600 nm ($OD_{600}$).

**Supplementary Figure 2-10. Distribution of '*Ca*. Desulfosporosinus nitrousreducens' strain PR and *Serratia* sp. strain MF in select publicly available soil metagenomes.** Metagenome datasets were downloaded from the European Nucleotide Archive (accession number PRJEB44414) with associated metadata available in a Supplemental Information/Source Data file (https://doi.org/10.1038/s41467-022-29161-3). (A) Geographical distribution of the soil metagenomes included in the analysis. Blue dots indicate a soil pH >7, red dots indicate a soil pH <7. (B) The partial importance (%) of different parameters, including the presence of *Serratia* sp. (based on short reads that align to the *Serratia* sp. strain MF genome), organic matter (OM content), $NO_3^-$ content, $NH_4^+$ content, C/N ratio, and pH for the relative abundance of '*Ca*. Desulfosporosinus nitrousreducens' strain PR based on Random Forest models (139). (C) Correlation between percentages of short read fragments aligned to the *Serratia* sp. strain MF and the '*Ca.* Desulfosporosinus nitrousreducens' strain PR genomes. The significance values for the correlations were calculated with the Pearson test (140) implemented in the ggpubr package (https://github.com/kassambara/ggpubr).

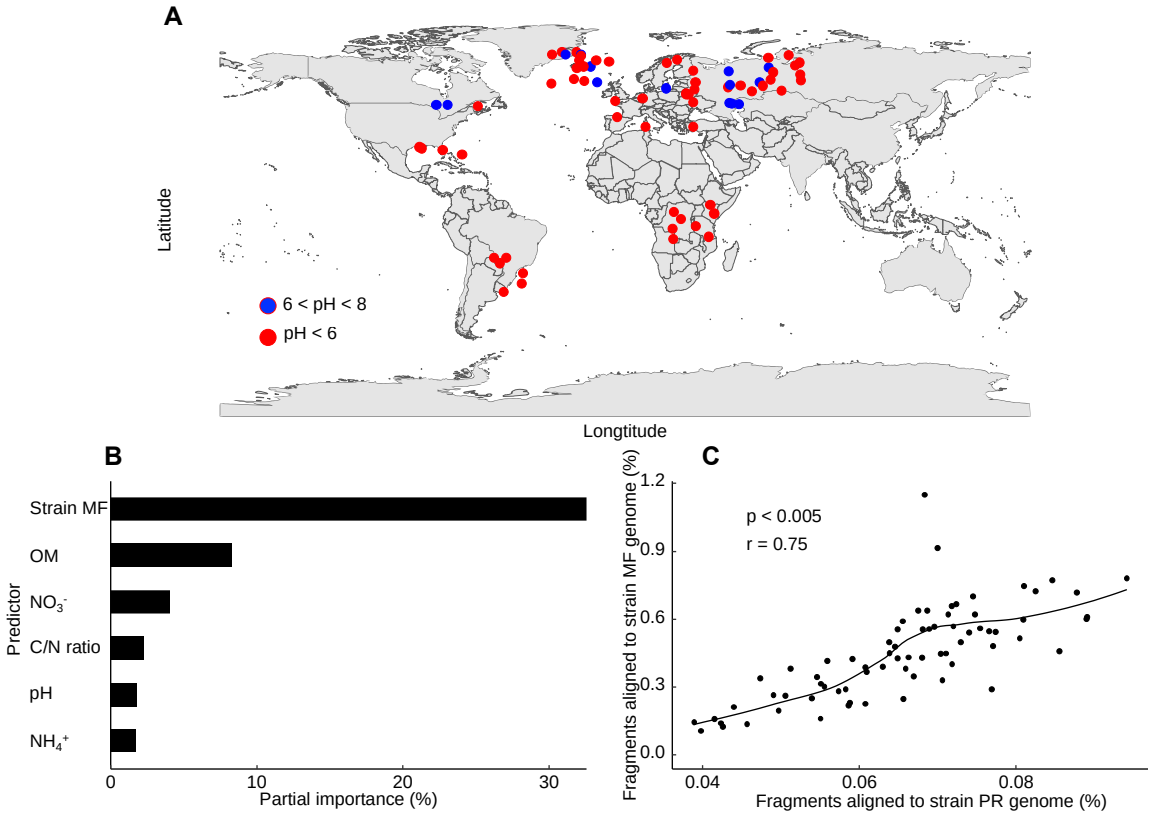
A
Latitude
Longtitude
6 < pH < 8
pH < 6
B
Predictor
Strain MF
OM
$NO_3^-$
C/N ratio
pH
$NH_4^+$
0
10
20
30
Partial importance (%)
C
Fragments aligned to strain MF genome (%)
1.2
0.9
0.6
0.3
0.0
p < 0.005
r = 0.75
0.04
0.06
0.08
Fragments aligned to strain PR genome (%)

**Table 2-1.** qPCR primers and probe designed for the enumeration of *Serratia* sp. strain MF and '*Ca*. Desulfosporosinus nitrousreducens' strain PR 16S rRNA genes.

| Target | Primer sequence | Probe |
|---|---|---|
| *Serratia* sp. | TGCTACAATTGGCGTATACAA (Ser_1316qF)<br>GACTACGACATACTTTATGA (Ser_1386qR) | None |
| *Desulfosporosinus* sp. | TGCTACAATGGCCGGTACAG (DS_1316qF)<br>CGAACTGAGACCGGCTTTCT (DS_1388qR) | FAM-AAGCTGTGAAGTGGAGCCAATC-MGB [a] |

[a] FAM: 6-Carboxyfluorescein attached to the 5' end of the probe. MGB: Minor Groove Binder that attached to the 3' end of the probe.

**Table 2-2.** Sequence information submitted to the NCBI database.

| **Dataset** | **Data type** | **Accession No.** |
|---|---|---|
| Enrichment culture (6th transfer) | Amplicon (16S V3-V4) | SRR24215177 |
| Enrichment culture (9th transfer) | Amplicon (16S V3-V4) | SRR24083098 |
| Co-culture EV (15th transfer) | SRA [a] | SRR24709127 |
| *Serratia* sp. (isolate) | SRA [a] | SRR24709126 |
| 16S rRNA gene (*Desulfosporosinus*) | Complete gene | OR076434 |
| 16S rRNA gene (*Serratia*) | Complete gene | OR076433 |
| '*Ca.* Desulfosporosinus nitrousreducens strain PR' | GenBank Assembly [b] | GCA_030954495.1 |
| *Serratia* sp. strain MF | GenBank Assembly [b] | GCA_030954505.1 |

[a] SRA: Sequence Read Archive (raw sequence data)

[b] Genome assembly constructed from SRA data

**Table 2-3.** Organismal and genomic information of microorganisms with reported $N_2O$ reduction capacity under different pH.

| **Organism** | **Genome NCBI acc no.** | **Reported pH range for $N_2O$ reduction** | ***nosZ* clade** | **Reference** |
|---|---|---|---|---|
| '*Ca*. Desulfosporosinus nitrousreducens' strain PR | GCA_030954495.1 | 4.5-6 | II | This work |
| *Desulfosporosinus meridiei* strain DSM 13257 | NC_018515.1 | ND | II | (12) |
| *Nitratiruptor labii* strain HRV44 | AP022826.1 | 5.4-6.4 | II | (105) |
| *Anaeromyxobacter dehalogenans* strain 2CP-1 | NC_011891.1 | ~7 | II | (12) |
| *Ferroglobus placidus* | NC_013849.1 | ND | II | (12) |
| *Azospira oryzae* | GCA_905120365.1 | ND | II | (12) |
| *Paracoccus denitrificans* strain DSM 413 | AL591688.1 | 7-8 | I | (38) |
| *Shewanella loihica* strain PV-4 | NC_009092.1 | 6-8 | I | (111) |
| *Alicycliphilus denitrificans* strain I51 | AP024172.1 | 6-9 | I | (110) |
| *Bradyrhizobium diazoefficiens* strain 110*spc*4 | NZ_CP032617.1 | 6-8 | I | (141) |

**Table 2-4.** Genomes used in phylogenomic analysis and classification of '*Ca*. Desulfosporosinus nitrousreducens'.

| **Organism** | **NCBI accession No. of genomes** |
|---|---|
| '*Ca*. Desulfosporosinus nitrousreducens' strain PR | GCA_030954495.1 |
| *Desulfosporosinus youngiae* DSM 17734 | NZ_CM001441.1 |
| *Desulfosporosinus orientis* DSM 765 | NC_016584.1 |
| *Desulfosporosinus metallidurans* strain OL | NZ_MLBF01000001.1 |
| *Desulfosporosinus meridiei* DSM 13257 | NC_018515.1 |
| *Desulfosporosinus lacus* DSM 15449 | NZ_FQXJ01000052.1 |
| *Desulfosporosinus hippie* DSM 8344 | NZ_fncp01000067.1 |
| *Desulfosporosinus fructosivorans* strain 63.6F | NZ_SPQQ01000010.1 |
| *Desulfosporosinus acidiphilus* SJ4 | NC_018068.1 |
| *Desulfosporosinus acididurans* strain M1 | NZ_LDZY01000001.1 |
| '*Ca*. Desulfosporosinus infrequens' | NZ_OMOF01000971.1 |
| *Syntrophobotulus glycolicus* DSM 8271 | NC_015172.1 |
| *Desulfitobacterium metallireducens* DSM 15288 | NZ_CP007032.1 |
| *Desulfitobacterium hafniense* DCB-2 | NC_011830.1 |

**Table 2-4 Continued**

| Organism | NCBI accession No. of genomes |
|---|---|
| *Desulfitobacterium dichloroeliminans* LMG P-21439 | NC_019903.1 |
| *Desulfitobacterium dehalogenans* ATCC 51507 | NC_018017.1 |
| *Desulfitobacterium chlororespirans* DSM 11544 | NZ_FRDN01000033.1 |
| *Dehalobacter restrictus* strain E1 | CANE01000102.1 |
| *Dehalobacter restrictus* strain 12DCA | NZ_CP046996.1 |
| *Dehalobacter restrictus* DSM 9455 | NZ_CP007033.1 |

**Table 2-5.** Amino acids and concentrations used to augment the growth medium for cultivation of '*Ca*. Desulfosporosinus nitrousreducens'. [a]

| Amino acid | Amino acid concentration (µM) | Carbon (µmol 100 mL medium$^{-1}$) |
|---|---|---|
| Alanine | 56 | 16.8 |
| Valine | 77 | 38.5 |
| Aspartate | 82 | 33.1 |
| Isoleucine | 38 | 22.9 |
| Methionine | 27 | 13.4 |
| Tyrosine | 16 | 14.9 |
| Histidine | 19 | 11.6 |
| Tryptophan | 10 | 10.8 |
| Glutamate | 68 | 34.0 |
| Proline | 86 | 43.5 |
| Arginine | 28 | 17.2 |
| Glycine | 40 | 8.0 |
| Threonine | 42 | 16.8 |
| Lysine | 69 | 41.1 |
| Serine | 76 | 22.9 |

[a] The addition of individual amino acids did not stimulate $N_2O$-dependent growth of '*Ca*. Desulfosporosinus nitrousreducens'. Similarly, a 5-amino acid mixture comprising alanine, valine, leucine, aspartate, and tyrosine did not promote $N_2O$ consumption. Weak and incomplete $N_2O$ reduction was observed in cultures that received a 6-amino acid mixture comprising alanine, valine, leucine, aspartate, tyrosine, and methionine. The 15-amino acid mixture (i.e., all amino acids listed in Table 5) supported growth of '*Ca*. Desulfosporosinus nitrousreducens' via hydrogenotrophic $N_2O$ reduction.

**Table 2-6.** Genome features of '*Ca.* Desulfosporosinus nitrousreducens' strain PR and *Serratia* sp. strain MF, and comparison to closest relatives.

| | **Organism** [a] | | | | |
|---|---|---|---|---|---|
| **Feature** | **(1)** | **(2)** | **(3)** | **(4)** | **(5)** |
| Genome size (bp) | 5,591,411 | 4,991,181 | 4,637,866 | 5,118,938 | 5,300,955 |
| Completeness (%) [b] | 99.5 | 99.1 | 92.3 | 98.0 | 95.6 |
| Contamination (%) [b] | 5.7 | 0.0 | 5.14 | 0.53 | 4.03 |
| GC content (%) | 44 | 42 | 41.5 | 58.8 | 59.5 |
| 5S rRNA genes | 8 | 8 | 8 | 8 | 8 |

**Table 2-7.** Genome features of '*Ca.* Desulfosporosinus nitrousreducens' strain PR and *Serratia* sp. strain MF, and close relatives.

| **Feature** | **Organism** [a] | | | | |
|---|---|---|---|---|---|
| | **(1)** | **(2)** | **(3)** | **(4)** | **(5)** |
| 23S rRNA genes | 1 | 8 | 11 [d] | 1 | 7 |
| tRNA genes | 105 | 66 | 67 | 81 | 91 |
| Coding sequences | 5,312 | 4,554 | 4,317 | 4,690 | 4,941 |
| Accession number | GCA_030954495.1 | GCA_000255115.3 | GCA_001029285.1 | GCA_030954505.1 | GCF_002220655.1 |

[a] (1) 'Ca. Desulfosporosinus nitrousreducens' strain PR (this study)

(2) *Desulfosporosinus acidiphilus* strain SJ4 (130)

(3) *Desulfosporosinus acididurans* strain M1 (104)

(4) *Serratia* sp. strain MF (this study)

(5) *Serratia marcescens* strain UMH3 (142)

[b] Genome completeness and contamination were evaluated based on the presence of 120 single copy genes using CheckM.

[c] Only partial 16S and 23S rRNA genes were found on *Desulfosporosinus acididurans* strain M1 genome.

# Chapter 3 Clade III $N_2O$-respiring microbes implicated in $N_2O$ reduction.

**Abstract**

Nitrous oxide ($N_2O$), a significant contributor to global warming and ozone depletion, has raised concerns over its increasing presence in the atmosphere. $N_2O$ consumption is limited to microorganisms known to possess clade I and clade II *nosZ* genes, but the $N_2O$ reduction activity progressively wanes with decreasing pH. Even more troublesome is the widespread phenomenon of soil acidification, a natural process accelerated by agricultural practices. In this study, we established enrichment cultures from acidic tropical forest soils (pH 4.4 to 4.9) and circumneutral regenerative agricultural soils (pH ~ 7), demonstrating sustained, growth-linked $N_2O$ reduction at an initial pH of 4.5. Characterization of the enrichment cultures suggest previously unknown clade II and a functional clade III $N_2O$ reducers obligately consume $N_2O$ at pH < 7. These results provide insight into the biodiversity and physiology of $N_2O$-reducing microorganisms, which have pivotal roles in curbing $N_2O$ emissions, especially in acidic soil systems.

## 3.1 Introduction

Nitrous oxide ($N_2O$, "laughing gas") is a powerful greenhouse gas with 298 times the warming potential of carbon dioxide ($CO_2$) over a lifetime of 100-year (51), and $N_2O$ is also a strong ozone depleting substance (1). $N_2O$ also interferes with biogeochemical processes such as methanogenesis, mercury methylation, and reductive dichlorination (55, 56, 143). The Foundation Platform F20 report emphasis of limiting global warming to 1.5ºC through curbing $CO_2$ emission (144); however, this effort could possibly be offset by the growing atmosphere $N_2O$ concentration (145). Natural and agricultural soils are primary natural and anthropogenic sources of $N_2O$, as a consequence of biological nitrogen fixation and increasing load of synthetic nitrogen fertilizer and manure, respectively (146, 147). Compilation of global $N_2O$ budget suggest that the natural and anthropogenic $N_2O$ emissions are 9.7 and 7.3 Tg N $y^{-1}$, respectively (3). Without putting $N_2O$ emissions under tight regulation, atmospheric $N_2O$ will continue to rise with the increasing demand of the exploding population growth for agricultural product, threatening global climate and ozone layer (148).

The rising $N_2O$ emissions across the globe indicate an imbalance between $N_2O$ formation versus consumption, with the rates of former process exceeding the latter. The most ancient origin (i.e., more than 2.7 billion years ago) of $N_2O$ is the iron mineral catalyzed abiotic process (7), which still occurs in modern tropic soils (5). The early anaerobic microbial life evolved $N_2O$ reductase, the only known enzyme catalyzing $N_2O$ reduction to date, to cope with tremendous $N_2O$ on Archaean earth prior to the great oxygen event (GOE) (7). Denitrification and aerobic nitrification appeared only shortly after the GOE (149), contribute to most $N_2O$ production on modern earth. Net positive $N_2O$ fluxes have been reported for peat land (150), forest (151), agricultural (152) and even permafrost soils (153), supporting the generalized paradigm that $N_2O$ production rates outweigh $N_2O$ consumption rates; however, net negative $N_2O$ fluxes, ranging from -0.0014 to -484 µg $N_2O$-N $m^{-2}$ $h^{-1}$, have been reported in pristine and agricultural ecosystems (154), suggesting some soils are a potential $N_2O$ sink. The net negative $N_2O$ fluxes measured in field sites could not differentiate $N_2O$ absorption (physical process) and its

transformation to $N_2$ (biotic process), and uncertainty exist in the underlying microbiology.

Microorganisms with *nosZ* gene encoding $N_2O$ reductase, known to include clade I and II, could reduce $N_2O$ for the objectives of denitrification, growth-linked respiration, detoxification and electron disposal (18). Soil pH is a key environmental factor influencing microbial $N_2O$ reduction (30). The pH optima of microbial $N_2O$ reduction in literature ranges from 7 to 8, and acidic pH was reported to interfere with $N_2O$ reductase assembly (38, 60), probably via disrupting the Cu cofactor associated histidine residue ligand (5). Most characterized $N_2O$ reducers with clade I *nosZ* could not consume $N_2O$ below pH 6 (38, 39, 110); however, recent advances reported an acidophilic soil bacterium, 'Ca. Desulfosporosinus nitrousreducens' strain PR with a clade II *nos* cluster, reduces $N_2O$ between pH 4.5 to 6 in a sustainable circulating manner (i.e., growth linked $N_2O$ respiration) (Guang, et al., 2023). A coincidental discovery of a clade II thermophile *Nitratiruptor labii*, respiring $N_2O$ between pH 5.4 to 6.4, extends the low pH $N_2O$ reduction to deep marine biosphere (105). Physiology and genetic differences exist between clade I and II $N_2O$ reducers. Clade II $N_2O$ reducers have higher substrate affinity for $N_2O$ (101) and a *nosB* gene, encoding a transmembrane protein of unknown function, has been found exclusively associated with clade II *nos* clusters (12). As such, a hypothesis was generated that low pH $N_2O$ reduction is a shared feature among clade II $N_2O$ reducers that warrants/requires a broader investigation on low pH $N_2O$ reducers. In this study, we enriched low pH $N_2O$-reducing microorganisms from acidic Luquillo Experimental Forest soils (pH 4.5 to 4.9, Puerto Rico) and circumneutral regenerative agricultural soils (pH ~7, Carthage, Tennessee). Characterization of the enrichment cultures revealed that microbial population responsible for low pH $N_2O$ reduction belong to previously unknown taxa. Clade II $N_2O$ reducers are enriched under rigorous acidic condition, validating the hypothesis that low pH $N_2O$ reduction is a shared feature among clade II $N_2O$ reducers. An unexpected, but surprising, discovery of this study is the identification of a functional novel clade (i.e., clade III) NosZ consuming $N_2O$ only at acidic pH.

## 3.2 Materials and Methods

### Soil sampling, microcosms and enrichment cultures

Acidic LEF (i.e., Sabana and Palm Nido sites) microcosms set up and performance were detailed in our prior study (44), and CFF soil (i.e., WS1, WS2, C1 and C1982) containing microcosms were set up in 160 mL glass serum bottles containing 100 mL of anoxic, completely synthetic, acidic (pH 4.5) basal salt medium following established procedure (Guang, et al., under review). A mass of 2.5-gram CFF soils were added to medium containing serum bottles in anaerobic chamber. Lactate and $N_2O$ served as electron donor and acceptors in all microcosms. $N_2O$ was monitored via sampling headspace gas during microcosm incubations.

Transfer cultures were established in 20 mL glass serum bottles containing 9 mL of completely synthetic medium as described with the 0.27 g $L^{-1}$ Tryptone-Soy Broth was augmented to the medium to meet potential nutrient requirement of auxotrophic microbes (Guang, et al., under review). The bottles with N2 headspace were sealed with butyl rubber stoppers (Bellco Glass, Vineland, NJ, USA) held in place with aluminum crimp caps and autoclaved. Measured medium pH ranges from 4.27 to 4.40 following autoclave. All subsequent amendments (i.e., filter-sterilized [0.2 µm polyethersulfone membrane filter] and undiluted gases) to the medium bottles were augmented with sterile plastic syringes and needles. Carbon source and electron donors used for transfer cultures are summarized in Table S2. $H_2$ and $N_2O$, 1-mL of each, were equilibrated for 24 hours in vessels prior to inoculation from corresponding microcosms showing $N_2O$ reduction activity. The microcosms were manually shaken for homogenization before 1 mL aliquots were transfer with 1-mL plastic syringes. Attempts of transition from microcosm to solids-free enrichment cultures, with lactate as carbon source and reducing equivalent, were unsuccessful. As such, carbon alternates plus $H_2$ were tested to resume $N_2O$ reduction activity in transfer cultures. Of note, 0.27 g $L^{-1}$ Tryptone-Soy Broth was augmented to the medium to meet potential nutrient requirement of auxotrophic microbes (Guang, et al., under review). Consecutive transfer in acidic basal salt medium occurred

when the initial dose of 10 mL $N_2O$ had been consumed, which yielded a total of six solid-free cultures showing $N_2O$ reduction activity with an initial pH of 4.5. All culture vessels were incubated in upright position at 30ºC in the dark without agitation.

**Comparative genomic analysis**

Comparative genomic analysis was conducted to identify organisms enriched with $N_2O$ dosing. Cultures grown in the presence or absence of $N_2O$ served as positive or negative controls, respectively. Following $N_2O$ depletion in corresponding cultures, biomass from 5 mL cell suspension samples were collected by centrifugation (10,000 x g, 20 min, 4 ºC), and genomic DNA was isolated from the cell pellets using the DNeasy PowerSoil Kit (Qiagen, Hilden, Germany). Short gun metagenomic sequencing was performed with NovaSeq at the University of Tennessee Genomics Core following published procedures (63). Short gun sequencing generated raw sequences ranging from 12.4 to 20.9 Gbp. Nonpareil v3.4.1 using the weighted NL2SOL algorithm was used to estimate the average coverage level of the metagenomic datasets (89). Quality control, assembly and metagenome assembled genome binning of short read were performed with nf-core/mag v2.1.0 (77) with Nextflow (65) using containerized software in singularity (66). Short read quality was evaluated with FastQC v0.11.9 (67), followed by quality filtering and Illumina adapter removal using fastp v0.20.1. (78). PhiX sequences removal was performed using Bowtie2 v2.4.2 (79) referencing genome GCA_002596845.1, ASM259684v1. Processed short reads from cultures amended with/without $N_2O$ were combined and co-assembled with Megahit2 v1.2.9 (80). Binning of coassemblys was conducted with MetaBAT2 v2.15 (81) and MaxBin v2.2.7 (155), and the resultant bins were refined using DASTools v1.1.6 (156). Metagenome-assembled genomes (MAGs) that passed quality control (completeness > 80%, contamination < 20%) of CheckM v1.2.1 (82) were dereplicated using dRep v3.4.2 (157) for further microbial community profiling. Protein-coding sequences on MAGs were predicted using Prokka v1.14.6 (137). Genome coverage of metagenomic assembled genomes (MAGs) of each metagenome were calculated with CoverM (https://github.com/wwood/CoverM). The coverage evenness of short reads on MAGs were assessed with in-house script

(https://github.com/rotheconrad/00_in-situ_GeneCoverage), based on distribution of high nucleotide identity reads across the reference genome sequences. Taxonomy classification of MAGs were performed using GTDB-TK v2.1.0 with classify workflow (91).

**Phylogenomic analysis**

Phylogenomic reconstruction was performed with genomes of the *Desulfosporosinus*, *Desulfitobacterium*, *Calidifontibacillus*, *Paludibacterium* genus available in the NCBI database. Conserved marker genes of the 20 reference genomes and 7 MAGs (constructed in this study) were identified and aligned with GTDB-TK (91). Phylogenomic relationships were inferred based on the alignment of 120 concatenated bacterial marker genes using RAxML-NG (92) with 1,000 bootstrap replicates. Implemented evolutionary model was selected based on the result of Modeltest-NG (93). Calculation of average amino acid identity (AAI) and hierarchical clustering of taxa based on AAI values were conducted with EzAAI (94). Graphical representation of tree topology and associated metadata were generated using the ggtreeExtra package (158).

**Computational analysis of *nos* operon cluster and NosZ structure modeling**

A total of 173 NosZ reference sequences were downloaded from pre-compiled models of ROCker (96), and was further clustered to 80 representative sequences (75% amino acid identity) to reduce tree topology complexity. Eleven NosZ amino acid sequences were identified and translated from *nosZ* genes in seven MAGs, and were aligned with the 80-representative reference NosZ sequences using MAFFT (97). A maximum likelihood tree of NosZ was constructed with RAxML-NG based on the output evolutionary model of Modeltest-NG. Preliminary phylogenetic analysis of NosZ revealed the deep-branching placement of MAG6 and MAG7 NosZ, and subsequent phylogenetic analysis included homolog amino acid sequences of the two NosZ in NCBI database. Amino acid identity of NosZ was calculated using FastAAI package (159). Accessory genes of the NosZ from a set of 9 genomes described in our prior study (12) were used as PSI-BLAST database to

query accessory genes on MAGs with predicted *nosZ* genes (160). Transmembrane helices in the proteins located downstream of NosZ were predicted with DeepTMHMM based on deep neural networks (90). Signal peptides of NosZ proteins were inferred with SignalP 6.0 (161). Visualization and annotation of phylogenetic tree and associated data was performed using ggtreeExtra package implemented in R (158). Signal peptide of Nos operon amino acid sequences were removed prior to structure prediction with the AlphaFold2 implemented in ColabFold (162). Membrane orientation of proteins was predicted using MembraneFold (163). Active sites (i.e., $Cu_A$ and $Cu_Z$ sites) of NosZ were predicted using AlphaFill (164). The best-predicted NosZ model was selected and loaded into ChimeraX for visualization (165).

**Comparative growth assays with enrichment cultures harboring clade III $N_2O$ reducers**

To validate the functionality of clade III NosZ, comparative growth assays were performed with cultures Sabana and WS2 in 160 mL vessels containing 100 mL medium described above. Replicate cultures amended with or without $N_2O$ were compared to verify the growth of clade III $N_2O$ reducers is $N_2O$-dependent. Cultures was also grown in pH 7 medium, where 30 mM bicarbonate replaces 50 mM $KH_2PO_4$, to testify the capacity of $N_2O$ reduction at circumneutral pH.

**Quantitative PCR**

SYBR Green quantitative PCR (qPCR) assays targeting the clade III *nosZ* genes of MAG6 and MAG7 were designed using Geneious Prime. Primer were examined by in silico analysis using the Primer-BLAST tool, and experimentally confirmed using 1,599 bp-long synthesized linear DNA of the respective *nosZ* genes of the MAG6 and MAG7 (Integrated DNA Technologies, USA). The two different nosZ genes could be amplified with the same primer set (395F-527R). For enumeration of clade III *nosZ* genes, 25 µL qPCR tubes received 10 µL 1X Power SYBR Green, 9.88 µL UltraPure nuclease-free water (Invitrogen, Carlsbad, CA, USA), 300 nM of each primer (395F:

GACCGTTTGGACCTCACCAT and 527R: CCGCCGGAAACATCGATTTC), and 2 µL template DNA. All qPCR assays were performed using an Applied Biosystems ViiA 7 system (Applied Biosystems, Waltham, MA, USA) with the following amplification conditions: 2 min at 50ºC and 10 min at 95ºC, followed by 40 cycles of 15 s at 95ºC and 1 min at 60ºC. The standard curves were generated using 10-fold serial dilutions of the linear DNA fragments carrying a complete sequence of MAG6 (1,599 bp) or MAG7 (1,599 bp) *nosZ* gene, covering the same 133-bp qPCR target region.

The qPCR standard curves established with the linear DNA fragments carrying complete MAG7 *nosZ* gene had slopes of -3.471, y-intercepts of 36.431, $R^2$ values of 0.998, and qPCR amplification efficiencies of 94.119%, respectively. The linear range spanned 8.54 to 8.54 x $10^8$ gene copies per reaction. The functional analysis indicated that both the MAG6 and the MAG7 carry a single *nosZ* gene, indicating that the enumeration of *nosZ* gene allows estimates of cell abundances.

## 3.3 Results

### Low pH $N_2O$ reducers enriched from circumneutral and acidic soils

The in-situ pH of Luquillo Experimental Forest and Caney Fork Farm soils ranged from 4.72 to 4.97 (43) and 6.74 to 6.98, respectively (Table 3-1). As such, the two type soils are representative acidic natural and circumneutral agricultural soils. $N_2O$ consumption at pH 4.5 was observed in all microcosms with corresponding soils (one microcosm set up for each soil) amended with lactate as a source of carbon and reducing equivalents, and the $N_2O$ reduction performance differed strikingly between the microcosms with LEF and CFF soils. The initial doses (10 mL, 4.16 mM nominal) of $N_2O$ in LEF microcosms were consumed following 4-month incubation (44), whereas complete disappearance of same amount of $N_2O$ was observed in CFF microcosms after two weeks. Transition from microcosm to soils-free enrichment cultures with lactate at pH 4.5 resulted in the loss of $N_2O$ reduction activity; subsequently alternative carbon sources and electron donors were tested aiming to resume $N_2O$ reduction activity in transfer cultures. The initiation of $N_2O$

reduction in CFF soil- and Sabana (LEF soil) soil-derived transfer cultures occurred with fumarate, whereas Palm Nido (LEF soil) soil-derived cultures required succinate, respectively (Table 3-2). Consecutive transfers performed in closed glass serum bottles (20 mL) containing defined pH 4.5 mineral salt medium (10 mL), tryptone-soy broth (0.1g $L^{-1}$), the respective carbon source (5 mM), and $H_2$ (10 mL, 4.16 mM nominal) yielded stable enrichment cultures that reduced $N_2O$ at rates ranging from 0.39 to 1.53 mM $day^{-1}$ (Supplementary Figure 3-1). Complete $N_2O$ consumption was not observed in cultures lacking $H_2$, indicating $H_2$ was the direct electron donor for $N_2O$ reduction. Over the course of the incubation, an increase in pH by 0.5 to 0.7 units was observed in enrichment cultures with carbon sources added at 5 mM concentration. With lower 0.5 mM concentrations, pH changes were <0.5 pH units, but the lag times for the initiation of $N_2O$ consumption increased.

Circumneutral (pH 7) soil microcosms were established with the CFF and PR soils, and transition from microcosms to soils-free transfer cultures (pH 7) was easily achieved in defined pH 7 medium with lactate; however, $N_2O$ reduction activity was abolished following the transitions from pH 7 to pH 4.5 medium. Consecutive transfers and dilution-to-extinction assays were further performed on WS2 and Sabana cultures in pH 7 medium amended with 5 mM lactate plus 10 mL (4.16 mM nominal) $N_2O$. The transfer procedure commenced in pH 7 medium rapidly resulted in highly enriched cultures; 16S rRNA based amplicon sequencing showed that *Azospira* population accounting for more than 99.9% of the total sequences in the pH 7 culture derived from Sabana soils.

**Novel species involved in low pH $N_2O$ reduction**

To identify the microbial taxa involved in low pH $N_2O$ reduction, shot-gun metagenome sequencing was performed to six different enrichment cultures grown with and without $N_2O$ (Supplementary Figure 3-2). Metagenomes of transfer cultures and the original soils were compared to evaluate the enrichment effort. Nonpareil analysis (Supplementary Figure 3-3) showed that the microbiota in PR- and CFF-soils and were highly diverse or poorly sequenced with sequence coverages ranging from 26.04% and 40.01% sequence

coverages. In contrast, the extracted community DNA of enrichment cultures were completely sequenced; the enrichment cultures had sequence coverages of at least 98.91%.

Population genome binning was performed with contigs from the coassembly (combining metagenomes from the same cultures with/without $N_2O$). Following quality assessment (completeness > 80% and contamination < 25%) and dereplication (95% ANI threshold), a total of 43 MAGs were retained for profiling microbial community (Supplementary Figure 3-3). Only small portions (5.53- 29.4%) of the short-read sequences could not be recruited to the high-quality MAGs, suggesting the 43 MAGs capture the diversity of each of the six enrichment cultures (Supplementary Figure 3-4). Community structures showed a strong impact of $N_2O$ on community composition (profiled based on high-quality MAGs). Specifically, MAGs representing the class *Desulfitobacteriia* accounted for 14.1% to 81.7% of the total short-read sequences in cultures fed with $N_2O$ except for C1. In the same cultures without $N_2O$, *Desulfitobacteriia* represented no more than 5% of the total sequences. In culture C1, *Bacilli* population showed strong relationship to $N_2O$ and contributed 23.2% of the total sequences (versus 1.15% without $N_2O$). Recruitment of metagenomes of LEF soils (n=2) and CFF soils (n=18) to the 43 high-quality MAGs was not successful, suggesting they have a low abundance, or are not representative population in the original soils.

To shed light on the $N_2O$ reducers enriched at pH 4.5, the 43 MAGs were annotated with Prokka and screened for *nosZ* genes. A total of 7 MAGs were predicted to possess at least one *nosZ* gene sequence, and 5 of the 7 MAGs were remarkably more abundant in cultures received $N_2O$. Interestingly, MAG7 representing *Desulfitobacterium* 1 population were consistently enriched in culture WS1, WS2, and C1982 though the initial inoculum source (soils) differed (Figure 3-1 A). In culture C1, MAG1 representing *Calidifontibacillus* was more abundant in the presence of $N_2O$, suggesting its growth is $N_2O$-dependent. MAG3 (*Desulfosporosinus* 1) and MAG2 (*Paludibacterium*) showed contrasting pattern in culture Palm; MAG3 and MAG2 were more abundant in the presence or absence of $N_2O$, respectively. Surprisingly, MAG4 (*Desulfosporosinus* 2)

exclusive to culture Palm amended with $N_2O$ was identical to '*Ca.* Desulfosporosinus nitrousreducens' strain PR (ANI > 99.9%) characterized in a co-culture (Guang, et al., 2023); while the partner bacterium *Serratia* sp. MF is not present in culture Palm. In culture Sabana, MAG6 representing a *Desulfitobacterium* 2 different from that present in CFF cultures (i.e., WS1, WS2, and C1982) was highly abundant (> 80%) in the presence of $N_2O$.

An insightful observation is that all *nosZ*-carrying MAGs recovered the low pH $N_2O$-reducing cultures represent previously unknown species in the corresponding genera (

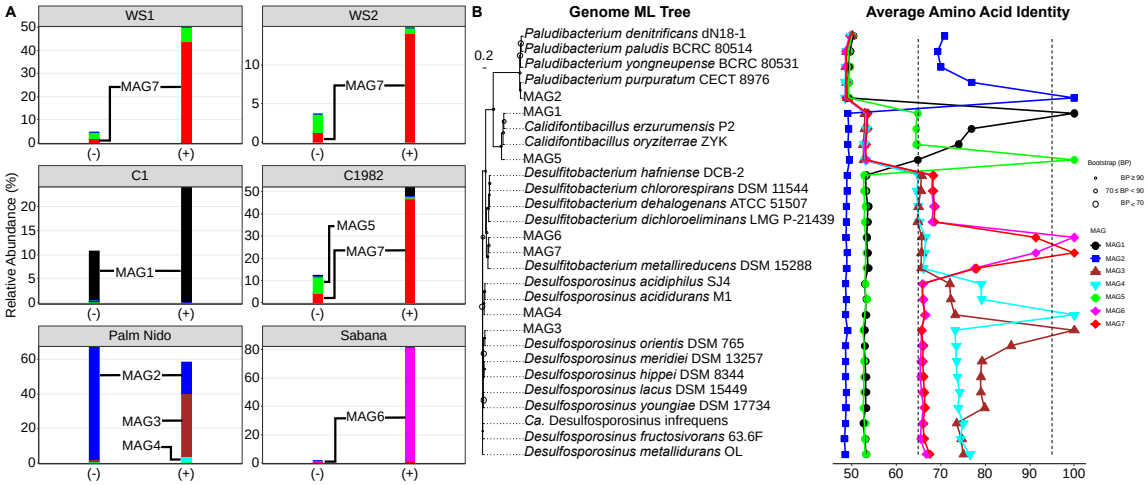


Figure **3-1** B). Albeit assigned to the same genus, the MAG3 and MAG4 are respectively more related to acidophilic *Desulfosporosinus* species (i.e., *D. acididurans* and *acidophilus*) and *Desulfosporosinus orientis*, none of which have the genetic machinery (*nos* operon) for $N_2O$ reduction. The MAG6 and MAG7 have the highest average amino acid identity (AAI: 91.3%) among the overall pairwise comparison, suggesting they represent different species that closely related to the *Desulfitobacterium metallireducens* lacking the *nos* gene cluster (166). MAG1 and MAG5 are affiliated with *Calidifontibacillus* species, among which two different *nos* gene clusters were found on the genome of *Calidifontibacillus oryziterrae* strain ZYK.

**Identification of clade III *nosZ***

A total of eleven *nosZ* genes were recovered from the seven high-quality MAGs. To demonstrate the *nosZ* of high-quality MAGs captures the comprehensive *nosZ* diversity in the twelve metagenomes, complete (> 500 bp) NosZ sequences were extracted from the coassembly (six in total) corresponding to each culture. Comparison of the assembly- and high-quality MAGs-derived NosZ (11 vs 11 genes) suggested the latter were sufficient to represent the overall NosZ diversity in the low pH $N_2O$-reducing enrichment cultures. MAGs representing *Desulfosporosinus* (MAG3 and 4), *Desulfitobacterium* (MAG6 and 7) and *Paludifontibacillus* (MAG2) species were predicted to have a single NosZ sequence, whereas four and two different NosZ sequences were found on MAG1 and MAG5 belonging to *Calidifontibacillus*. Initial phylogenetic analyses placed NosZ sequences derived from acidic enrichment cultures to either clade I or clade II (Supplementary Figure 3-5). However, the deep-branching placement of MAG6- and MAG7-NosZ suggest they do not belong to either clade I or clade II, as the pairwise identity calculated for the two NosZ to other NosZ is no more than 30%. As such, the NosZ sequences of MAG6 and MAG7 were blasted against NCBI nr database, and the top 21 best hit sequences were included in following phylogenetic analyses (Figure 3-2).

Phylogenetic analyses including the reference-, acidic cultures-derived NosZ and the putative NosZ identified three independent NosZ lineages (Figure 3-2A), with the clade I and clade II being described previously (12, 22). MAG2 *nosZ*, associated with a clade I *nos* operon cluster (i.e., *nosZDFYL*, Figure 3-2 B), was clustered with clade I group. The *nosZ* genes of MAG1, 3, 4 and 5, followed immediately by a *nosB*, fell into clade II group. Interestingly, the multiple *nos* operon clusters of the same MAGs (i.e., MAG1 and 5) showed different structures (Figure 3-2 C). For instance, one of the four *nos* operon clusters from MAG1 lacks the *nosB* gene, encoding a transmembrane protein of unknown gene. Moreover, the four *nosZ* recovered from MAG1 shared no more than 72.5% amino acid identity (Supplementary Figure 3-6). These observations suggest *nosZ* diversification occurrs within individual population. The deep-branching *nosZ* genes recovered from MAG6 and 7, and the putative *nosZ*, most of which are recovered from metagenomic based studies, constituted a previously unknown clade and is hereafter

referred as clade III (Figure 3-2 D). Interestingly, clade III harbors MAGs representing *Nitrospira* bacterium, contradicting current recognition that *nosZ* genes are not found in *Nitrospira* (167). Most of the clade III NosZ (20 of 23 sequences) have a N-terminal Sec signal peptide, a feature shared with clade II NosZ. The clade III is coincided with the novel *nosZ* clade previously proposed in a metagenomic study of groundwater (168), yet the $N_2O$ reduction capacity of the *nosZ* requires experimental verification. The MAG6- and MAG7-*nosZ* and the putative *nosZ* genes all encode a N-terminal seven blade beta-propeller domain ($Cu_Z$ center) and a C-terminal cupredoxin domain ($Cu_A$ center), a characteristic found in both clade I and clade II *nosZ* (169). Among the clade I and II type NosZ, the Cuz-binding motifs associated with the first two histidine residues, DxHH, exhibited 100% conservation. Less conserved histidine residues were found in the $Cu_Z$-binding motifs of the putative clade *nosZ* (i.e., DxHx).

**Structural and functional validation of clade III *nosZ* in enrichment cultures**

Structure of the NosZ and closely related proteins (i.e., *nos* gene cluster) recovered from MAG6 were predicted using Alphafold2 with templates in PDB100 database as query structures. High-confidence structures were obtained for the corresponding protein sequences (Supplementary Figure 3-7), as assessed by the sequence coverage and predicted per-residue confidence measure (pLDDT). Among the eight protein sequences, NosZ and two hypothetical proteins were predicted to be periplasmic lipoprotein, whereas other proteins are cytoplasmic membrane-bounding or anchored. Specifically, a homodimer structure (pLDDT > 90) was predicted for NosZ, with two copper containing active sites present (Figure 3-3 A). Two conserved histidine and cysteine residues are associated with the electron transfer site (i.e., $Cu_A$), whereas seven conserved histidine residues are associated with the catalytic site (i.e., $Cu_Z$). An unexpected observation is an additional tyrosine associated with $Cu_Z$ site (Figure 3-3 B), but the physiology implication of this tyrosine in $Cu_Z$ site remains to be demonstrated yet.

Microbial profiling of transfer cultures suggested the same clade III $N_2O$ reducers, MAG7, was consistently selected in culture WS1, C1982 and WS2

(

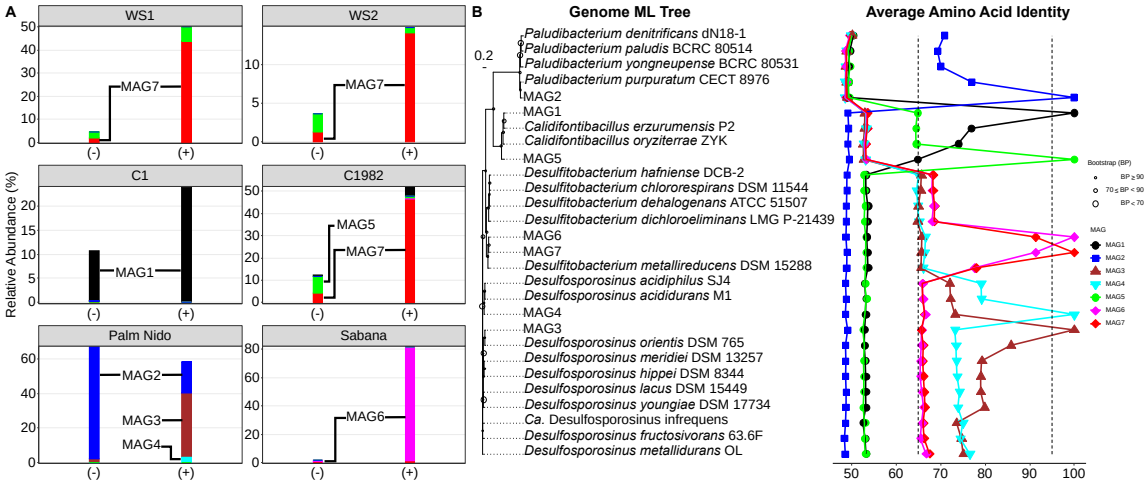


Figure **3-1** A); while MAG6 was only enriched in culture Sabana. As such, the culture WS2 and Sabana was maintained for further study. Following consecutive transfers were performed on culture Sabana and WS2, with which a 27$^{th}$ Sabana and 15$^{th}$ WS2 transfer cultures harboring the clade III $N_2O$ reducers were obtained. Subsequently triplicate cultures Sabana and WS2 growing in acidic medium consumed the initial dose of $N_2O$ (i.e., 416 µmol) over a 3-day incubation (Figure 3-3 C). In contrast, cultures incubated in circumneutral pH medium showed no $N_2O$ consumption over 10-day incubation. Consistent with $N_2O$ consumption, cells (measured by qPCR-targeting clade III *nosZ* gene) representing MAG6 in culture Sabana and MAG7 in culture WS2 increased by (25.7 ± 2.9) and (14.5 ± 2.8) folds, respectively (Table 3-5). Growth yields of (8.3 ± 1.1) x $10^8$ and (3.2 ± 0.9) x $10^{10}$ cells mmol $N_2O^{-1}$ were determined for MAG6 and MAG7 in culture Sabana and WS2, respectively. In control cultures omitting $N_2O$, increase in cells representing MAG6 and MAG7 was not substantial (less than 1-fold increase), suggesting their growth is $N_2O$-dependent under the conditions tested. No growth of MAG6 and MAG7 was observed in pH 7 cultures in the presence of $N_2O$, demonstrating

the $N_2O$ reduction activity of the clade III $N_2O$ reducers (i.e., MAG6 and MAG7) is limited to acidic pH.

Comparative Reverse Transcriptional qPCR (RT-qPCR) analyses were performed on cultures (Sabana and WS2) that were actively consuming $N_2O$, with cultures omitting $N_2O$ served as control. The transcribed *nosZ* in cultures Sabana and WS2 received $N_2O$ reached (44.7 ± 11.4) and (107 ± 51.8) copies ng $RNA^{-1}$, respectively; whereas the transcribed *nosZ* decreased to (9.65 ± 4.38) and (24.6 ± 20.1) copies ng $RNA^{-1}$ in cultures Sabana and WS2 omitting $N_2O$, respectively. Significance analyses ($p < 0.05$) suggest that the *nosZ* transcriptions were enhanced by (4.91 ± 0.9) and (5.13 ± 1.64) folds in cultures Sabana and WS2 in the presence of $N_2O$, respectively (Fig. 4, inset graph). The *nosZ* transcripts were lower than (2.9 ± 3.33) copies ng $RNA^{-1}$ in all cultures received $N_2O$ incubated at pH 7, an observation consistent to the ceased $N_2O$ reduction activity. In line with RT-qPCR results, the amount of assembled clade III NosZ (measured by metaproteomic) increased by (1.4 ± 1.5) and (2.3 ± 0.4) folds in Sabana and WS2 cultures responding to the $N_2O$ amendment, with the increase in WS2 cultures being significant ($p < 0.05$).

### 3.4 Discussion

The present study challenged the decade-lasting view that NosZ are divided into clade I and II lineages. The discovery of $N_2O$-dependent respiratory growth of clade III $N_2O$ reducers advances the understanding of *nosZ* diversity involved in $N_2O$ reduction, and has far-reaching implication in underexplored soil microbial $N_2O$ reduction potentials. Current approaches (e.g., sequencing and qPCR) estimating soil $N_2O$ reduction potential only target clade I and clade II NosZ (170), leaving the clade III NosZ out of consideration, tentatively due to the failure in identification and cultivation of members of clade III lineage. A metagenome-based study suggested the putative clade III $N_2O$ reducers (i.e., *Nitrospinota* and *Nitrospira* bacterium) are present in groundwater and the NosZ was transcriptional active (168); however, the $N_2O$ reduction capacity of members in clade III was still not resolved. We demonstrated the growth supporting $N_2O$ reduction

of two population (MAG6 and MAG7) have a clade III *nosZ* gene, which provides experimental evidence the clade III NosZ is of functionality. The function of clade III NosZ was validated with multiple lines of evidence: Comparative growth assays of culture WS2 and Sabana revealed the $N_2O$-dependent respiratory growth; AlphaFold prediction of clade III NosZ showed a homo-dimeric structure containing the electron transfer $Cu_A$ site and catalytic $Cu_Z$ site; RT-qPCR and proteomics analyses suggest NosZ expression depends on $N_2O$ amendment. Although the in-situ detection in soil samples (LEF soils) with qPCR assays targeting the clade III *nosZ* (MAG6 and MAG7-NosZ) gene was unsuccessful, enrichment of the clade III $N_2O$ reducers from distant biomes (CFF and LEF) illustrated they represent rare biosphere but readily responsive to $N_2O$. Distribution of the clade III NosZ warrants further investigation of environmental samples, which would possibly leverage the genomic potential of $N_2O$ reduction in various ecosystems.

In this study, we sampled soils from circumneutral (pH ~ 7) sub-tropical agricultural (i.e., CFF) (171) and acidic (4.5 < pH < 5.0) tropical forest sites (i.e., LEF) (43) that represent contrasting soil types. We showed that continuous cultivation and enrichment of microorganisms directly using exogenous $N_2O$ under acidic conditions is a successful strategy to obtain acidic $N_2O$ respiring microorganisms and characterize them. The unusual cultivation strategy (alternate carbon source [fumarate and succinate] plus $H_2$) resulted in the enrichment of seven previously unknown *nosZ*-carrying bacteria, all of which belong to the genus (i.e., *Calidifontibacillus*, *Desulfosporosinus* and *Desulfitobacterium*) have not been implicated in $N_2O$ reduction yet (i.e., lack experimental validation). In contrast, cultivation and enrichment of the same soils (i.e., Sabana) performed at pH 7 derived well-studied microorganisms (i.e., *Azospira*) (110, 172), representing most cells (accounting > 99% of the 16S rRNA amplicons) in the cultures following less than fifteen consecutive transfers; however, those pH 7 transfer cultures cannot consume $N_2O$ in pH 4.5 medium. This finding is consistent to generalized observation: $N_2O$ reducers obtained under circumneutral conditions are incapable of low pH $N_2O$ reduction (36, 38, 39), and maintaining acidic pH is crucial to cultivate acidic

$N_2O$ reducers (Guang, et al., 2023). Interestingly, the acidophilic '*Ca.* Desulfosporosinus nitrousreducens' strain PR in a consortium consisted of two population, derived from El Verde Field station, was also enriched in the low pH $N_2O$-reducing culture derived from Palm Nido soil. The two sites, El Verde field station and Palm Nido, have contrasting soil physicochemical parameters such as elevation (453 m for EV and 634 m for PN) and represent different life zones (43). A coincidental observation is the clade III *nosZ*-carrying MAG7 was consistently selected in cultures enriched from the soils from three separate sites in CFF. The same population could be readily enriched from different soils lend strong experimental credibility to the hypothesis that low pH $N_2O$ reducing microorganisms are more widely distributed than first thought (Guang, et al., 2023).

pH has been considered the major factor limiting $N_2O$ reduction activity in acidic biomes (e.g., soils and oceans) (37, 173), and was explained by microbial failure to assemble functional NosZ under acidic conditions (pH < 6) (40). The generalized paradigm was recently challenged by the acidophilic $N_2O$-reducing '*Ca.* Desulfosporosinus nitrousreducens' strain PR with a clade II *nos* operon cluster (Guang, et al., 2023) and the deep-sea isolate, *Niratiruptor labii* HRV44 (105). The 'Ca. Desulfosporosinus nitrousreducens' strain PR was enriched from the acidic tropical forest (pH < 5), thus raised a question: Does acidophilic $N_2O$ reducers exist in circumneutral soils? The successful enrichment of $N_2O$-reducing cultures under acidic conditions from circumneutral CFF soils suggest that low pH $N_2O$ reducers are not limited to acidic soils. The naturally acidic sites on the Earth are known to thrive a variety of acidophilic microorganisms (45), whereas the circumneutral soil are overlooked source of acidophiles. Soils are complex matrixes with high pH heterogeneity, and pH varies by as much as 1.3 pH among samples less than 50 cm apart (46). The microbial metabolism could have led to more contrasting pH at finer scale: the microscale varied by 2 pH in spots localized closely (less than 5 mm) following straw patch amendment (47). Obviously, acidic microsites could occur in circumneutral CFF soils and harbor the acidophilic $N_2O$-reducing microorganisms. This finding has far-reaching implications in

predicting $N_2O$ emissions as the acidophilic $N_2O$ reducing microorganisms would thrive to cope with increased $N_2O$ emissions associated with soil acidification.

Prior to this study, $N_2O$ reducers were known to include clade I and II, with the former mostly possess all genes involved in denitrification of $NO_3^-$ to $N_2$ (23). Physiology and genomic features distinguish clade I versus clade II NosZ, suggesting niche differentiation may exist within and between the two clades. The NosZ is a periplasmic enzyme, which must be transported across inner membrane. Clade I NosZ are translocated in a folded state using the Twi-arginine pathway (Tat-pathway) whereas clade II NosZ are translocated as unfolded protein via the general secretion route (Sec-pathway) (12). The translocation pathway may influence the pH range of clade I and II NosZ. Metagenomic investigation of acidic LEF soils suggest that clade II *nosZ* dominated the *nosZ* gene pool ( > 10% of total *nosZ* reads) (43), and pH selected for different clade II $N_2O$ reducers in the LEF soils-derived microcosms (44). Coincidently, $N_2O$ consumption activity in acidic microcosms increased proportionally with the clade II *nosZ* abundance (5). In line with prior studies, our comparative metagenome analyses with soils-free cultures grown with/without $N_2O$ amendment identifies that all active $N_2O$ reducing microorganisms possess clade II or clade III (with Sec peptide) *nosZ*, suggesting low pH $N_2O$ reduction may be a shared feature in clade II and clade III $N_2O$ reducers. Growth of the clade I *nosZ*-carrying microorganism (MAG2, *Paludibacterium*) in culture Palm was $N_2O$-independent at pH 4.5, suggesting its growth depends on fumarate fermentation. This observation is consistent to the failure of $N_2O$ reduction by *Ensifer meliloti* (clade I) at pH 6, whereas oxygenic respiration was not influenced at pH 6 (39). A possible explanation is the oxygen respiration and fumarate fermentation occur in cytoplasm, where the pH was maintained relatively stable via homeostasis; however, $N_2O$ reduction occurs in periplasm, where the pH is more impacted by external environments.

Genomic and Phenotypic differences have been documented in clade I and clade II $N_2O$ reducers, implicating niche differentiation existing between the two evolutionary distinct lineages (12). For example, the co-occurrence rate of *nosZ* and *nirK*/*nirS* was much higher in clade I (83%) than clade II $N_2O$ reducers (49%) (23), suggesting clade II $N_2O$

reducers are more likely to be obligate $N_2O$ sink. Furthermore, kinetic study demonstrated that clade II and clade I $N_2O$ reducers are more likely to acclimate oligotrophic and eutrophic conditions, respectively (101). Therefore, oligotrophic conditions rich with $N_2O$ are proposed to favor growth of clade II over clade I $N_2O$ reducers. Indeed, laboratory enrichment documented that clade II outweigh clade I $N_2O$ reducers when $N_2O$ was the sole electron acceptor, while clade I $N_2O$ reducers were more abundant with $NO_3^-$ as electron acceptor (174). In contrast, most $N_2O$ reducers isolated on eutrophic medium (i.e., Tryptone-Soy Agar) were close relatives to clade I associated taxa and produced $N_2O$ via denitrification (116). In current research, clade II $N_2O$ reducers acclimated cultures growing in oligotrophic medium (containing 1% v/v TSB) in response to $N_2O$ additives. The enriched clade II $N_2O$-reducing organisms are of concern in bioaugmentation perspective as they are predicted to be non-denitrifiers (i.e., lack *nirS*/*nirK* genes) and are potential $N_2O$ scavengers in soils. Soils become net $N_2O$ sources when $N_2O$-producing rates exceed $N_2O$-reducing rates (154), while soils turn to be net $N_2O$ sink when $N_2O$-consuming organisms outcompete $N_2O$-producing organisms (175). Acidic soils have long been considered major $N_2O$ emitters as acidic conditions favor $N_2O$ formation over its consumption in denitrifying organisms (38, 40). As such, the non-denitrifying organisms reducing $N_2O$ under acidic conditions offer a golden opportunity to shift acidic soils into net $N_2O$ sinks if their growths are favored over denitrifying organisms.

The $N_2O$ reduction was hypothesized an ancient trait that appeared before or after the ‘great oxygen event (GOE)’, 2.8-2.5 Gyr before present (23). Phylogenetic analysis indicated *nosZ* has evolved predominantly via vertical inheritance and some instances of horizontal gene transfer (HGT) (176, 177). Following the definition of clade II lineage, phylogenetic diversity of *nosZ* and microbial taxa have been greatly expanded (12). In contrast to the narrow distribution of clade I *nosZ* among *Proteobacteria* phyla, the clade II *nosZ* appeared to be shared by evolutionary distant phyla (e.g., *Firmicutes* and *Chloroflexi*) (22). Furthermore, the increasing clade II *nosZ* diversity indicated its potential in mitigating $N_2O$ emissions from diverse soil ecosystems. For example, *nosZ*

has not been detected from the genomes of *Actinobacteria* or *Acidobacteria* that are associated with low resource availability and low pH conditions in terrestrial ecosystems during the past decades (23). However, in-depth characterization of microbial communities in tundra soils identified *nosZ*-carrying organisms affiliated with *Acidobacteria*, associated with acidic conditions (24), implying its role in $N_2O$ consumption was underexplored.

The clade II and III *nosZ* genes acquired in current research expanded the *nosZ* diversity associated with low pH $N_2O$ reduction. Organisms carry clade II *nosZ* genes are classified as *Desulfosporosinus*, *Calidifontibacillus* and clade III *nosZ*-carrying organisms are affiliated with *Desulfitobacterium*. In consistent to previous studies (22, 178), the *nosZ* phylogeny of *Calidifontibacillus* and *Bacillales* showed congruence to the hierarchical taxonomic classification, suggesting the *nosZ* genes were attained via vertical heritance events within these taxa. Incongruence between *nosZ* and taxonomic phylogeny was observed for *Desulfitobacterium* and *Desulfosporosinus* population, suggesting higher diversification within the taxa. The deep-branching subclade comprising *Desulfitobacterium nosZ* was unexpected, as the *nosZ* of *Desulfitobacterium* are defined as clade II. In supporting the evolutionary difference, the multiple sequence alignment analysis identified partially conserved histidine ligands of the $Cu_z$ center within the clade. In addition, the NosD protein (encoded by *nosD*), delivering $Cu^{2+}$ to $Cu_z$ center in *Pseudomonas stutzeri* (clade I lineage) (169), was absent in the deep-branching *Desulfitobacterium nosZ* clade. However, the assembly machinery may differ between clade I, II and III $N_2OR$ as the folding processes occur in different cell compartments (cytoplasm vs. periplasm) (23). Therefore, the role of *nosD* in the deep-branching *nosZ* cluster remains questionable. Taken together, the deep-branching *nosZ* clade was proposed a putative novel *nosZ* lineage specialized in low pH $N_2O$ reduction.

## Appendix

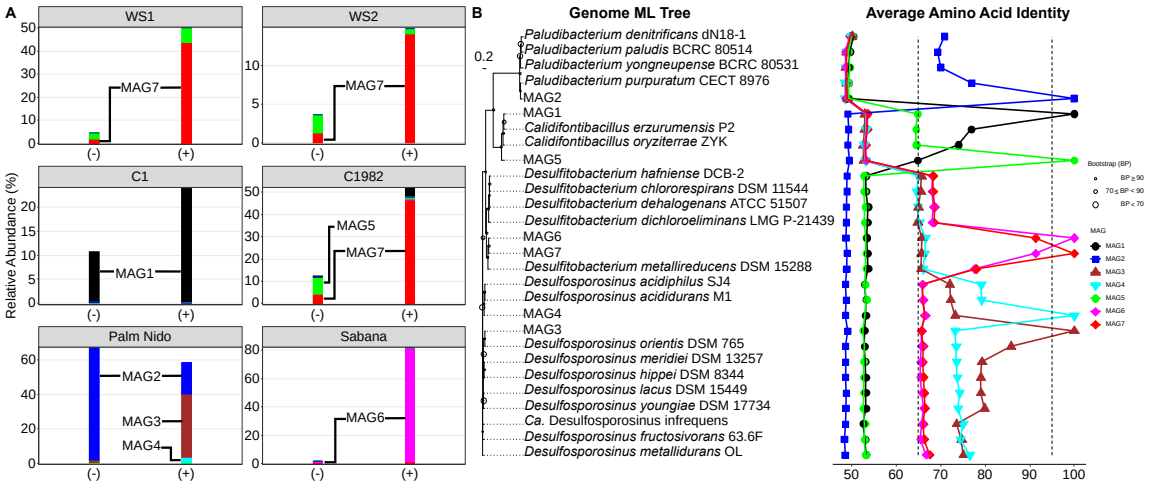


**Figure 3-1. Novel microbial guilds implicated in $N_2O$ reduction.** (A) Distribution of putative $N_2O$-reducing population in transfer cultures with (+) or without (-) $N_2O$ amendment. The relative abundance (% of the total metagenome fragments) of MAGs was calculated using CoverM (https://github.com/wwood/CoverM). Taxonomy was assigned to MAGs using GTDB-TK (91). Displayed are MAGs predicted to have at least one *nosZ* gene based on Prokka annotation (137). The comprehensive microbial community profiled with the 43 high-quality MAGs are summarized in Fig. S4. (B). Phylogenomic analyses of *nosZ*-carrying MAGs recovered from low pH $N_2O$-reducing cultures. The tree topology was obtained from the Maximum Likelihood (ML) tree by using RAxML-NG (92), inferred from a 120 conserved marker genes alignment of 20 complete genomes (selected based on GTDB-TK results) (91) and 7 MAGs. The top scale bar indicates 0.2 amino acid substitution rates per site. Sizes of open circles alongside the branches of each sublineage indicate bootstrap percentages obtained by RAxML-NG. The pairwise genome-wide AAI calculated for each MAGs are shown on the right, with the scale displayed on the bottom. Values for each comparison for a given MAGs are connected by lines, and the comparison to self is indicated as 100%. Pair-wise AAI values of 65-95% (i.e., data points fall between the dashed lines) are indicative of

species boundary (179). The color legend corresponds to the bar and line colors in panel (A) and (B).

**Figure 3-2. Phylogenetic trees showing the placement of acidic cultures derived NosZ (green) among the reference NosZ (black) and putative NosZ (red).** (A) Unrooted phylogenetic tree of NosZ showing three independent clades (i.e., I, II and III). The tree topology was inferred from RAxML-NG. Bootstrap values are displayed as white (> 90%), grey (70 < BP < 90) and black circles (< 70%). (B) Phylogenetic tree showing clade I NosZ with branches belonging to clade II and clade III collapsed. (C) Phylogenetic tree showing clade II NosZ with branches belonging to clade I and clade III collapsed. (D) Phylogenetic tree showing clade III NosZ with branches belonging to clade I and clade II collapsed. Of note, the MAG4 *nos* gene cluster is identical to '*Ca.* Desulfosporosinus nitrousreducens' in a co-culture reported in a prior study (Guang, et al., 2023). Accessory genes associated with *nosZ* are displayed as oriented arrows and gene designation is represented by color legend in panel D.

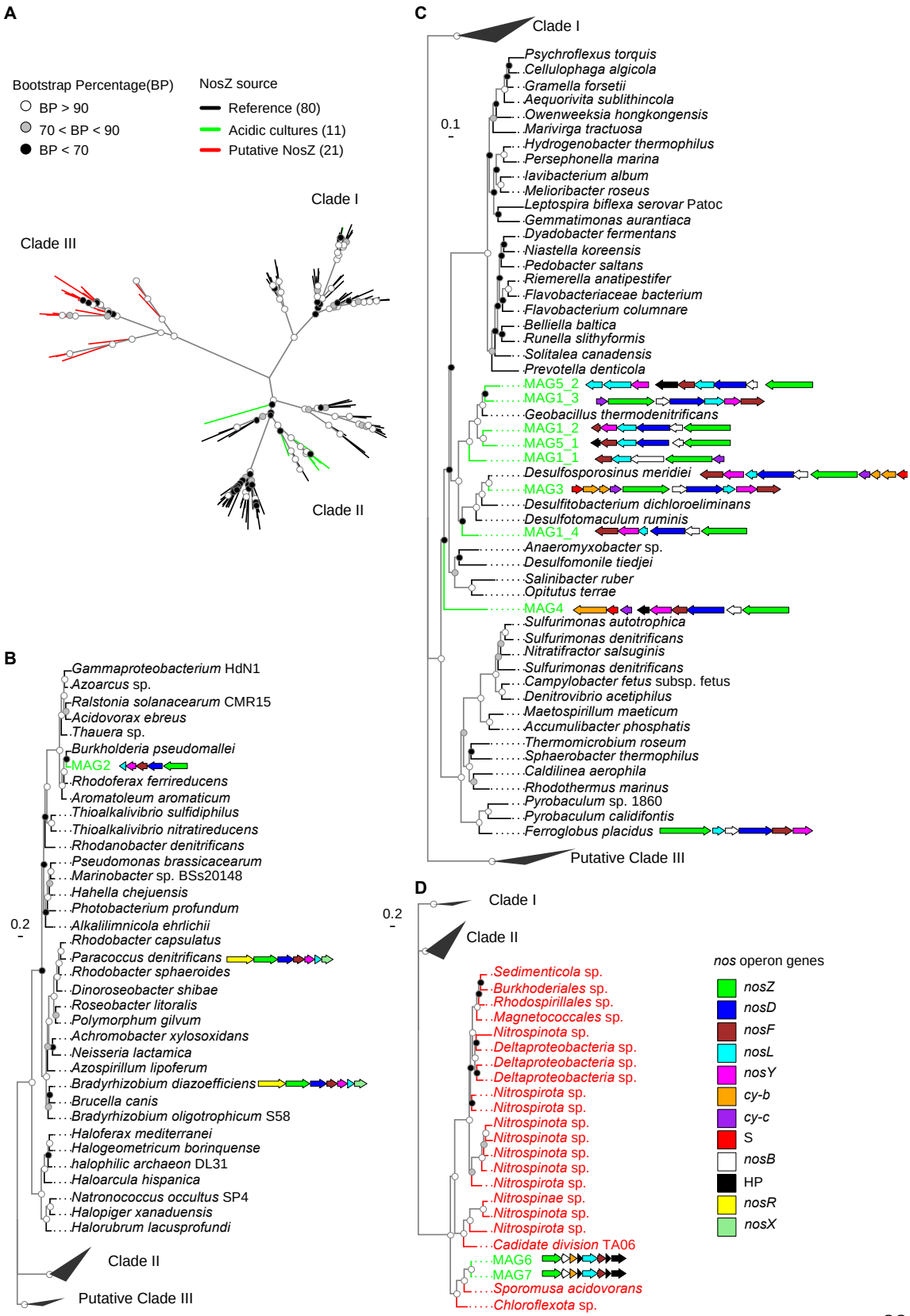
A
Bootstrap Percentage(BP)
BP > 90
70 < BP < 90
BP < 70
NosZ source
Reference (80)
Acidic cultures (11)
Putative NosZ (21)
Clade I
Clade III
Clade II
B
Gammaproteobacterium HdN1
Azoarcus sp.
Ralstonia solanacearum CMR15
Acidovorax ebreus
Thauera sp.
Burkholderia pseudomallei
MAG2
Rhodoferax ferrireducens
Aromatoleum aromaticum
Thioalkalivibrio sulfidiphilus
Thioalkalivibrio nitratireducens
Rhodanobacter denitrificans
Pseudomonas brassicacearum
Marinobacter sp. BSs20148
Hahella chejuensis
Photobacterium profundum
Alkalilimnicola ehrlichii
Rhodobacter capsulatus
Paracoccus denitrificans
Rhodobacter sphaeroides
Dinoroseobacter shibae
Roseobacter litoralis
Polymorphum gilvum
Achromobacter xylosoxidans
Neisseria lactamica
Azospirillum lipoferum
Bradyrhizobium diazoefficiens
Brucella canis
Bradyrhizobium oligotrophicum S58
Haloferax mediterranei
Halogeometricum borinquense
halophilic archaeon DL31
Haloarcula hispanica
Natronococcus occultus SP4
Halopiger xanaduensis
Halorubrum lacusprofundi
0.2
Clade II
Putative Clade III
C
Clade I
Psychroflexus torquis
Cellulophaga algicola
Gramella forsetii
Aequorivita sublithincola
Owenweeksia hongkongensis
Marivirga tractuosa
Hydrogenobacter thermophilus
Persephonella marina
Iavibacterium album
Melioribacter roseus
Leptospira biflexa serovar Patoc
Gemmatimonas aurantiaca
Dyadobacter fermentans
Niastella koreensis
Pedobacter saltans
Riemerella anatipestifer
Flavobacteriaceae bacterium
Flavobacterium columnare
Belliella baltica
Runella slithyformis
Solitalea canadensis
Prevotella denticola
0.1
MAG5_2
MAG1_3
Geobacillus thermodenitrificans
MAG1_2
MAG5_1
MAG1_1
Desulfosporosinus meridiei
MAG3
Desulfitobacterium dichloroeliminans
Desulfotomaculum ruminis
MAG1_4
Anaeromyxobacter sp.
Desulfomonile tiedjei
Salinibacter ruber
Opitutus terrae
MAG4
Sulfurimonas autotrophica
Sulfurimonas denitrificans
Nitratifractor salsuginis
Sulfurimonas denitrificans
Campylobacter fetus subsp. fetus
Denitrovibrio acetiphilus
Maetospirillum maeticum
Accumulibacter phosphatis
Thermomicrobium roseum
Sphaerobacter thermophilus
Caldilinea aerophila
Rhodothermus marinus
Pyrobaculum sp. 1860
Pyrobaculum calidifontis
Ferroglobus placidus
Putative Clade III
D
Clade I
Clade II
0.2
Sedimenticola sp.
Burkhoderiales sp.
Rhodospirillales sp.
Magnetococcales sp.
Nitrospinota sp.
Deltaproteobacteria sp.
Deltaproteobacteria sp.
Deltaproteobacteria sp.
Nitrospirota sp.
Nitrospirota sp.
Nitrospinota sp.
Nitrospinota sp.
Nitrospinota sp.
Nitrospinota sp.
Nitrospirota sp.
Nitrospinae sp.
Nitrospinota sp.
Nitrospirota sp.
Cadidate division TA06
MAG6
MAG7
Sporomusa acidovorans
Chloroflexota sp.
nos operon genes
nosZ
nosD
nosF
nosL
nosY
cy-b
cy-c
S
nosB
HP
nosR
nosX

**Figure 3-3. Structural and functional validation of clade III NosZ.** (A). The NosZ enzyme is a homodimer in head-to-tail orientation with the tetranuclear $Cu_Z$ active site located in the N-terminal, seven-bladed β-propeller domain and the binuclear $Cu_A$ site in the C-terminal cupredoxin domain. The $Cu_A$–$Cu_Z$ distance within one monomer is around 42.5 Å (i.e., $Cu_A$-A to $Cu_Z$-A) and thus too large for efficient electron transfer. Instead, the $Cu_A$ site of one monomer is at a distance of only 10.5 Å from $Cu_Z$ in the other monomer ($Cu_A$-A to $Cu_Z$-B) (B). Conserved residues associated with $Cu_A$ and $Cu_Z$ sites. Two histidine and cysteine residues are conserved in $Cu_A$ site, and seven histidine residues are conserved in $Cu_Z$ site. The Y163 residue enclosed in red is an unexpected (lacking in clade I and clade II NosZ) tyrosine associated with $Cu_Z$ site. (C) Comparative growth assays performed with 27$^{th}$ Sabana and (D) 15$^{th}$ WS2 transfers cultures. Green and red lines indicate $N_2O$ reduction performance in different pH (4.5 and 7) medium. Green bars represent the cells (pH 4.5) enumerated with specific primers targeting the clade III *Desulftobacterium nosZ*. Fold changes of *nosZ* transcripts (orange bars) and assembled NosZ protein (yellow bars) are calculated based on corresponding cultures grown in pH 4.5 medium with (+) and without (-) $N_2O$ amendment. Of note, growth of clade III $N_2O$ reducers was not substantial in cultures without $N_2O$. Data represent averages of triplicate incubations and error bars represent standard deviations (n=3). Error bars are not shown when smaller than the symbol.

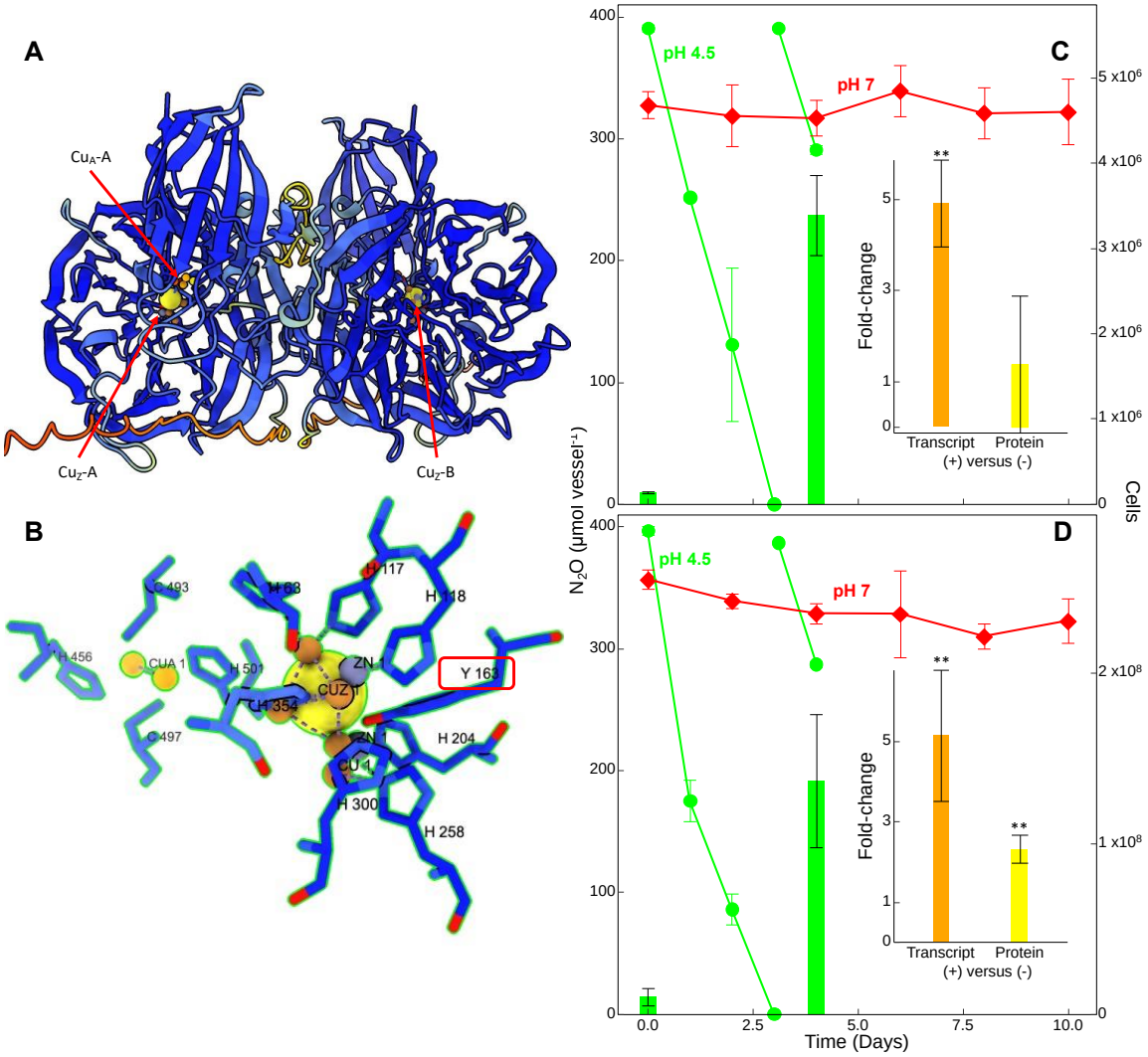
A
Cu$_A$-A
Cu$_Z$-A
Cu$_Z$-B
B
C 493
H 68
H 117
H 118
H 456
CUA 1
H 501
ZN 1
CUZ 1
Y 163
CU 354
C 497
ZN 1
H 204
CU 1
H 300
H 258
C
D
pH 4.5
pH 7
N$_2$O (µmol vessel$^{-1}$)
Cells
Fold-change
Transcript
Protein
(+) versus (-)
Time (Days)
0.0
2.5
5.0
7.5
10.0

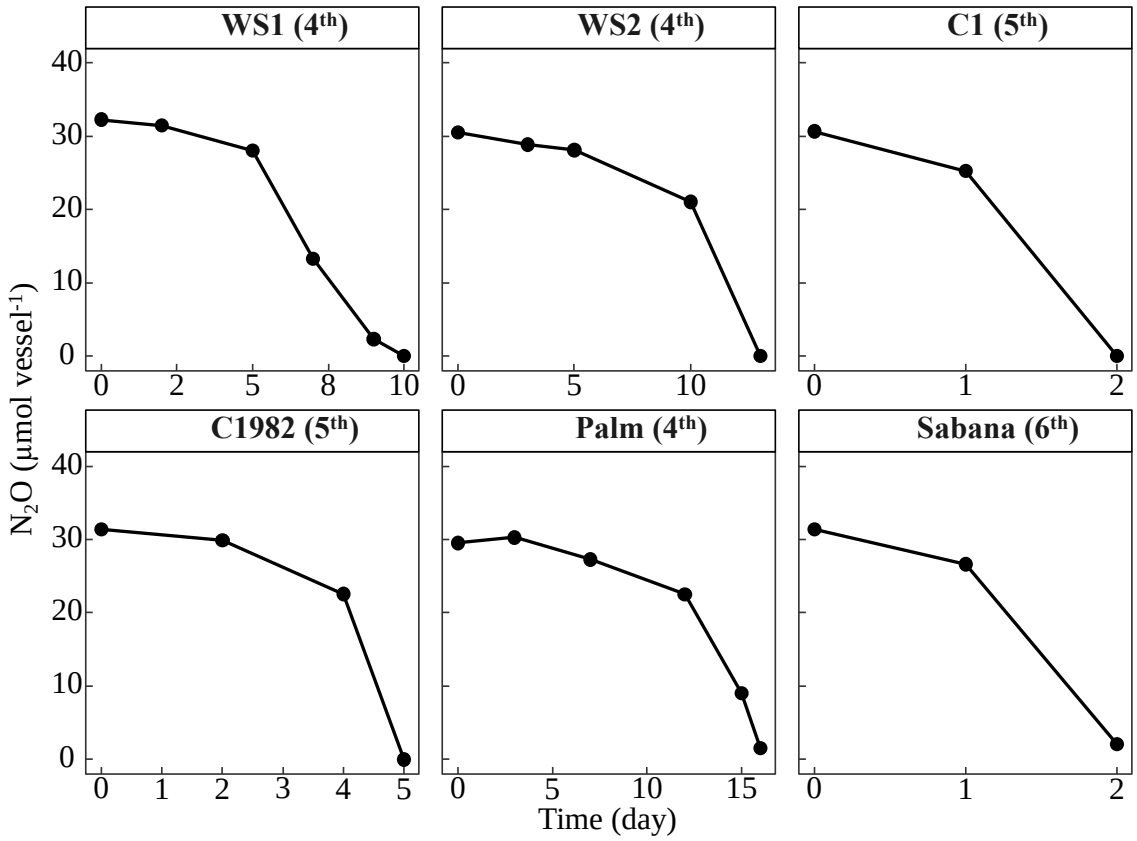


**Supplementary Figure 3-1. Low pH $N_2O$ reduction of transfer cultures derived from farm and tropical soils.** Numbers inside parenthesis indicate the transfer generations. For example, panel labeled as WS1 ($4^{th}$) showed $N_2O$ data collected from $4^{th}$ WS1 transfer culture. Data were collected from single experiment.

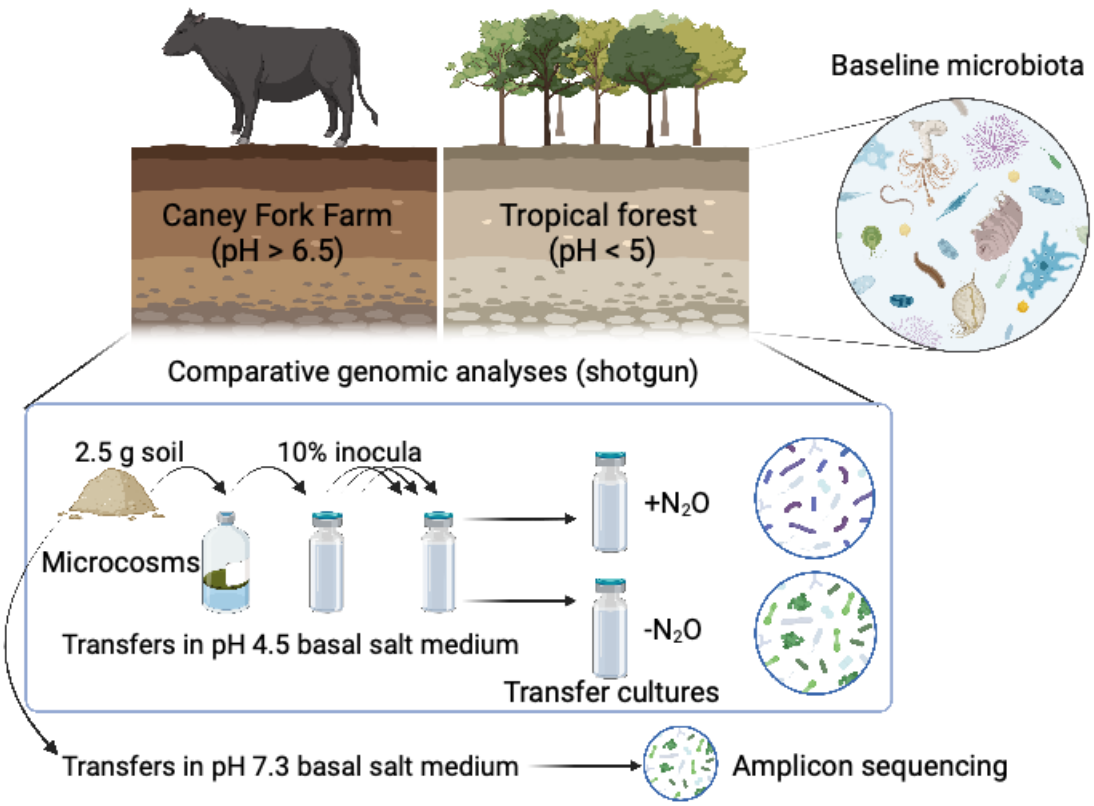


**Supplementary Figure 3-2. Schematic of establishing low pH $N_2O$ reducing cultures.** Shotgun metagenomic sequencing was applied to original Caney Fork Farm and Puerto Rico Soils to study the baseline microbiota. Soil samples from Caney Fork Farm and Puerto Rico Forest were subsequently used to establish pH 4.5 and 7 soil microcosms. Consecutive transfers were performed in pH 4.5 and 7 basal salt medium and derived solids-free cultures. Comparative shotgun metagenomic analyses were conducted with corresponding pH 4.5 cultures with or without $N_2O$ substrate. Amplicon sequencing targeting 16S V3-V4 regions was performed on cultures transferred in pH 7 basal salt medium.

**Supplementary Figure 3-3. Nonpareil analysis of soil- and enrichment cultures' metagenomes.** (A) Nonpareil curves of PR soil- and derived enrichment cultures. (B) Nonpareil curves of CFF soil- and derived enrichment cultures. Open circles represent the estimated average coverage of the datasets obtained and projections based on model fitting to reach 95% and 99% coverage are indicated (horizontal dashed lines). The arrows at the bottom represent sequencing effort required to achieve 50% coverage.

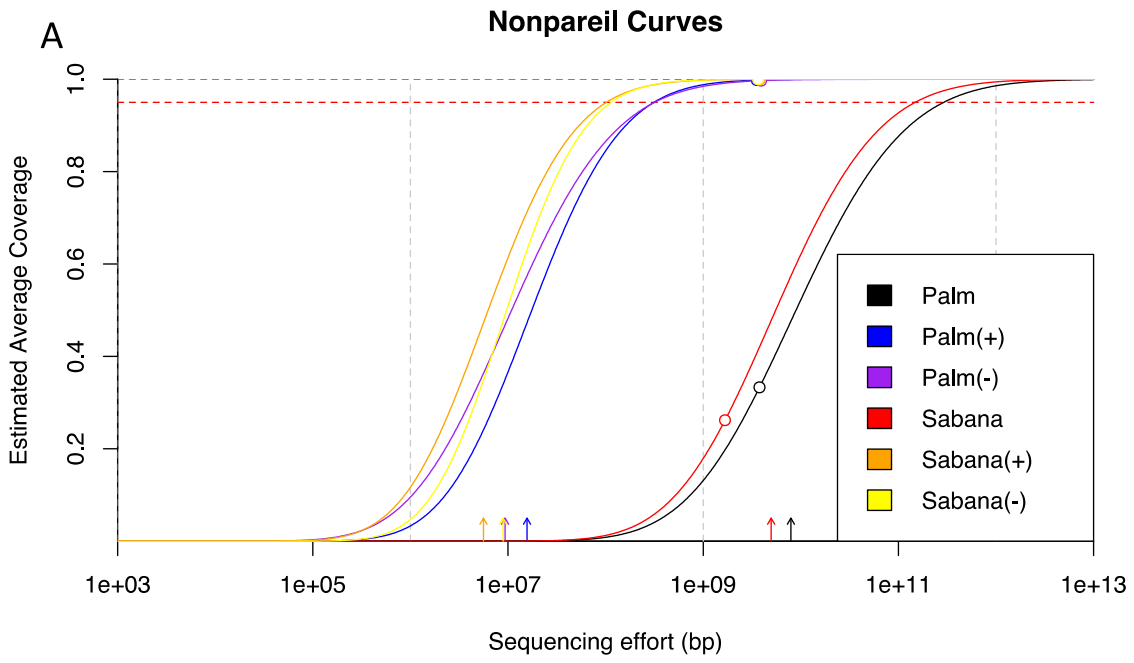
A
Nonpareil Curves
Estimated Average Coverage
0.2
0.4
0.6
0.8
1.0
1e+03
1e+05
1e+07
1e+09
1e+11
1e+13
Sequencing effort (bp)
Palm
Palm(+)
Palm(-)
Sabana
Sabana(+)
Sabana(-)

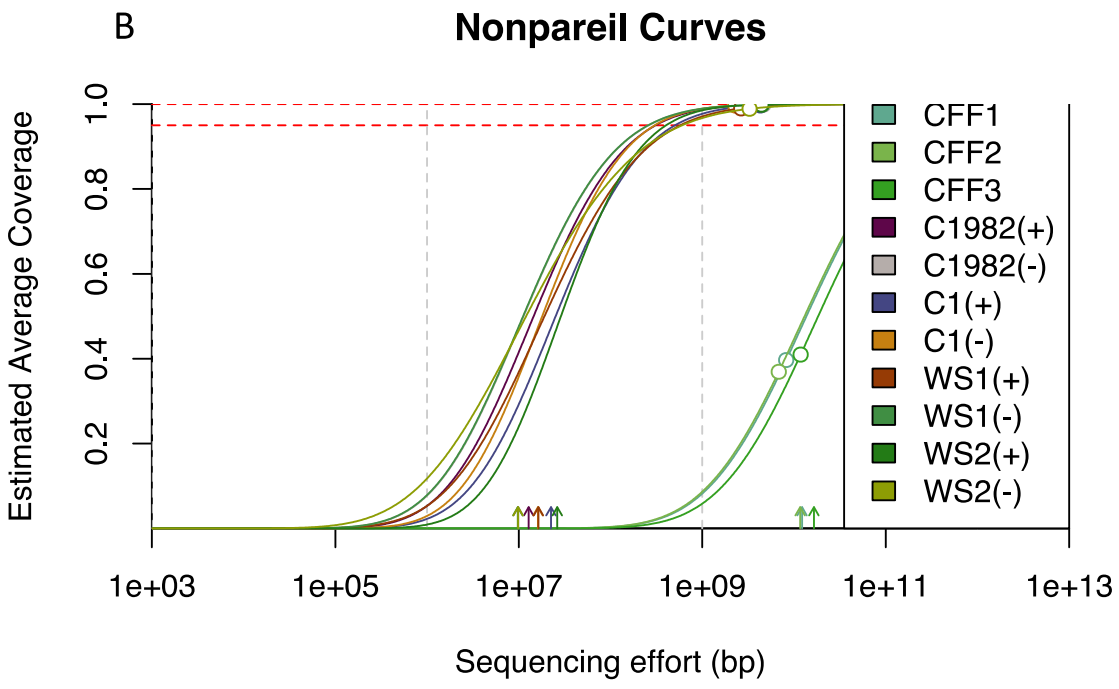
B
Nonpareil Curves
Estimated Average Coverage
0.2
0.4
0.6
0.8
1.0
1e+03
1e+05
1e+07
1e+09
1e+11
1e+13
Sequencing effort (bp)
CFF1
CFF2
CFF3
C1982(+)
C1982(-)
C1(+)
C1(-)
WS1(+)
WS1(-)
WS2(+)
WS2(-)

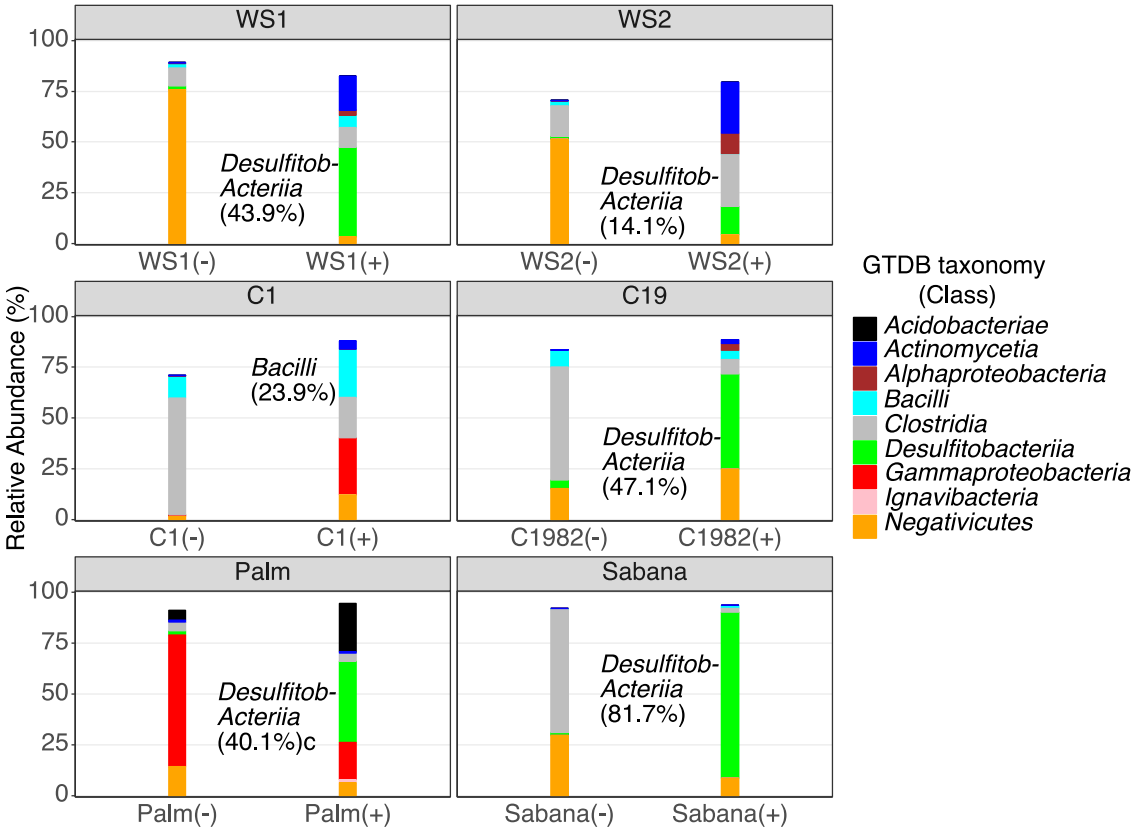


**Supplementary Figure 3-4. Microbial community constructed with high-quality MAGs.** Relative abundance of MAGs in each metagenome was calculated with CoverM. Taxonomy was assigned to MAGs using GTDB-TK. Microbial community was displayed at class level with ggplot package. T axa highlighted with text are population selectively growing in the presence of $N_2O$.

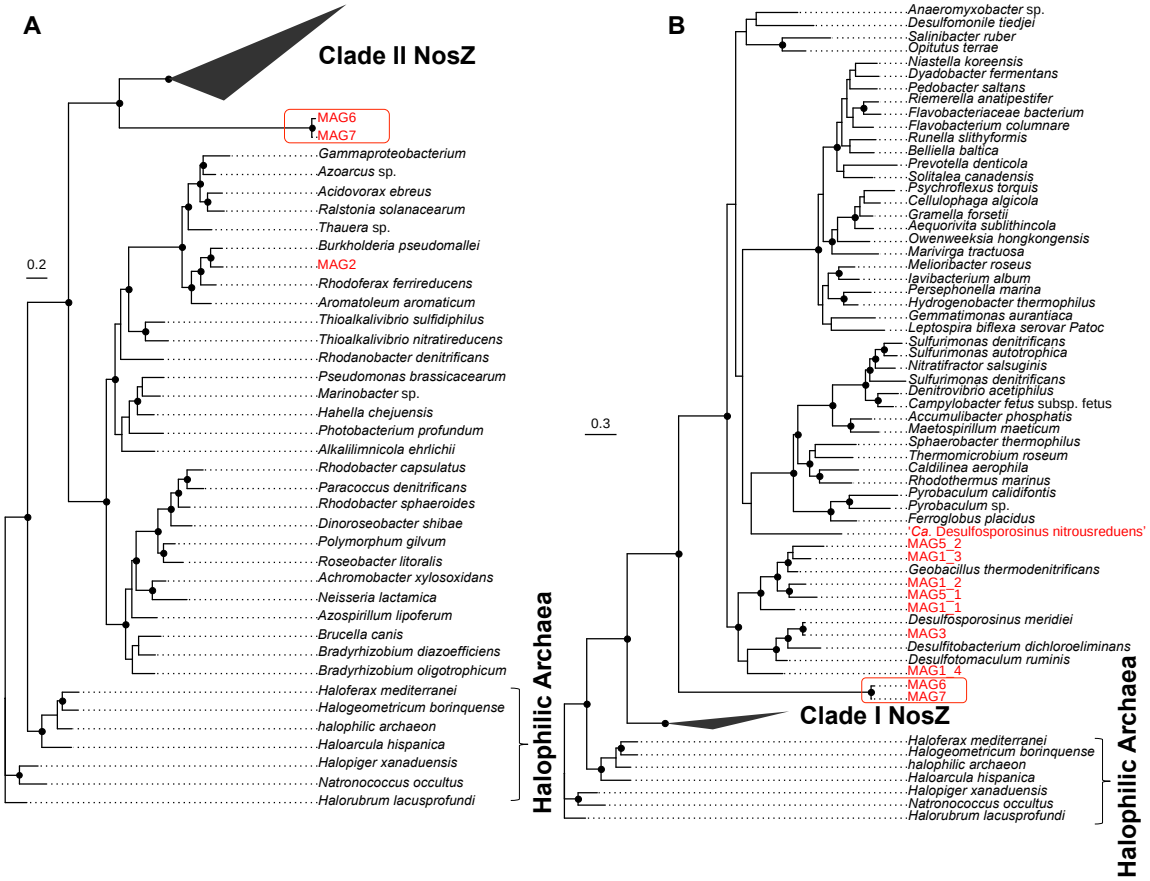


**Supplementary Figure 3-5. Preliminary phylogenetic analyses allude to the clade III *nosZ* genes recovered from acidic $N_2O$-reducing cultures.** (A) clade I and (B) clade II *nosZ* are shown separately for readers' convenience. The branch labels in black indicate the 80 referecen *nosZ* genes, whereas branch labels in red indicate the *nosZ* genes recovered from acidic $N_2O$-reducing cultures. Bifurcation with bootstrap values over 75% are indicated with closed circle symbols. Tree scales indicate amino acid substitution rates. The *nosZ* genes (MAG6 and 7) not cluster with either clade I or clade II are enclosed in red.

| | MAG1_1 | MAG1_2 | MAG1_3 | MAG1_4 | MAG2 | MAG3 | MAG4 | MAG5_1 | MAG5_2 | MAG6 | MAG7 |
|---|---|---|---|---|---|---|---|---|---|---|---|
| MAG1_1 | NA | 64.5 | 64.2 | 58.0 | 31.8 | 55.7 | 42.2 | 60.9 | 59.9 | 25.0 | 24.7 |
| MAG1_2 | 64.5 | NA | 72.3 | 54.6 | 31.4 | 52.8 | 41.7 | 75.0 | 66.9 | 23.6 | 24.1 |
| MAG1_3 | 64.2 | 72.3 | NA | 56.0 | 31.6 | 54.2 | 42.2 | 69.5 | 72.0 | 23.9 | 24.2 |
| MAG1_4 | 58.0 | 54.6 | 56.0 | NA | 32.1 | 61.1 | 46.0 | 54.8 | 55.9 | 25.9 | 25.6 |
| MAG2 | 31.8 | 31.4 | 31.6 | 32.1 | NA | 32.2 | 27.5 | 29.9 | 29.7 | 23.1 | 23.1 |
| MAG3 | 55.7 | 52.8 | 54.2 | 61.1 | 32.2 | NA | 42.9 | 52.3 | 53.8 | 24.8 | 24.7 |
| MAG4 | 42.2 | 41.7 | 42.2 | 46.0 | 27.5 | 42.9 | NA | 44.7 | 41.0 | 21.4 | 21.5 |
| MAG5_1 | 60.9 | 75.0 | 69.5 | 54.8 | 29.9 | 52.3 | 44.7 | NA | 67.8 | 23.5 | 23.2 |
| MAG5_2 | 59.9 | 66.9 | 72.0 | 55.9 | 29.7 | 53.8 | 41.0 | 67.8 | NA | 23.5 | 23.5 |
| MAG6 | 25.0 | 23.6 | 23.9 | 25.9 | 23.1 | 24.8 | 21.4 | 23.5 | 23.5 | NA | 97.0 |
| MAG7 | 24.7 | 24.1 | 24.2 | 25.6 | 23.1 | 24.7 | 21.5 | 23.2 | 23.5 | 97.0 | NA |

**Supplementary Figure 3-6. Heatmap showing amino acid identity between the NosZ recovered from high-quality MAGs.** Numbers inside cells represent the pairwise sequence identity (%) between two NosZ. Four and two different NosZ are found on MAG1 and MAG5, respectively. The MAG6 and MAG7 NosZ share no more than 30% to reference NosZ shown as black labels in Fig. S5.

## AlphaFold models

| | NosZ | NosB | Cyt-B | H122 | NosL | NosF | H125 | H126 |
|---|---|---|---|---|---|---|---|---|
| | $N_2O$ reductase | Part of ABC transporter? | Cytochrome | Met-rich β-barrel lipoprotein | Met-rich ABC transporter | Part of ABC transporter | Unknown | β propeller |
| | periplasmic lipoprotein | cytoplasmic membrane | cytoplasmic membrane | periplasmic lipoprotein | cytoplasmic membrane | cytoplasm | cytoplasmic membrane-anchored | periplasmic lipoprotein |
| | dimer | monomer | monomer | monomer | monomer? | dimer | monomer | monomer |

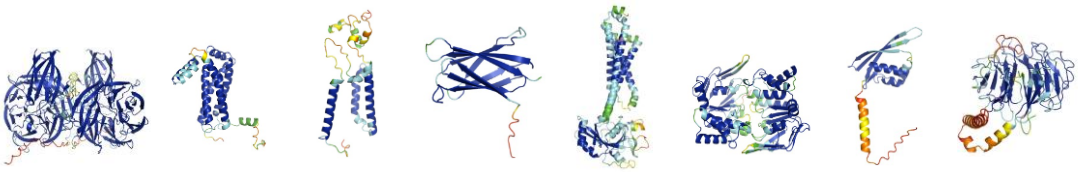

| | | | | | | | | |
|---|---|---|---|---|---|---|---|---|
| **monomer** | | **88.9** | 77.4 | **88.4** | **83.9** | | **80.8** | **84.6** |
| **dimer** | **91.8 (0.92, 0.91)** | 83.2 (0.8, 0.78) | | | 72.3 (0.52, 0.443) | 88.5 (0.77, 0.64) | | |

**Scores**
monomers: pLDDT
dimers: pLDDT (pTM, ipTM)

**Supplementary Figure 3-7. AlfphaFold2 predicted structures of proteins located closely to NosZ.** Signalp 6.0 was used to identify and remove signal peptides prior to structure prediction. The corresponding membrane orientations of proteins were predicted using MembraneFold.

**Table 3-1.** Metadata associated with soils used for enrichment procedure.

| Soil Samples (Location [a]) | Longitude | Latitude | pH [b] | Tree [c] |
|---|---|---|---|---|
| Sabana (LEF) | -65.7296575 | 18.317758 | 4.72 | *Dacryodes excelsa* |
| Palm Nido (LEF) | -65.798597 | 18.295042 | 4.97 | *Sierra Palm* |
| WS1 (CFF) | -85.910731 | 36.243253 | 6.74 | Winter-East-AA-005 |
| WS2 (CFF) | -85.910401 | 36.243113 | 6.87 | Winter-East-AA-013 |
| C1 (CFF) | -85.909630 | 36.241153 | 6.96 | Winter-East-AA-061 |
| C1982 (CFF) | -85.909575 | 36.241508 | 6.98 | Winter-East-AA-053 |

[a] Location: LEF refers to Luquillo Experimental Forest located in Puerto Rico; CFF refers to Caney Fork Farm located in Carthage, Tennessee. [b] pH of LEF soils were reported in a prior study (43) and CFF soil pH was measured by mixing 2.5 gram fresh soils with 10 mL deionized water (1:4) in this study. [c] The CFF soils are associated with labelled trees aiming for long-term monitoring; WS1 and WS2 are associated with trees that inoculated with Symbionts to Advance Food and Energy (SAFE) fertilizer whereas C1 and C1982 are soils close to trees not receiving any fertilizer. Sabana and Palm Nido sites is dominated by Dacryodes excelsa and Sierra Palm, respectively.

**Table 3-2.** Substrates provided to the $N_2O$-reducing cultures during the enrichment process.

| Culture [a] | Carbon source [b] | Electron acceptor | Electron donor |
|---|---|---|---|
| WS1 (6th) | 5 mM Fumarate | 4.16 mM $N_2O$ (nominal) | 4.16 mM $H_2$ (nominal) |
| WS2 (6th) | 5 mM Fumarate | 4.16 mM $N_2O$ (nominal) | 4.16 mM $H_2$ (nominal) |
| C1 (7th) | 5 mM Fumarate | 4.16 mM $N_2O$ (nominal) | 4.16 mM $H_2$ (nominal) |
| C1982 (7th) | 5 mM Fumarate | 4.16 mM $N_2O$ (nominal) | 4.16 mM $H_2$ (nominal) |
| Sabana (9th) | 5 mM Fumarate | 4.16 mM $N_2O$ (nominal) | 4.16 mM $H_2$ (nominal) |
| Palm Nido (9th) | 5 mM Succinate | 4.16 mM $N_2O$ (nominal) | 4.16 mM $H_2$ (nominal) |

[a] Numbers inside parenthesis indicate the corresponding cultures were subjected to shot-gun sequencing efforts. [b] In addition to fumarate/succinate, 1% (v/v) Tryptone-Soy Broth was augmented as growth nutrient.

**Table 3-3.** Analyses of high-quality MAGs using the Microbial Genome Atlas (MiGA) [a].

| MAG ID [b] | Completeness | Contamination | Closest relative [c] | AAI [d] |
|---|---|---|---|---|
| C1982-MAG1 [e] | 92.2 | 5.7 | *Calidifontibacillus erzurumensis* | 76.9 |
| Palm-MAG2 [e] | 94.4 | 0.9 | *Paludibacterium purpuratum* | 77.0 |
| Palm-MAG3 [e] | 97.0 | 1.6 | *Desulfosporosinus orientis* | 85.8 |
| Palm-MAG4 [e] | 99.5 | 6.0 | *Desulfosporosinus acididurans* | 79.2 |
| C1982-MAG5 [e] | 95.6 | 2.4 | *Calidifontibacillus erzurumensis* | 64.6 |
| Sabana-MAG6 [e] | 98.9 | 2.6 | *Desulfitobacterium_metallireducens* | 77.7 |
| WS2-MAG7 [e] | 98.9 | 2.0 | *Desulfitobacterium_metallireducens* | 78.0 |
| Palm-MAG8 | 95.0 | 0.6 | *Clostridium celerecrescens* | 92.0 |
| Sabana-MAG9 | 99.4 | 0.6 | *Clostridium sphenoides* | 97.4 |
| Sabana-MAG10 | 95.4 | 3.7 | *Variimorphobacter saccharofermentans* | 64.9 |

**Table 3-3.** Continued

| MAG ID [b] | Completeness | Contamination | Closest relative [c] | AAI [d] |
|---|---|---|---|---|
| Palm-MAG11 | 100 | 9.0 | *Pelosinus fermentans* | 75.4 |
| C1-MAG12 | 97.9 | 1.4 | *Sinanaerobacter chloroacetimidivorans* | 68.0 |
| Sabana-MAG13 | 85.2 | 5.8 | *Pseudoclostridium thermosuccinogenes* | 55.0 |
| Sabana-MAG14 | 98.6 | 5.0 | *Ectobacillus_panaciterrae* | 65.0 |
| C1-MAG15 | 97.2 | 3.1 | *Clostridium homopropionicum* | 84.2 |
| C1-MAG16 | 84.8 | 2.8 | *Clostridium magnum* | 83.7 |
| Palm-MAG17 | 99.9 | 9.08 | *Clostridium aciditolerans* | 89.3 |
| WS2-MAG18 | 85.1 | 2.3 | *Clostridium thailandense* | 92.2 |
| Sabana-MAG19 | 89.7 | 8.9 | *Clostridium rhizosphaerae* | 62.9 |
| WS2-MAG20 | 97.4 | 1.1 | *Clostridium swellfunianum* | 63.3 |

**Table 3-3.** Continued

| MAG ID [b] | Completeness | Contamination | Closest relative [c] | AAI [d] |
|---|---|---|---|---|
| C1982-MAG21 | 97.2 | 6.6 | *Clostridium rhizosphaerae* | 93.2 |
| WS2-MAG22 | 89.7 | 22.6 | *Clostridium swellfunianum* | 63.3 |
| WS2-MAG23 | 96.6 | 2.8 | *Clostridium rhizosphaerae* | 63.7 |
| C1-MAG24 | 99.3 | 19.5 | *Clostridium rhizosphaerae* | 64.3 |
| WS2-MAG25 | 90.8 | 6.8 | *Clostridium swellfunianum* | 60.1 |
| C1-MAG26 | 98.0 | 0.7 | *Clostridium homopropionicum* | 84.2 |
| Palm-MAG27 | 98.7 | 1.0 | *Caproiciproducens galactitolivorans* | 67.3 |
| WS2-MAG28 | 98.0 | 4.7 | *Dendrosporobacter quercicolus* | 58.3 |
| Palm-MAG29 | 97.8 | 0 | *Paracidobacterium acidisoli* | 50.8 |
| WS2-MAG30 | 99.4 | 1.4 | *Dendrosporobacter quercicolus* | 58.7 |

**Table 3-3.** Continued

| MAG ID [b] | Completeness | Contamination | Closest relative [c] | AAI [d] |
|---|---|---|---|---|
| C1-MAG31 | 97.2 | 0.5 | *Propionicimonas paludicola* | 66.3 |
| Palm-MAG32 | 97.2 | 1.8 | *Propionicimonas paludicola* | 63.9 |
| WS1-MAG33 | 99.5 | 1.2 | *Microbacterium algeriense* | 83.9 |
| WS1-MAG34 | 98.8 | 0 | *Microbacterium aurum* | 95.8 |
| WS2-MAG35 | 99.2 | 0.3 | *Cellulomonas fimi* | 63.2 |
| WS1-MAG36 | 99.1 | 0.8 | *Sphingomonas echinoides* | 95.0 |
| WS2-MAG37 | 98.1 | 5.0 | *Sphingomonas echinoides* | 97.3 |
| C1-MAG38 | 100 | 1.4 | *Pseudomonas nicosulfuronedens* | 97.2 |
| Palm-MAG39 | 84.6 | 10.7 | *Oscillibacter ruminantium* | 71.0 |
| Palm-MAG40 | 85.9 | 1.36 | *Muriventricola aceti* | 66.1 |

**Table 3-3.** Continued

| MAG ID [b] | Completeness | Contamination | Closest relative [c] | AAI [d] |
|---|---|---|---|---|
| C1-MAG41 | 98.0 | 3.02 | *Ruminiclostridium hungatei* | 66.8 |
| Palm-MAG42 | 90.2 | 7.0 | *Sporolituus thermophilus* | 57.1 |
| Palm-MAG43 | 98.0 | 1.1 | *Melioribacter roseus* | 50.7 |

[a] MAG completeness and contamination were calculated using CheckM package. [b] Prefix (e.g., Sabana and Palm) of MAG ID indicates the metagenomes from where a MAG was constructed. [c] Closest relatives and associated [d] Average Amino Acid Identity (AAI) calculated using MiGA. [e] MAGs carry at least one *nosZ* gene.

**Table 3-4.** Statistics of the high-quality *nosZ*-carrying MAGs.

| MAG id | Contigs | Size (Mbp) | GC content (%) | CDS [b] | tRNA [c] | rRNA d |
|---|---|---|---|---|---|---|
| MAG1 | 69 | 4.2 | 38.0 | 4163 | 53 | 15 |
| MAG2 | 85 | 3.7 | 62.1 | 3461 | 59 | 4 |
| MAG3 | 106 | 5.3 | 46.4 | 4926 | 70 | 12 |
| MAG4 [a] | 94 (84) | 5.6 (5.6) | 44.7 (44.8) | 5239 (5231) | 41 (40) | 7 (8) |
| MAG5 | 31 | 4.14 | 38.3 | 4052 | 72 | 5 |
| MAG6 | 105 | 4.5 | 41.3 | 4394 | 40 | 5 |
| MAG7 | 45 | 4.14 | 41.0 | 3976 | 43 | 5 |

[a] MAG4 is identical to the genome of '*Ca.* Desulfosporosinus nitrousreducens' strain PR and numbers inside parenthesis are the genome characteristics reported in prior study (Guang, et al., 2023). [b] CDS: coding sequences. [c] tRNA: transfer RNA. [d] rRNA: ribosomal RNA.

**Table 3-5.** Growth of clade III $N_2O$ reducers is $N_2O$- and pH- dependent. [a]

| Population | $N_2O$ supply | Medium pH | Cells (mL $^{-1}$) [b] | Cells (mL $^{-1}$) [c] |
|---|---|---|---|---|
| MAG6 (Sabana) | Yes | 4.5 | 1.3 (0.1) x $10^5$ | 3.4 (0.5) x $10^6$ |
| | No | 4.5 | 3.0 (0.6) x $10^4$ | 4.7 (0.8) x $10^4$ |
| | Yes | 7 | 7.5 (2.7) x $10^3$ | 1.5 (0.6) x $10^4$ |
| MAG7 (WS2) | Yes | 4.5 | 1.0 (0.5) x $10^7$ | 1.4 (0.4) x $10^8$ |
| | No | 4.5 | 1.5 (0.3) x $10^6$ | 2.8 (1.5) x $10^6$ |
| | Yes | 7 | 1.6 (0.2) x $10^6$ | 1.7 (0.2) x $10^6$ |

[a] Growth of clade III $N_2O$ reducers (i.e., MAG6 and MAG7) were measured in mixed cultures (culture Sabana and WS2, respectively) with *nosZ*-targeting primers. [b] Cells measured immediately following vessels received inoculum. [c] Cells in pH-4.5 and -7 cultures were measured at 4- and 10-day, respectively.

# Chapter 4 Geochemical factors control $N_2O$ reduction under low pH conditions

**Abstract**

Nitrous oxide ($N_2O$) is a greenhouse gas exacerbating ozone depletion and global warming. Microorganisms synthesizing $N_2O$ reductase are the only sink of $N_2O$. However, the $N_2O$ reduction process is regulated by environmental factors (e.g., oxygen content, pH and copper ions). Acidic soils had long been considered $N_2O$ emitters because laboratory efforts studying denitrification showed a strong preference for circumneutral pH conditions for complete reduction to environmentally benign dinitrogen gas. Field observations and the recent discovery of bacteria with a preference of low pH $N_2O$ reduction suggest the microbiology is not limiting $N_2O$ consumption under acidic conditions. Laboratory cultivation experiments explored the geochemical controls of acidophilic and neutrophilic $N_2O$ reducing co-culture EV and *Dechloromonas aromatica* strain RCB, respectively. The results revealed geochemical factors (i.e., nitrogen oxyanions, $Cu^{2+}$ and $Na_2S$), instead of pH, were limiting low pH $N_2O$ reduction by co-culture EV. Temporal nitrogen oxyanions (i.e., $NO_3^-$ and $NO_2^-$) dosing experiments demonstrated different mechanisms behind $NO_3^-$ and $NO_2^-$ inhibition on low pH $N_2O$ reduction. $Cu^{2+}$ and $Na_2S$ dosing experiments revealed multidimensional effect of sulfide on $N_2O$ reduction. The start-up concentration of copper toxicity (0.5 mM) on $N_2O$-dependent growth was much lower than that reported for $NO_3^-$-dependent growth. These observations together suggest that geochemical factors other than pH are limiting $N_2O$ reduction in acidic soils.

## 4.1 Introduction

Nitrous oxide ($N_2O$) is a long-lived greenhouse gas with ozone destruction potential and is of environmental significance for global warming. Increases in atmospheric $N_2O$ are predicted to cause a 2-4% decline of the total ozone column by the end of 21$^{st}$ century (180). Biotic and coupled biotic-abiotic processes in terrestrial and aquatic ecosystems are the primary $N_2O$ sources (181, 182). The $N_2O$-forming and -consuming processes are regulated by multiple environmental factors such as temperature, oxygen partial pressure, pH, copper availability, and electron donor availability (40, 183-186). The only known biological $N_2O$ sink is the microbial transformation of $N_2O$ to $N_2$ catalyzed by $N_2O$ reductase ($N_2OR$) (17), which was previously considered a weak process in acidic soils (40, 41). Current paradigm of low pH $N_2O$ reduction is that the assembly of $N_2O$ reductase is impaired under acidic pH conditions (38, 40, 41). However, a deep-sea isolate, *Nitratiruptor* sp., respires $N_2O$ between pH 5.4 to 6.4, contradicting the recognition that $N_2O$ reductase cannot be assembled under acidic conditions (105). We have enriched clade II *nosZ*-carrying organisms capable of respiring $N_2O$ under strong acidic conditions (Guang, et al., unpublished work) from tropical forest soils and managed agricultural soils, implicating microbiology is not limiting $N_2O$ reduction activities in acidic soils. Thus, a better understanding on the limiting factors of $N_2O$ reduction activities is needed to manage $N_2O$ emissions from acidic soils.

$N_2OR$, encoded by the *nosZ* gene, is a periplasmic multicopper protein consisting of two distinct copper centers, designated $Cu_A$ and $Cu_Z$ (17) and strictly requires copper as a metal cofactor (187). The binuclear $Cu_A$ center channels electrons to the tetranuclear $Cu_Z$ center where $N_2O$ reduction to $N_2$ occurs (188). Copper-limiting conditions impacts the assembly of functional $N_2OR$. For example, methanobactin produced by some methanotrophs, and the formation of CuS with a solubility product of $8.5 \times 10^{-45}$ (189), effectively sequester copper and inhibits $N_2O$ reduction (127, 190, 191). Under circumneutral pH conditions, the addition of copper ions ($Cu^{2+}$) recovered $N_2O$ reduction activity (191, 192). However, due to limited cultivable organisms with capability of $N_2O$

reduction at pH < 5, the impact of copper sequestration by sulfide on $N_2O$ reduction under acidic conditions remains unclear.

$NO_3^-$ and $NO_2^-$ are key precursors of $N_2O$ availabilities and have been implicated as key environmental factors controlling $N_2O$ formation (32, 193). [need ref that shows that $NO_3^-$ and $NO_2^-$ are N2O precursors. Then need refs that show that $NO_3^-$ and $NO_2^-$ concentrations impacts N2O formation (e.g., Sukhwan Yoon's paper with Shewanella loihica). Net $N_2O$ emission was result from $N_2O$ production outpacing $N_2O$ consumption, presumably due to geochemical favoring $N_2O$ production or inhibiting $N_2O$ consumption (38, 128, 185). For example, intracellular competition for electrons directed towards $NO_3^-$ versus $N_2O$ reduction in denitrifying organisms (converting $NO_3^-$ to $N_2$) can explain the impact of $NO_3^-$ on $N_2O$ reduction activity (194). $NO_2^-$ also impacts $N_2O$ reduction and stalled $N_2OR$ activity was observed in laboratory incubations (195, 196). Previous paradigm that denitrifying organisms are the key $N_2O$ consumers had been argued by the discovery of clade II $N_2O$ reducers, most of which lack the *nirK* and *nirS* genes to denitrify (12). Therefore, denitrification is considered a modular microbial process, consisting of step-by-step reductions of oxidized nitrogen species ($NO_3^- \rightarrow NO_2^- \rightarrow N_2O \rightarrow N_2$). The impact of nitrogen oxyanions on [new section. now you are bringing up the modularity issue. This needs to be explicitly explained] $N_2O$-reducing bacteria that cannot denitrify may differ from that on denitrifying $N_2O$ reducers. The case studies investigating the effect of nitrogen oxyanions on $N_2O$ reduction was limited to neutral pH conditions (197). Our former work documented that organisms performing low pH $N_2O$ reduction are incapable of denitrification with *nirK* and *nirS* genes absent (Guang, et al., unpublished work). Therefore, those cultures offer an opportunity to study the impact of nitrogen oxyanion on low pH $N_2O$ reduction.

While some progress has been made to understand the complex organisms-environment interactions that govern $N_2O$ reduction at circumneutral pH, our understanding of factors controlling $N_2OR$ activity at low pH are unclear. This research was conducted to test the hypothesis: geochemical factors, instead of pH, is limiting microbiology of low pH $N_2O$ reduction. Specifically, copper, sulfide and nitrogen oxyanions limitations on low pH

$N_2O$ reduction by culture EV were evaluated. The *Desulfosprosinus nitrousreducens* habituating culture EV reduces $N_2O$ with $H_2$ as electron donor. To compare the impact of geochemical factors on acidic $N_2O$ reduction to that on neutral $N_2O$ reduction, hydrogenotrophic $N_2O$-reducing *Dechloromonas aromatica* strain RCB was cultivated in parallel.

## 4.2 Materials and Methods

### Microorganisms and cultivation.

Co-Culture EV, consisting of pyruvate-fermenting *Serratia marcescens* strain MF and $N_2O$-respiring *Desulfosporosinus nitrousreducens*, was enriched from acidic tropical forest soil (Guang, et al, unpublished work). After the establishment of the stable co-culture, it was maintained in the laboratory via repeated transfers in defined mineral salt medium with $N_2O$ as the sole electron acceptor and $H_2$ as the electron donor. Co-Culture EV was cultivated in 160-mL serum bottles containing 100 mL phosphate-buffered (50 mM, pH 4.5) anoxic mineral salt medium reduced with L-cysteine (0.2 mM) as described with the following modifications (Guang, et al, unpublished work). A volume of 1 mL stock solution of mixed amino acid was added to the vessels prior to inoculation served as growth nutrient. The stock solution of amino acid contains (g $L^{-1}$): alanine (0.5); aspartic acid (1); proline (1); tyrosine (0.3); histidine (0.3); tryptophan (0.2); arginine (0.5); isoleucine (0.5); methionine (0.4); glycine (0.3); threonine (0.5); valine (0.9); lysine (1); glutamate (1); serine (0.8). *Dechloromonas aromatica* strain RCB was maintained in 160-mL serum bottles containing 100 mL bicarbonate-buffered (30 mM, pH 7.3) anoxic mineral salt medium reduced with L-cysteine (0.2 mM) as described (101). Ten mL (416 µmol) of $H_2$ and $N_2O$ were added using plastic syringes and equilibrated over-night prior to the inoculation of co-culture EV or *D. aromatica* strain RCB.

**Abiotic controls of $N_2O$ reduction at low pH.**

$N_2O$ reduction by the co-culture EV was examined in the presence of copper chloride ($CuCl_2$) at the concentration ranging from 0 to 0.5 mM. To precipitate the residual copper carried from the parent culture, sodium sulfide ($Na_2S$) was added at a final concentration of 0.2 mM in cultures that did not receive $CuCl_2$. $N_2O$ reduction of co-culture EV and *D. aromatica* strain RCB was evaluated in the presence of $Na_2S$ (0.2 or 1 mM) with excessive $CuCl_2$ (0.22 or 1.02 mM). Cultures omitting $CuCl_2$ severed as negative controls. Additional time-serial dosing experiments were conducted to evaluate the toxicity of $Na_2S$ to co-culture EV and *D. aromatica* strain RCB. Briefly, cultures amended with $Na_2S$ (0.2 or 1 mM) were incubated for the first week followed by the addition of excessive $CuCl_2$ (0.22 or 1.02 mM) to resuscitate $N_2O$ respiration. To investigate the effect of nitrate and nitrite on $N_2O$ reduction by co-culture EV, growth experiments were conducted in the presence of nitrate or nitrite (0.1, 0.5 or 1 mM). $Na_2S$, nitrate and nitrite were added to the cultures when half of the initially added $N_2O$ was consumed to assess their impact on the activity of pre-synthesized $N_2O$ reductase.

**Analytical procedures.**

$N_2O$ were analyzed via manually injecting 100 µL headspace samples into an Agilent 3000A Micro-Gas Chromatograph (Palo Alto, CA, USA) equipped with Plot Q and molecular sieve columns coupled with thermal conductivity detection as described (101). Aqueous gas concentrations were calculated from the headspace concentrations based on the Henry's law using published Henry's constant for $N_2O$ ($2.4\times10^{-4}$) (102).

$$C_{aq} = \frac{C_g}{H} \times \frac{1}{24.86}$$ Equation 1 Henry's law

$C_{aq}$, $C_g$ and H are the aqueous gas concentration, the headspace gas concentration, and Henry's constant (dimensionless), respectively. Five-point standard curves for $N_2O$ spanned a concentration rage of 8,333 to 133,333 ppmv. The total amount of $N_2O$ in vessels was calculated by combining the gaseous and aqueous $N_2O$. Average $N_2O$ reduction rates at different pH were calculated as below:

$$v(N_2O) = \frac{c(N_2O_m - N_2O_n)}{m-n}$$ Equation 2

$v(N_2O)$ is the average $N_2O$ reduction rate; c represents $N_2O$ concentration (unit: µmole vessel$^{-1}$); n and m represent timepoint prior to measurable $N_2O$ consumption observed and at $N_2O$ depletion. $NO_3^-$ and $NO_2^-$ were measured using the Dionex IC 2100 system (Sunnyvale, CA, USA) as described (198).

## 4.3 Results

### $N_2O$ reduction by culture EV and D. aromatica strain RCB require copper

Culture EV enriched from acidic forest soils harbors a non-denitrifying *Serratia marcescens* population and an obligate $N_2O$-reducing *Desulfosporosinus nitrousreducens* which only reduces $N_2O$ to $N_2$ between pH 4.5 to 6 (Figure 4-1 A). *Dechloromonas aromatica* strain RCB carries all genes required for canonical denitrification and grows with $NO_3^-$ or $N_2O$ as sole electron acceptor (Figure 4-1 B). A genomic feature shared by *Desulfosporosinus nitrousreducens* and *Dechloromonas aromatica* strain RCB is the *hyp*-type NiFe hydrogenase, which is consistent to their capability of utilizing hydrogen gas as the sole electron donor.

Culture EV cultivated at pH 4.5 and *Dechloromonas aromatica* strain RCB grown at pH 7 reduced $N_2O$ at similar rates with $Cu^{2+}$ concentrations ranging from 0.0005 to 0.05 mM over a 6-day incubation (Figure 4-1 C, D). $N_2O$ reduction was not observed in either culture EV or *Dechloromonas aromatica* strain RCB received 0.2 mM sulfide. Sulfide precipitates $Cu^{2+}$ to form CuS with a solubility product constant of $8.5 \times 10^{-45}$ indicating the dissolved, bioavailable $Cu^{2+}$ concentration is no more than $4.25 \times 10^{-38}$ nM. $N_2O$ reduction was completely inhibited when the $Cu^{2+}$ concentration exceeded 0.5 mM, presumably due to toxic effects.

**Effects of copper and $Na_2S$ on $N_2O$ reduction**

In both culture EV (grown at pH 4.5) and the axenic culture of *D. aromatica* strain RCB (grown at pH 7) receiving copper at the concentration of 0.02 mM, $N_2O$ was depleted within 6 days. $N_2O$ reduction was prohibited in all cultures of EV and *D. aromatica* strain RCB amended with 0.2 mM $Na_2S$ or 1 mM $Na_2S$ alone (Figure 4-2). Average $N_2O$ reduction rates in culture EV received both $Na_2S$ and $CuCl_2$ (35.5 ± 1.22 and 34.5 ± 0.26 µmol $N_2O$ $day^{-1}$) were about half of that received 0.02 mM $CuCl_2$ only (66.1 ± 0.46 µmol $N_2O$ $day^{-1}$, Figure 4-2 A). Culture EV amended with 0.2 mM $Na_2S$ plus 0.22 mM $CuCl_2$ consumed the initially added $N_2O$ following an incubation of 11 days. A lag phase of 10-day was observed for Culture EV amended with 1 mM $Na_2S$ plus 1.02 mM $CuCl_2$ to initiate $N_2O$ reduction (Figure 4-2 C). Similar average $N_2O$ reduction rates of *D. aromatica* strain RCB were observed in cultures with both $Na_2S$ and $CuCl_2$ (70.9 ± 0.84 and 70.0 ± 2.32 µmol $N_2O$ $day^{-1}$), and in cultures with $CuCl_2$ only (70.1 ± 0.84 µmol $N_2O$ $day^{-1}$, Figure 4-2 B). No lag phase was observed for *D. aromatica* strain RCB received excessive copper (0.2 mM $Na_2S$ plus 0.22 mM $CuCl_2$ or 1 mM $Na_2S$ plus 1.02 mM $CuCl_2$) to initiate $N_2O$ reduction (Figure 4-2 D). The different $N_2O$ reduction phenotype of culture EV responding to low and high $Na_2S$ concentration raised a question: does $Na_2S$ exert toxicity to $N_2O$-reducing organisms at high concentrations under acidic conditions? Therefore, excessive $CuCl_2$ (0.22 or 1.02 mM) was added to cultures of El and *D. aromatica* strain RCB pre-exposed to low and high $Na_2S$. $CuCl_2$ dosing initiated $N_2O$ reduction in cultures of both EV and *D. aromatica* strain RCB exposed to low $Na_2S$ concentration (0.2 mM) but not to high $Na_2S$ concentration (1 mM) (Figure 4-3 A, B). In contrast, $N_2O$ reduction was stalled in culture EV and *Dechloromonas aromatica* strain RCB immediately following $Na_2S$ dosing (Figure 4-3 C, D), suggesting the of $Na_2S$ over copper against pre-synthesized $N_2O$ reductase.

**Effects of nitrogen oxyanion on low pH $N_2O$ reduction.**

$N_2O$ reduction by culture EV was prohibited in the presence of 0.1 mM to 1 mM $NO_3^-$ and 0.01 mM to 1 mM $NO_2^-$ (Figure 4-4 A, B). Culture EV received a concentration of

0.01 mM $NO_3^-$ or 0.001 mM $NO_2^-$ exhibited comparable $N_2O$ reduction activities as cultures without $NO_3^-$ or $NO_2^-$, suggesting the threshold concentrations of $NO_3^-$ and $NO_2^-$ inhibition on $N_2O$ reduction by culture EV are between 0.01 to 0.1 mM and 0.001 to 0.01 mM, respectively. Following a 3-day incubation, culture EV reduced approximately half of the initial amount of $N_2O$, subsequent $NO_2^-$ (1 mM) but not $NO_3^-$ dosing (1 mM) stalled $N_2O$ reduction immediately (Figure 4-4 C). In contrast, $NO_2^-$ dosing in *Dechloromonas aromatica* strain RCB transiently inhibit $N_2O$ reduction, suggesting $NO_2^-$ exerted a monopoly on electron against $N_2O$ reduction (Figure 4-4 D).

**4.4 Discussion**

Geochemical factors are important regulators controlling $N_2O$ flux in soils (199) and their impact on $N_2O$ reduction have been extensively studied under circumneutral pH conditions (185, 191, 196). However, the regulation of geochemistry over low pH $N_2O$ reduction remains elusive due to limited cultivable organisms. The isolation of organism that reduces $N_2O$ under acidic conditions (pH <5) (Guang, et al., unpublished work) offers an opportunity to study how geochemical factors impact $N_2O$ reduction under acidic conditions. In this study, we demonstrated that $N_2O$-dependent growth of culture EV was abolished in the presence of either $NO_3^-$ or $NO_2^-$, implicating that nitrogen oxyanions, instead of pH itself, may be the limiting factor of $N_2O$ reduction in acidic soils.

Acidic soils are considered as $N_2O$ emitters because of the inability of $N_2O$ reduction under acidic conditions. A previous study focused on denitrifying organisms attributed the abolished $N_2O$ reduction to pH interference on $N_2O$ reductase assembly (40). However, we enriched a co-culture harboring *Desulfosporosinus* bacteria capable of sustaining $N_2O$ reduction under acidic conditions (pH ~ 4.5) (Guang, et al., unpublished work). Here, we demonstrate that $NO_2^-$ has a lethal (inhibitory?) effect on both $N_2O$-dependent growth and the activity of pre-synthesized $N_2O$ reductase of culture EV under acidic conditions. Meanwhile $NO_2^-$ only exert a transient inhibitory effect on $N_2O$ reduction by *Dechloromonas aromatica* strain RCB via scavenging electrons, which is

consistent to previous studies focused on neutralophilic denitrifying organisms (110, 196). In addition, $NO_3^-$ prevents $N_2O$-dependent growth while exerts no effect on pre-synthesized $N_2O$ reductase activity of co-culture EV. The adverse impact of $NO_3^-$ on $N_2O$-dependent growth of *Desulfosporosinus nitrousreducens* was unexpected. Though high soil $NO_3^-$ content (10 mM, equivalent to 44.9 mg N $kg^{-1}$ soil) was reported to inhibit $N_2O$ reduction in soil incubations (200), there is no example of $NO_3^-$ regulation over $N_2O$ reduction in cultures. The theory of electron competition between $NO_3^-$ and $N_2O$ derived from denitrifying *Bradyrhizobia* genera (194, 201) is not sufficient to explain the observation of non-denitrifying culture EV. An alternative explanation is that the presence of $NO_3^-$ only interferes the assembly of $N_2O$ reductase while the already assembled enzymes are still functioning. These observations together suggested that genotype varying $N_2O$ reducers respond differently to nitrogen oxyanions.

Cu is a co-factor involved in the assembly of functional $N_2O$ reductase (17). In this research, cultivation experiments with culture EV and *Dechloromonas aromatica* strain RCB demonstrated that Cu at nM level is sufficient for the assembly of $N_2O$ reductase under both acidic and circumneutral pH conditions. A previous study proposed that $H_2S$ yielded from cysteine during anaerobic incubation may sequester copper and impede $N_2O$ reduction (202). However, in our cysteine-amended medium, $N_2O$ reduction of both culture EV and *Dechloromonas aromatica* strain RCB was not impacted until exogenous $Na_2S$ was added. Furthermore, the onset concentration of Cu (0.5 mM) toxicity on $N_2O$-dependent growth was much lower than that previously reported (20 mM) on $NO_3^-$-dependent growth (202). These observations are informative to soil environments where $N_2O$ is the sole energy source for microbial growth.

Sulfide has been long considered as a potent inhibitor of $N_2O$ reduction and previous studies derived two possible mechanisms: (I) ionic $S^{2-}$ and $HS^-$ formulated $H_2S$ exerts toxicity on organisms (203); (II) sequestration of copper by $S^{2-}$ (191). Here we demonstrate that the effect of sulfide on $N_2O$ reduction is multidimensional by parallelly cultivating two $N_2O$-respiring organisms under either acidic or circumneutral pH conditions. Copper dosing resuscitated $N_2O$ reduction inhibited low concentration of

$Na_2S$ (0.2 mM) in culture EV grown at pH 4.5 and *Dechloromonas aromatica* strain RCB (grown at pH 7), suggested copper sequestration to be the major cause of stalled $N_2O$ reduction in the scenario. This observation is consistent with previous incubation experiments with sludge and an axenic culture where divalent metal dosing restored sulfide-inhibited $N_2O$ reduction (191, 192). However, if organisms could recover $N_2O$ reduction activity following the exposure to high concentrations of $Na_2S$ were not considered in those studies. In this study, high concentration of $Na_2S$ (1 mM) exerted irreversible inhibition on $N_2O$ reduction in culture EV and *Dechloromonas aromatica* strain RCB, suggesting the onset concentration of sulfide toxicity is pH independent. Furthermore, the toxicity of copper and sulfide could be counteracted via precipitation, implicating interactions between geochemical factors indirectly regulate $N_2O$ reduction activity.

## Appendix

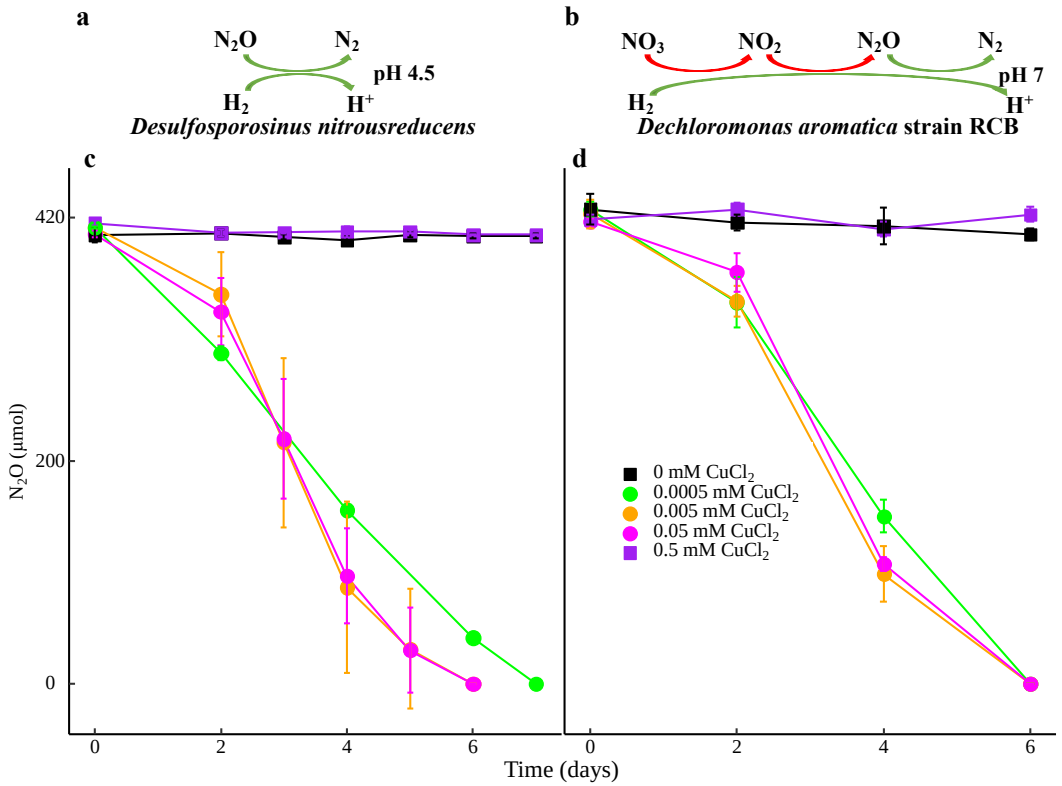


**Figure 4-1. Effects of copper on $N_2O$ reduction.** Nitrous oxide transformation of culture EV (a) and *D. aromatica* strain RCB (b). $N_2O$ reduction in culture EV (c) and *D. aromatica* strain RCB (d) amended with varying concentrations of $CuCl_2$. Cultures received 0.2 mM $Na_2S$ sequestering residual copper were referred as 0 mM $CuCl_2$. The data represent the averages of triplicate incubations and error bars represent the standard deviations (n=3). Error bars are not shown if smaller than the symbol.

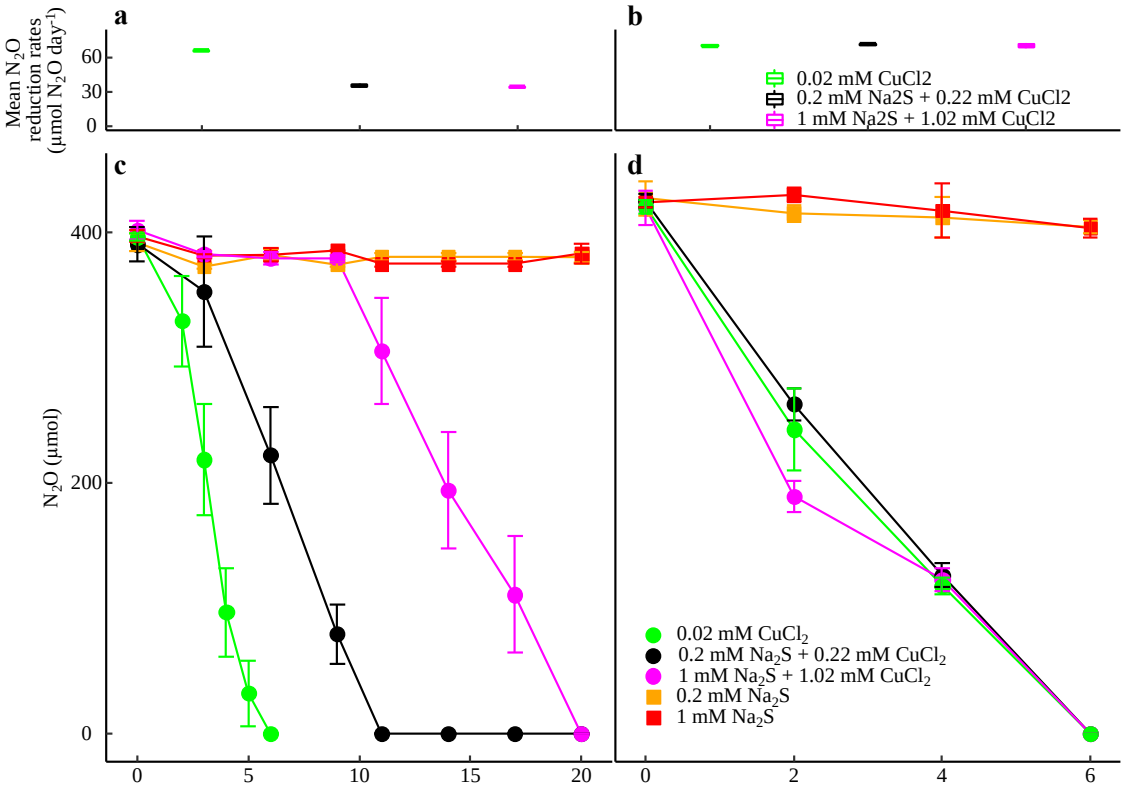


**Figure 4-2. Effect of $Na_2S$ on $N_2O$ reduction.** Mean $N_2O$ reduction rates of culture EV (a) and *D. aromatica* strain RCB (b) in the presence or absence of $Na_2S$. $N_2O$ reduction in culture EV (c) and *D. aromatica* strain RCB (d) received either $CuCl_2$ or $Na_2S$ and cultures amended with excess $CuCl_2$ and $Na_2S$. The data represent the averages of triplicate incubations and error bars represent the standard deviations (n=3). Error bars are not shown if smaller than the symbol.

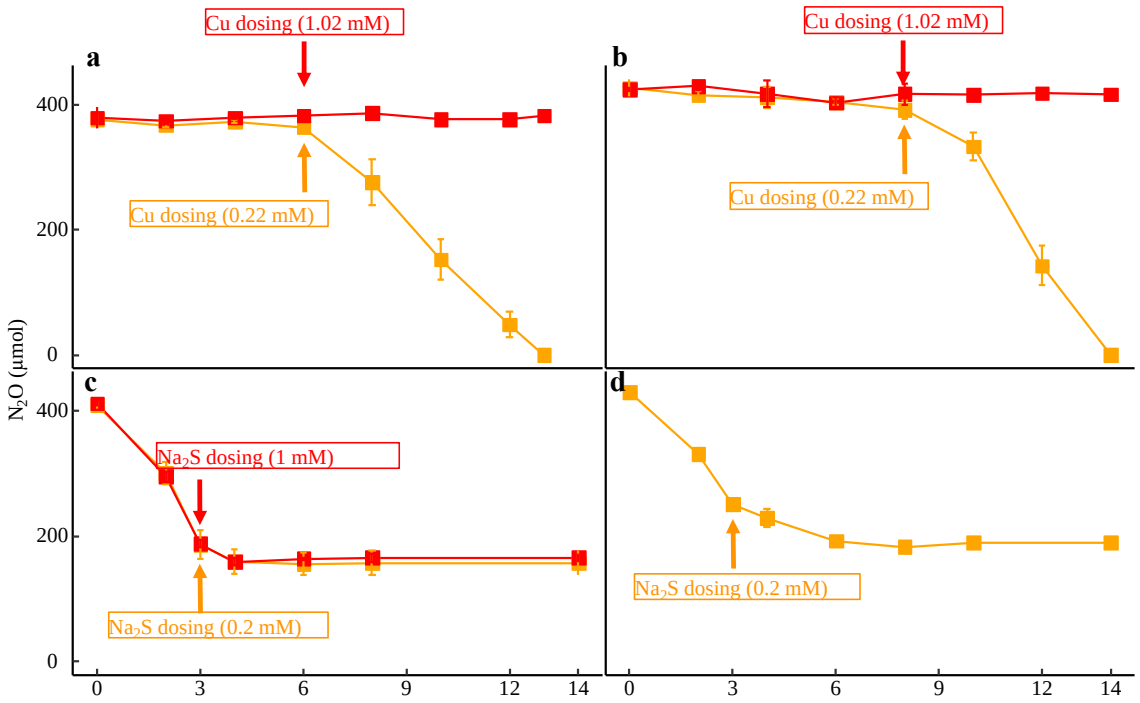


**Figure 4-3. Reversible and irreversible inhibition of $Na_2S$ on $N_2O$ reduction.** $N_2O$ reduction of culture EV following $CuCl_2$ (a) or $Na_2S$ dosing (c). $N_2O$ reduction by *D. aromatica* strain RCB following $CuCl_2$ (c) or $Na_2S$ dosing (d). Arrows indicate $CuCl_2$ or $Na_2S$ dosing. The data represent the averages of triplicate incubations and error bars represent the standard deviations (n=3). Error bars are not shown if smaller than the symbol.

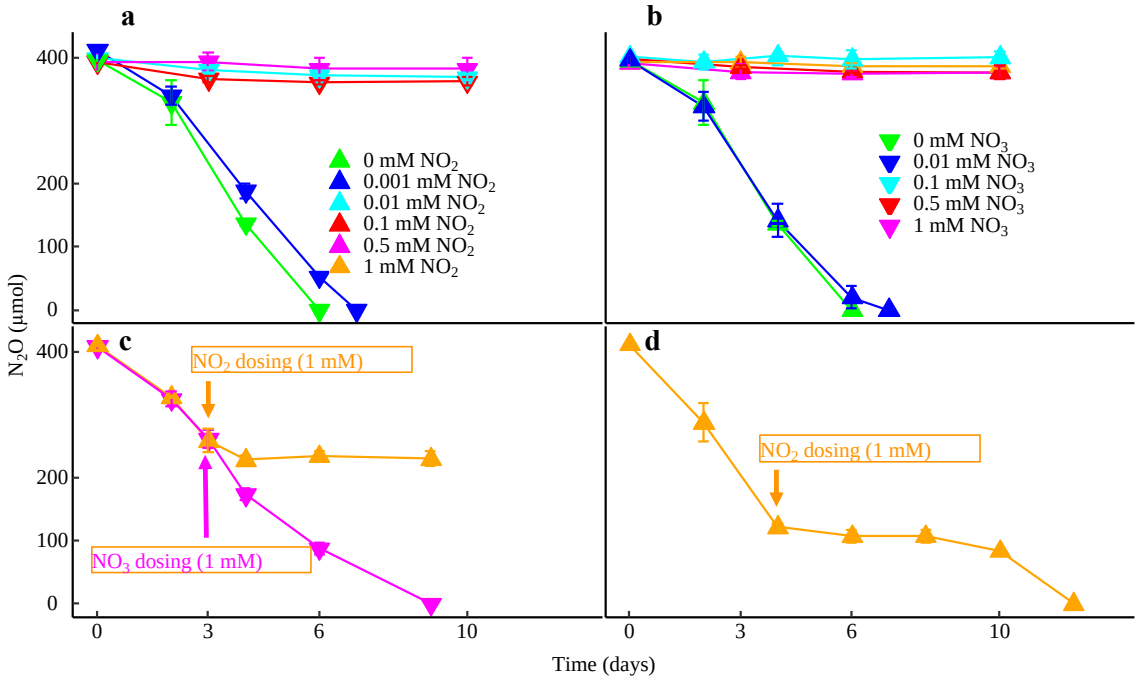


**Figure 4-4. Inhibition of nitrogen oxyanions on $N_2O$ reduction by culture EV.** $N_2O$ reduction in culture EV received varying concentrations of $NO_2^-$ (a) or $NO_3^-$ (b). $N_2O$ reduction in culture EV (c) and *Dechlromonas aromatica* strain RCB (d) following nitrogen oxyanion dosing. The data represent the averages of triplicate incubations and error bars represent the standard deviations (n=3). Error bars are not shown if smaller than the symbol.

## Summary and Conclusion

Soil health is being degraded across the globe due to exploitation, mismanagement, and anthropogenic practices. One important parameter of soil health is pH, but regions around the world are experiencing soil acidification due to natural processes accelerated by acidic precipitation/deposition and agricultural practices that rely on nitrogen fertilizer and the growth of legumes. Nitrogen fertilizer input also leads to the formation of $N_2O$, a substance linked to climate warming and interference with biogeochemical processes such as methanogenesis, mercury turnover, and reductive dechlorination.

The imbalance between $N_2O$ formation and consumption is a key issue, with the rise in global $N_2O$ emission indicating that $N_2O$ formation is outpacing consumption. This is partly due to the contrasting pH optima of processes involved in $N_2O$ formation (pH 5-6) versus consumption (pH~7). While some studies have reported $N_2O$ consumption in acidic soil laboratory microcosms and ecosystems, soil heterogeneity and associated microscale patchiness of pH conditions make generalized conclusions difficult.

Attempts to demonstrate low pH $N_2O$ reduction in denitrifying enrichment and axenic cultures have so far failed to demonstrate growth-linked $N_2O$ reduction and the sustainability of such a process. The only known sink for $N_2O$ are microorganisms expressing $N_2O$ reductase, a periplasmic enzyme that catalyzes the conversion of $N_2O$ to environmentally benign dinitrogen. Studies have shown that pH interferes with NosZ maturation, limiting microbial $N_2O$ reduction to circumneutral pH environments.

However, chapter 2 has shown that organisms capable of low pH $N_2O$ reduction exist, at least, in acidic soils. We demonstrated an intricate organismal interaction between two populations derived from El Verde soil, revealing a commensal relationship between a pyruvate fermenting *Serratia* population and an $N_2O$-reducing *Desulfosporosinus* population. Growth experiments illustrated that the *Serratia* population fermented pyruvate to acetate, formate, and CO2, while the *Desulfosporosinus* population only grew with $N_2O$. The *Desulfosporosinus* population reduced $N_2O$ at a narrow range of pH (4.5

to 6), which contradicts previous observations that model denitrifier *Paracoccus denitrificans* only reduces $N_2O$ above pH 6. The difference in $N_2O$ reduction behavior may be due to differences in enzyme assembly strategies.

In chapter 3, Enrichment cultures were established with acidic tropical forest soil and circumneutral soil retrieved from an organic farm practicing regenerative agriculture. Comparative metagenome analysis revealed $N_2O$ reduction under acidic conditions was associated with microbial growth. Further analysis suggested that low pH $N_2O$ reducers cannot perform canonical denitrification and that phylogenetic analysis of NosZ genes illustrated a preference of acidic pH over clade II $N_2O$ reducers. Two novel subclades were also identified with the *nosZ* sequences from the enrichment cultures.

Although the existence of soil microorganisms capable of low pH $N_2O$ reduction has been demonstrated, the in-situ $N_2O$ emissions from acidic soils are generally higher than those from circumneutral pH soils. Chapter 4 shows that $N_2O$ reduction of the El Verde co-culture is sensitive to geochemical factors such as copper and nitrogen oxyanions. These factors could play a role in limiting $N_2O$ reduction in acidic soils, explaining why $N_2O$ reducers stay inactive even when they reside in such environments.

In conclusion, the study of low pH $N_2O$ reduction in soil microorganisms provides valuable insights into the role of microbial communities in mitigating the impacts of anthropogenic activities on soil health and global climate change. The findings suggest that the reduction of $N_2O$ in acidic soils is not only possible but also linked to the presence of specific microbial populations with unique functional and physiological characteristics. However, the complex interactions between soil biogeochemistry and microbial communities make it difficult to generalize the findings and predict their implications at a larger scale. Further research is needed to better understand the factors that regulate the activity of $N_2O$ reducers in different soil types and under different environmental conditions to develop effective strategies for sustainable soil management and climate change mitigation.

## References


1. A. R. Ravishankara, J. S. Daniel, R. W. Portmann, Nitrous oxide ($N_2O$): The dominant ozone-depleting substance emitted in the 21st century. *Science* **326**, 123-125 (2009).
2. R. L. Thompson *et al.*, Acceleration of global N2O emissions seen from two decades of atmospheric inversion. *Nature Climate Change* **9**, 993-998 (2019).
3. H. Tian *et al.*, A comprehensive quantification of global nitrous oxide sources and sinks. *Nature* **586**, 248-256 (2020).
4. M. M. M. Kuypers, H. K. Marchant, B. Kartal, The microbial nitrogen-cycling network. *Nature Reviews Microbiology* **16**, 263-276 (2018).
5. S. Buessecker *et al.*, Coupled abiotic-biotic cycling of nitrous oxide in tropical peatlands. *Nat. Ecol. Evol.*, 1-10 (2022).
6. D. E. Canfield, A. N. Glazer, P. G. Falkowski, The Evolution and Future of Earth’s Nitrogen Cycle. *Science* **330**, 192-196 (2010).
7. S. Buessecker *et al.*, Mineral-catalysed formation of marine NO and $N_2O$ on the anoxic early Earth. *Nature Geoscience* 10.1038/s41561-022-01089-9 (2022).
8. J. R. Onley, S. Ahsan, R. A. Sanford, F. E. Loffler, Denitrification by Anaeromyxobacter dehalogenans, a Common Soil Bacterium Lacking the Nitrite Reductase Genes nirS and nirK. *Applied and Environmental Microbiology* **84** (2017).
9. F. Picardal, Abiotic and Microbial Interactions during Anaerobic Transformations of Fe(II) and NOX. *Frontiers in Microbiology* **3** (2012).
10. J. H. Butler, L. I. Gordon, Rates of nitrous oxide production in the oxidation of hydroxylamine by iron (III). *Inorganic Chemistry* **25**, 4573-4577 (1986).
11. J. Bremner, A. Blackmer, S. Waring, Formation of nitrous oxide and dinitrogen by chemical decomposition of hydroxylamine in soils. *Soil Biology and Biochemistry* **12**, 263-269 (1980).
12. R. A. Sanford *et al.*, Unexpected nondenitrifier nitrous oxide reductase gene diversity and abundance in soils. *Proc. Natl. Acad. Sci. U.S.A.* **109**, 19709-19714 (2012).
13. S. A. Higgins, C. W. Schadt, F. E. Löffler, P. B. Matheny, Phylogenomics Reveal the Dynamic Evolution of Fungal Nitric Oxide Reductases and Their Relationship to Secondary Metabolism. *Genome Biology and Evolution* **10**, 2474-2489 (2018).
14. S. R. Pauleta, M. S. P. Carepo, I. Moura, Source and reduction of nitrous oxide. *Coordination Chemistry Reviews* **387**, 436-449 (2019).
15. M. S. Coyne, D. D. Focht, Nitrous Oxide Reduction in Nodules: Denitrification or N<sub>2</sub> Fixation? *Applied and Environmental Microbiology* **53**, 1168-1170 (1987).
16. A. T. Fernandes *et al.*, The multicopper oxidase from the archaeon Pyrobaculum aerophilum shows nitrous oxide reductase activity. *The FEBS Journal* **277**, 3176-3189 (2010).
17. K. Brown *et al.*, A novel type of catalytic copper cluster in nitrous oxide reductase. *Nature Structural Biology* **7**, 191-195 (2000).

18. J. Shan *et al.*, Beyond denitrification: The role of microbial diversity in controlling nitrous oxide reduction and soil nitrous oxide emissions. *Global Change Biology* **27**, 2669-2683 (2021).
19. J. J. Moura, I. Moura, L. B. Maia, *Enzymes for Solving Humankind's Problems* (Springer, 2021).
20. D. Park, H. Kim, S. Yoon, Nitrous oxide reduction by an obligate aerobic bacterium, *Gemmatimonas aurantiaca* Strain T-27. *Appl. Environ. Microbiol.* **83**, AEM.00502-00517 (2017).
21. M. J. Sullivan, A. J. Gates, C. Appia-Ayme, G. Rowley, D. J. Richardson, Copper control of bacterial nitrous oxide emission and its impact on vitamin $B_{12}$-dependent metabolism. *Proc. Natl. Acad. Sci. U.S.A.* **110**, 19926-19931 (2013).
22. C. M. Jones, D. R. H. Graf, D. Bru, L. Philippot, S. Hallin, The unaccounted yet abundant nitrous oxide-reducing microbial community: a potential nitrous oxide sink. *The ISME Journal* **7**, 417-426 (2013).
23. S. Hallin, L. Philippot, F. E. Löffler, R. A. Sanford, C. M. Jones, Genomics and ecology of novel $N_2O$-reducing microorganisms. *Trends Microbiol.* **26**, 43-55 (2018).
24. I. S. Pessi *et al.*, In-depth characterization of denitrifier communities across different soil ecosystems in the tundra. *Environmental Microbiome* **17**, 30 (2022).
25. N. Van Breemen, J. Mulder, J. Van Grinsven, Impacts of acid atmospheric deposition on woodland soils in the Netherlands: II. Nitrogen transformations. *Soil Science Society of America Journal* **51**, 1634-1640 (1987).
26. D. T. a. S. Niu, A global analysis of soil acidification caused by nitrogen additi. *Environmental Research Letters* **10** (2015).
27. L. F. Schulte-Uebbing, A. H. W. Beusen, A. F. Bouwman, W. de Vries, From planetary to regional boundaries for agricultural nitrogen pollution. *Nature* **610**, 507-512 (2022).
28. N. Gruber, J. N. Galloway, An Earth-system perspective of the global nitrogen cycle. *Nature* **451**, 293 (2008).
29. M. Bahram *et al.*, Structure and function of the soil microbiome underlying $N_2O$ emissions from global wetlands. *Nat. Commun.* **13**, 1430 (2022).
30. J.-M. Blum *et al.*, The pH dependency of N-converting enzymatic processes, pathways and microbes: effect on net $N_2O$ production. *Environ. Microbiol.* **20**, 1623-1640 (2018).
31. M.-Y. Jung *et al.*, Indications for enzymatic denitrification to $N_2O$ at low pH in an ammonia-oxidizing archaeon. *ISME J.* **13**, 2633-2638 (2019).
32. S. Yoon, C. Cruz-Garcia, R. Sanford, K. M. Ritalahti, F. E. Loffler, Denitrification versus respiratory ammonification: environmental controls of two competing dissimilatory NO3(-)/NO2(-) reduction pathways in Shewanella loihica strain PV-4. *Isme j* **9**, 1093-1104 (2015).
33. N. Y. N. Lim, Å. Frostegård, L. R. Bakken, Nitrite kinetics during anoxia: The role of abiotic reactions versus microbial reduction. *Soil Biology and Biochemistry* **119**, 203-209 (2018).

34. R. N. Van Den Heuvel, E. Van Der Biezen, M. S. M. Jetten, M. M. Hefting, B. Kartal, Denitrification at pH 4 by a soil-derived *Rhodanobacter*-dominated community. *Environ. Microbiol.* **12**, 3264-3271 (2010).
35. Y. Yang *et al.*, Organohalide respiration with chlorinated ethenes under low pH conditions. *Environ. Sci. Technol.* **51**, 8579-8588 (2017).
36. K. R. Jonassen *et al.*, A dual enrichment strategy provides soil-and digestate-competent nitrous oxide-respiring bacteria for mitigating climate forcing in agriculture. *mBio*, e00788-00722 (2022).
37. Y. Wang *et al.*, Soil pH as the chief modifier for regional nitrous oxide emissions: New evidence and implications for global estimates and mitigation. *Global Change Biology* **24**, e617-e626 (2018).
38. L. Bergaust, Y. Mao, R. Bakken Lars, Å. Frostegård, Denitrification response patterns during the transition to anoxic respiration and posttranscriptional effects of suboptimal pH on nitrogen oxide reductase in *Paracoccus denitrificans*. *Appl. Environ. Microbiol.* **76**, 6387-6396 (2010).
39. E. Bueno *et al.*, Anoxic growth of *Ensifer meliloti* 1021 by $N_2O$-reduction, a potential mitigation strategy. *Front. Microbiol.* **6** (2015).
40. B. Liu, Å. Frostegård, L. R. Bakken, Impaired reduction of $N_2O$ to $N_2$ in acid soils is due to a posttranscriptional interference with the expression of *nosZ*. *mBio* **5**, e01383-01314-e01383 (2014).
41. Å. Frostegård, S. H. W. Vick, N. Y. N. Lim, L. R. Bakken, J. P. Shapleigh, Linking meta-omics to the kinetics of denitrification intermediates reveals pH-dependent causes of $N_2O$ emissions and nitrite accumulation in soil. *ISME J.* 10.1038/s41396-021-01045-2 (2021).
42. C. Carreira, R. F. Nunes, O. Mestre, I. Moura, S. R. Pauleta, The effect of pH on *Marinobacter hydrocarbonoclasticus* denitrification pathway and nitrous oxide reductase. *J. Biol. Inorg. Chem.* **25**, 927-940 (2020).
43. S. Karthikeyan *et al.*, Metagenomic characterization of soil microbial communities in the Luquillo experimental forest (Puerto Rico) and implications for nitrogen cycling. *Appl. Environ. Microbiol.* 10.1128/aem.00546-21, AEM.00546-00521 (2021).
44. Y. Sun *et al.*, pH selects for distinct $N_2O$-reducing microbiomes in tropical soil microcosms. **In Review**.
45. A. Sharma, D. Parashar, T. Satyanarayana, "Acidophilic Microbes: Biology and Applications" in Biotechnology of Extremophiles: Advances and Challenges, P. H. Rampelotto, Ed. (Springer International Publishing, Cham, 2016), 10.1007/978-3-319-13521-2_7, pp. 215-241.
46. R. B. Jackson, M. M. Caldwell, Geostatistical patterns of soil heterogeneity around individual perennial plants. *J. Ecol.* **81**, 683-692 (1993).
47. K. Zhu, X. Ye, H. Ran, P. Zhang, G. Wang, Contrasting effects of straw and biochar on microscale heterogeneity of soil $O_2$ and pH: Implication for $N_2O$ emissions. *Soil Biol. Biochem.* **166**, 108564 (2022).
48. R. Lal, Soil health and carbon management. *Food Energy Secur.* **5**, 212-222 (2016).

49. N. S. Bolan, M. J. Hedley, "Role of carbon, nitrogen, and sulfur cycles in soil acidification" in Handbook of soil acidity. (CRC Press, 2003), pp. 43-70.
50. K. W. T. Goulding, Soil acidification and the importance of liming agricultural soils with particular reference to the United Kingdom. *Soil Use Manage.* **32**, 390-399 (2016).
51. D. A. Lashof, D. R. Ahuja, Relative contributions of greenhouse gas emissions to global warming. *Nature* **344**, 529-531 (1990).
52. IPCC (2022) Climate Change 2022: Mitigation of Climate Change. Working Group III Contribution to the IPCC Sixth Assessment Report. in *Contribution of Working Group I to the Fourth Assessment Report of the Intergovernmental Panel*.
53. J. H. Guo *et al.*, Significant acidification in major Chinese croplands. *Science* **327**, 1008-1010 (2010).
54. C. Meng *et al.*, Global soil acidification impacts on belowground processes. *Environ. Res. Lett.* **14**, 074003 (2019).
55. Y. Yin *et al.*, Nitrous oxide is a potent inhibitor of bacterial reductive dechlorination. *Environ. Sci. Technol.* **53**, 692-701 (2019).
56. L. Zhang *et al.*, Inhibition of methylmercury and methane formation by nitrous oxide in Arctic tundra soil microcosms. *Environ. Sci. Technol.* **57**, 5655-5665 (2023).
57. K. Palmer, C. Biasi, M. A. Horn, Contrasting denitrifier communities relate to contrasting $N_2O$ emission patterns from acidic peat soils in Arctic tundra. *ISME J.* **6**, 1058-1077 (2012).
58. K. R. Jonassen *et al.*, Nitrous oxide respiring bacteria in biogas digestates for reduced agricultural emissions. *ISME J.* **16**, 580-590 (2022).
59. J. K. Thomsen, T. Geest, R. P. Cox, Mass spectrometric studies of the effect of pH on the accumulation of intermediates in denitrification by *Paracoccus denitrificans*. *Appl. Environ. Microbiol.* **60**, 536-541 (1994).
60. A. Olaya-Abril *et al.*, Effect of pH on the denitrification proteome of the soil bacterium *Paracoccus denitrificans* PD1222. *Sci. Rep.* **11**, 17276 (2021).
61. F. E. Löffler, R. A. Sanford, K. M. Ritalahti, "Enrichment, cultivation, and detection of reductively dechlorinating bacteria" in Methods in Enzymology. (Academic Press, 2005), vol. 397, pp. 77-111.
62. F. E. Loffler, R. A. Sanford, J. M. Tiedje, Initial characterization of a reductive dehalogenase from *Desulfitobacterium chlororespirans* Co23. *Appl. Environ. Microbiol.* **62**, 3809-3813 (1996).
63. G. Chen *et al.*, Anaerobic microbial metabolism of dichloroacetate. *mBio* **12**, e00537-00521 (2021).
64. A. Klindworth *et al.*, Evaluation of general 16S ribosomal RNA gene PCR primers for classical and next-generation sequencing-based diversity studies. *Nucleic Acids Res.* **41**, e1-e1 (2012).
65. P. Di Tommaso *et al.*, Nextflow enables reproducible computational workflows. *Nat. Biotechnol.* **35**, 316-319 (2017).

66. G. M. Kurtzer, V. Sochat, M. W. Bauer, Singularity: Scientific containers for mobility of compute. *PLOS ONE* **12**, e0177459 (2017).
67. S. Andrews, FastQC: a quality control tool for high throughput sequence data. *Cambridge, UK: Babraham Institute* https://www.bioinformatics.babraham.ac.uk/projects/fastqc/ (2010).
68. M. Martin, Cutadapt removes adapter sequences from high-throughput sequencing reads. *EMBnet. J.* **17**, 3 (2011).
69. B. J. Callahan *et al.*, DADA2: High-resolution sample inference from Illumina amplicon data. *Nat. Methods* **13**, 581-583 (2016).
70. T. Seemann, *barrnap 0.9: rapid ribosomal RNA prediction*. https://github.com/tseemann/barrnap (2013).
71. C. Quast *et al.*, The SILVA ribosomal RNA gene database project: improved data processing and web-based tools. *Nucleic Acids Res.* **41**, D590-D596 (2012).
72. E. Bolyen *et al.*, Reproducible, interactive, scalable and extensible microbiome data science using QIIME 2. *Nat. Biotechnol.* **37**, 852-857 (2019).
73. Y. Chen *et al.*, Parallel-Meta Suite: Interactive and rapid microbiome data analysis on multiple platforms. *iMeta* **1**, e1 (2022).
74. F. E. Löffler, Q. Sun, J. Li, J. M. Tiedje, 16S rRNA gene-based detection of tetrachloroethene-dechlorinating *Desulfuromonas* and *Dehalococcoides* species. *Appl. Environ. Microbiol.* **66**, 1369-1374 (2000).
75. J. Ye *et al.*, Primer-BLAST: A tool to design target-specific primers for polymerase chain reaction. *BMC Bioinformatics* **13**, 134 (2012).
76. K. M. Ritalahti *et al.*, Quantitative PCR targeting 16S rRNA and reductive dehalogenase genes simultaneously monitors multiple *Dehalococcoides* strains. *Appl. Environ. Microbiol.* **72**, 2765-2774 (2006).
77. S. Krakau, D. Straub, H. Gourlé, G. Gabernet, S. Nahnsen, nf-core/mag: a best-practice pipeline for metagenome hybrid assembly and binning. *NAR Genom. Bioinform.* **4** (2022).
78. S. Chen, Y. Zhou, Y. Chen, J. Gu, fastp: an ultra-fast all-in-one FASTQ preprocessor. *Bioinformatics* **34**, i884-i890 (2018).
79. B. Langmead, S. L. Salzberg, Fast gapped-read alignment with Bowtie 2. *Nat. Methods* **9**, 357-359 (2012).
80. D. Li, C.-M. Liu, R. Luo, K. Sadakane, T.-W. Lam, MEGAHIT: an ultra-fast single-node solution for large and complex metagenomics assembly via succinct de Bruijn graph. *Bioinformatics* **31**, 1674-1676 (2015).
81. D. D. Kang *et al.*, MetaBAT 2: an adaptive binning algorithm for robust and efficient genome reconstruction from metagenome assemblies. *PeerJ* **7**, e7359 (2019).
82. D. H. Parks, M. Imelfort, C. T. Skennerton, P. Hugenholtz, G. W. Tyson, CheckM: assessing the quality of microbial genomes recovered from isolates, single cells, and metagenomes. *Genome Res.* **25**, 1043-1055 (2015).
83. K. Gemayel, A. Lomsadze, M. Borodovsky, MetaGeneMark-2: Improved Gene Prediction in Metagenomes. *bioRxiv* 10.1101/2022.07.25.500264, 2022.2007.2025.500264 (2022).

84. C. Camacho *et al.*, BLAST+: architecture and applications. *BMC Bioinformatics* **10**, 421 (2009).
85. A. Bairoch, R. Apweiler, The SWISS-PROT protein sequence database and its supplement TrEMBL in 2000. *Nucleic Acids Res.* **28**, 45-48 (2000).
86. T. Aramaki *et al.*, KofamKOALA: KEGG Ortholog assignment based on profile HMM and adaptive score threshold. *Bioinformatics* **36**, 2251-2252 (2019).
87. R. Overbeek *et al.*, The SEED and the Rapid Annotation of microbial genomes using Subsystems Technology (RAST). *Nucleic Acids Res.* **42**, D206-D214 (2013).
88. L. M. Rodriguez-R, K. T. Konstantinidis, The enveomics collection: a toolbox for specialized analyses of microbial genomes and metagenomes. *PeerJ Preprints* (2016).
89. L. M. Rodriguez-R, K. T. Konstantinidis, Nonpareil: a redundancy-based approach to assess the level of coverage in metagenomic datasets. *Bioinformatics* **30**, 629-635 (2013).
90. J. Hallgren *et al.*, DeepTMHMM predicts alpha and beta transmembrane proteins using deep neural networks. *bioRxiv* 10.1101/2022.04.08.487609, 2022.2004.2008.487609 (2022).
91. P.-A. Chaumeil, A. J. Mussig, P. Hugenholtz, D. H. Parks, GTDB-Tk: a toolkit to classify genomes with the Genome Taxonomy Database. *Bioinformatics* **36**, 1925-1927 (2019).
92. A. M. Kozlov, D. Darriba, T. Flouri, B. Morel, A. Stamatakis, RAxML-NG: a fast, scalable and user-friendly tool for maximum likelihood phylogenetic inference. *Bioinformatics* **35**, 4453-4455 (2019).
93. D. Darriba *et al.*, ModelTest-NG: a new and scalable tool for the selection of DNA and protein evolutionary models. *Mol. Biol. Evol.* **37**, 291-294 (2019).
94. D. Kim, S. Park, J. Chun, Introducing EzAAI: a pipeline for high throughput calculations of prokaryotic average amino acid identity. *J. Microbiol.* **59**, 476-480 (2021).
95. G. Yu, D. K. Smith, H. Zhu, Y. Guan, T. T.-Y. Lam, ggtree: an r package for visualization and annotation of phylogenetic trees with their covariates and other associated data. *Methods Ecol. Evol.* **8**, 28-36 (2017).
96. L. H. Orellana, L. M. Rodriguez-R, K. T. Konstantinidis, ROCker: accurate detection and quantification of target genes in short-read metagenomic data sets by modeling sliding-window bitscores. *Nucleic Acids Res.* **45**, e14-e14 (2016).
97. K. Katoh, D. M. Standley, MAFFT multiple sequence alignment software version 7: improvements in performance and usability. *Mol. Biol. Evol.* **30**, 772-780 (2013).
98. S. P. Dearth *et al.*, Metabolome changes are induced in the arbuscular mycorrhizal fungus Gigaspora margarita by germination and by its bacterial endosymbiont. *Mycorrhiza* **28**, 421-433 (2018).
99. W. Lu *et al.*, Metabolomic analysis via reversed-phase ion-pairing liquid chromatography coupled to a stand alone orbitrap mass spectrometer. *Anal. Chem.* **82**, 3212-3221 (2010).

100. M. F. Clasquin, E. Melamud, J. D. Rabinowitz, LC-MS data processing with MAVEN: A metabolomic analysis and visualization engine. *Curr. Protoc. Bioinformatics* **37**, 14.11.11-14.11.23 (2012).
101. S. Yoon, S. Nissen, D. Park, R. A. Sanford, F. E. Löffler, Nitrous oxide reduction kinetics distinguish bacteria harboring clade I NosZ from those harboring clade II NosZ. *Appl. Environ. Microbiol.* **82**, 3793-3800 (2016).
102. R. Sander, Compilation of Henry's law constants (version 4.0) for water as solvent. *Atmos. Chem. Phys.* **15**, 4399-4981 (2015).
103. P. Keawmanee, C. Rattanakreetakul, R. Pongpisutta, Microbial reduction of fumonisin B1 by the new isolate *Serratia marcescens* 329-2. *Toxins* **13**, 638 (2021).
104. I. Sánchez-Andrea, A. J. M. Stams, S. Hedrich, I. Ňancucheo, D. B. Johnson, *Desulfosporosinus acididurans* sp. nov.: an acidophilic sulfate-reducing bacterium isolated from acidic sediments. *Extremophiles* **19**, 39-47 (2015).
105. M. Fukushi *et al.*, Biogeochemical implications of $N_2O$-reducing thermophilic Campylobacteria in deep-sea vent fields, and the description of *Nitratiruptor labii* sp. nov. *iScience* **23**, 101462 (2020).
106. I. Kristoficova, C. Vilhena, S. Behr, K. Jung, BtsT, a novel and specific pyruvate/$H^+$ symporter in *Escherichia coli*. *J. Bacteriol.* **200**, e00599-00517 (2018).
107. P.-H. Wang *et al.*, Refined experimental annotation reveals conserved corrinoid autotrophy in chloroform-respiring *Dehalobacter* isolates. *ISME J.* **11**, 626-640 (2017).
108. N. Rascio, N. La Rocca, "Biological Nitrogen Fixation" in Encyclopedia of Ecology, S. E. Jørgensen, B. D. Fath, Eds. (Academic Press, Oxford, 2008), https://doi.org/10.1016/B978-008045405-4.00273-1, pp. 412-419.
109. J. W. Erisman, M. A. Sutton, J. Galloway, Z. Klimont, W. Winiwarter, How a century of ammonia synthesis changed the world. *Nature Geosci.* **1**, 636-639 (2008).
110. Y. Zhou *et al.*, Nitrous oxide-sink capability of denitrifying bacteria impacted by nitrite and pH. *Chem. Eng. J.* **428**, 132402 (2022).
111. H. Kim, D. Park, S. Yoon, pH control enables simultaneous enhancement of nitrogen retention and $N_2O$ reduction in *Shewanella loihica* Strain PV-4. *Front. Microbiol.* **8** (2017).
112. M. P. Highton, L. R. Bakken, P. Dörsch, L. Molstad, S. E. Morales, Nitrite accumulation and impairment of $N_2O$ reduction explains contrasting soil denitrification phenotypes. *Soil Biol. Biochem.* **166**, 108529 (2022).
113. L. Alldredge Alice, Y. Cohen, Can microscale chemical patches persist in the sea? Microelectrode study of marine snow, fecal pellets. *Science* **235**, 689-691 (1987).
114. M. C. v. Loosdrecht, J. Lyklema, W. Norde, A. J. Zehnder, Influence of interfaces on microbial activity. *Microbiol. Rev.* **54**, 75-87 (1990).
115. I. Sánchez-Andrea, A. J. M. Stams, R. Amils, J. L. Sanz, Enrichment and isolation of acidophilic sulfate-reducing bacteria from Tinto River sediments. *Environ. Microbiol. Rep.* 10.1111/1758-2229.12066, 672-678 (2013).

116. P. Lycus *et al.*, Phenotypic and genotypic richness of denitrifiers revealed by a novel isolation strategy. *ISME J.* **11**, 2219-2232 (2017).
117. J. Čuhel *et al.*, Insights into the effect of soil pH on $N_2O$ and $N_2$ emissions and denitrifier community size and activity. *Appl. Environ. Microbiol.* **76**, 1870-1878 (2010).
118. K. Palmer, A. Horn Marcus, Actinobacterial nitrate reducers and Proteobacterial denitrifiers are abundant in $N_2O$-metabolizing palsa peat. *Appl. Environ. Microbiol.* **78**, 5584-5596 (2012).
119. P. Natale, T. Brüser, A. J. M. Driessen, Sec- and Tat-mediated protein secretion across the bacterial cytoplasmic membrane—Distinct translocases and mechanisms. *Biochim. Biophys. Acta* **1778**, 1735-1756 (2008).
120. C. Xianke, "Thriving at low pH: Adaptation mechanisms of acidophiles" in Acidophiles, L. Jianqiang, C. Linxu, L. Jianqun, Eds. (IntechOpen, Rijeka, 2021), 10.5772/intechopen.96620, pp. Ch. 3.
121. C. Baker-Austin, M. Dopson, Life in acid: pH homeostasis in acidophiles. *Trends Microbiol.* **15**, 165-171 (2007).
122. K. Zengler, L. S. Zaramela, The social network of microorganisms—how auxotrophies shape complex communities. *Nat. Rev. Microbiol.* **16**, 383-390 (2018).
123. M. Embree, K. Liu Joanne, M. Al-Bassam Mahmoud, K. Zengler, Networks of energetic and metabolic interactions define dynamics in microbial communities. *Proc. Natl. Acad. Sci. U.S.A.* **112**, 15450-15455 (2015).
124. M. T. Mee, J. J. Collins, G. M. Church, H. H. Wang, Syntrophic exchange in synthetic microbial communities. *Proc. Natl. Acad. Sci. U.S.A.* **111**, E2149-E2156 (2014).
125. M. T. Croft, A. D. Lawrence, E. Raux-Deery, M. J. Warren, A. G. Smith, Algae acquire vitamin $B_{12}$ through a symbiotic relationship with bacteria. *Nature* **438**, 90-93 (2005).
126. M. Jiang, X. Zheng, Y. Chen, Enhancement of denitrification performance with reduction of nitrite accumulation and $N_2O$ emission by *Shewanella oneidensis* MR-1 in microbial denitrifying process. *Water Res.* **169**, 115242 (2020).
127. J. Chang *et al.*, Enhancement of nitrous oxide emissions in soil microbial consortia via copper competition between Proteobacterial methanotrophs and denitrifiers. *Appl. Environ. Microbiol.* **87**, e02301-02320 (2021).
128. Y. Pan, L. Ye, B.-J. Ni, Z. Yuan, Effect of pH on $N_2O$ reduction and accumulation during denitrification by methanol utilizing denitrifiers. *Water Res.* **46**, 4832-4840 (2012).
129. H. Hippe, E. Stackebrandt, "*Desulfosporosinus*" in Bergey's Manual of Systematics of Archaea and Bacteria. (2015), https://doi.org/10.1002/9781118960608.gbm00660, pp. 1-10.
130. D. Alazard, M. Joseph, F. Battaglia-Brunet, J.-L. Cayol, B. Ollivier, *Desulfosporosinus acidiphilus* sp. nov.: a moderately acidophilic sulfate-reducing bacterium isolated from acid mining drainage sediments. *Extremophiles* **14**, 305-312 (2010).

131. I. A. Panova *et al.*, *Desulfosporosinus metallidurans* sp. nov., an acidophilic, metal-resistant sulfate-reducing bacterium from acid mine drainage. *Int. J. Syst. Evol. Microbiol.* **71** (2021).
132. A. V. Mardanov *et al.*, Genomic insights into a new acidophilic, copper-resistant *Desulfosporosinus* isolate from the oxidized tailings area of an abandoned gold mine. *FEMS Microbiol. Ecol.* **92** (2016).
133. P. Petzsch *et al.*, Genome sequence of the moderately acidophilic sulfate-reducing *Firmicute Desulfosporosinus acididurans* (Strain M1$^T$). *Genome Announc.* **3**, 10.1128/genomea.00881-00815 (2015).
134. M. Pester *et al.*, Complete genome sequences of *Desulfosporosinus orientis* DSM765$^T$, *Desulfosporosinus youngiae* DSM17734$^T$, *Desulfosporosinus meridiei* DSM13257$^T$, and *Desulfosporosinus acidiphilus* DSM22704$^T$. *J. Bacteriol.* **194**, 6300-6301 (2012).
135. S. Xu *et al.*, Linking $N_2O$ emissions from biofertilizer-amended soil of tea plantations to the abundance and structure of $N_2O$-reducing microbial communities. *Environ. Sci. Technol.* **52**, 11338-11345 (2018).
136. N. Gao *et al.*, Inoculation with nitrous oxide ($N_2O$)-reducing denitrifier strains simultaneously mitigates $N_2O$ emission from pasture soil and promotes growth of pasture plants. *Soil Biol. Biochem.* **97**, 83-91 (2016).
137. T. Seemann, Prokka: rapid prokaryotic genome annotation. *Bioinformatics* **30**, 2068-2069 (2014).
138. C. A. Ruiz-Perez, R. E. Conrad, K. T. Konstantinidis, MicrobeAnnotator: a user-friendly, comprehensive functional annotation pipeline for microbial genomes. *BMC Bioinformatics* **22**, 11 (2021).
139. A. Liaw, M. Wiener, Classification and regression by randomForest. *R news* **2**, 18-22 (2002).
140. A. J. Bishara, J. B. Hittner, Testing the significance of a correlation with nonnormal data: Comparison of Pearson, Spearman, transformation, and resampling approaches. *Psychol. Methods* **17**, 399-417 (2012).
141. E. Bueno *et al.*, Regulation of the emissions of the greenhouse gas nitrous oxide by the soybean endosymbiont bradyrhizobium diazoefficiens. *Int. J. Mol. Sci.* **23**, 1486 (2022).
142. L. Dabos *et al.*, SME-4-producing *Serratia marcescens* from Argentina belonging to clade 2 of the *S. marcescens* phylogeny. *J. Antimicrob. Chemother.* **74**, 1836-1841 (2019).
143. S. Buessecker *et al.*, Microbial communities and interactions of nitrogen oxides with methanogenesis in diverse peatlands of the Amazon basin. *Front. Microbiol.* **12** (2021).
144. S. Teske, C. Briggs, S. Miyake (2022) Limit global warming to 1.5° C—Renewable Target Mapping for the G20; Report prepared by the University of Technology Sydney, Institute for Sustainable Futures (UTS/ISF). (Australia).
145. S. Zaehle, P. Ciais, A. D. Friend, V. Prieur, Carbon benefits of anthropogenic reactive nitrogen offset by nitrous oxide emissions. *Nat. Geosci.* **4**, 601-605 (2011).

146. D. S. Reay *et al.*, Global agriculture and nitrous oxide emissions. *Nature Climate Change* **2**, 410-416 (2012).
147. K. Butterbach-Bahl, E. M. Baggs, M. Dannenmann, R. Kiese, S. Zechmeister-Boltenstern, Nitrous oxide emissions from soils: how well do we understand the processes and their controls? *Philos. Trans. R. Soc. Lond., B, Biol. Sci.* **368**, 20130122 (2013).
148. D. Tilman, C. Balzer, J. Hill, B. L. Befort, Global food demand and the sustainable intensification of agriculture. *Proc. Natl. Acad. Sci. U.S.A.* **108**, 20260-20264 (2011).
149. E. K. Moore, B. I. Jelen, D. Giovannelli, H. Raanan, P. G. Falkowski, Metal availability and the expanding network of microbial metabolisms in the Archaean eon. *Nat. Geosci.* **10**, 629-636 (2017).
150. Q. Cui *et al.*, Effects of warming on $N_2O$ fluxes in a boreal peatland of Permafrost region, Northeast China. *Sci. Total Environ.* **616-617**, 427-434 (2018).
151. A. W. Quebbeman *et al.*, A Severe Hurricane Increases Carbon Dioxide and Methane Fluxes and Triples Nitrous Oxide Emissions in a Tropical Forest. *Ecosystems* **25**, 1754-1766 (2022).
152. A. M. Weitz, E. Linder, S. Frolking, P. M. Crill, M. Keller, $N_2O$ emissions from humid tropical agricultural soils: effects of soil moisture, texture and nitrogen availability. *Soil Biol. Biochem.* **33**, 1077-1093 (2001).
153. C. Voigt *et al.*, Nitrous oxide emissions from permafrost-affected soils. *Nat. Rev. Earth Environ.* **1**, 420-434 (2020).
154. L. Chapuis-Lardy, N. Wrage, A. Metay, J.-L. Chotte, M. Bernoux, Soils, a sink for $N_2O$? A review. *Global Chang. Biol.* **13**, 1-17 (2007).
155. Y.-W. Wu, B. A. Simmons, S. W. Singer, MaxBin 2.0: an automated binning algorithm to recover genomes from multiple metagenomic datasets. *Bioinformatics* **32**, 605-607 (2015).
156. C. M. K. Sieber *et al.*, Recovery of genomes from metagenomes via a dereplication, aggregation and scoring strategy. *Nat. Microbiol.* **3**, 836-843 (2018).
157. M. R. Olm, C. T. Brown, B. Brooks, J. F. Banfield, dRep: a tool for fast and accurate genomic comparisons that enables improved genome recovery from metagenomes through de-replication. *ISME J.* **11**, 2864-2868 (2017).
158. S. Xu *et al.*, ggtreeExtra: Compact visualization of richly annotated phylogenetic data. *Mol. Biol. Evol.* **38**, 4039-4042 (2021).
159. K. Konstantinidis *et al.*, FastAAI: Efficient estimation of genome average amino acid identity and phylum-level relationships using tetramers of universal proteins. (2022).
160. S. F. Altschul *et al.*, Gapped BLAST and PSI-BLAST: a new generation of protein database search programs. *Nucleic Acids Research* **25**, 3389-3402 (1997).
161. F. Teufel *et al.*, SignalP 6.0 predicts all five types of signal peptides using protein language models. *Nature Biotechnology* **40**, 1023-1025 (2022).
162. M. Mirdita *et al.*, ColabFold: making protein folding accessible to all. *Nat. Methods* **19**, 679-682 (2022).

163. S. Gutierrez, W. G. Tyczynski, W. Boomsma, F. Teufel, O. Winther, MembraneFold: Visualising transmembrane protein structure and topology. *bioRxiv* 10.1101/2022.12.06.518085, 2022.2012.2006.518085 (2022).
164. M. L. Hekkelman, I. de Vries, R. P. Joosten, A. Perrakis, AlphaFill: enriching AlphaFold models with ligands and cofactors. *Nat. Methods* **20**, 205-213 (2023).
165. T. D. Goddard *et al.*, UCSF ChimeraX: Meeting modern challenges in visualization and analysis. *Protein Sci.* **27**, 14-25 (2018).
166. T. Kruse *et al.*, Comparative genomics of the genus Desulfitobacterium. *FEMS Microbiology Ecology* **93** (2017).
167. S. Meng *et al.*, Ecological distribution and function of comammox *Nitrospira* in the environment. *Appl. Microbiol. Biotechnol.* **107**, 3877-3886 (2023).
168. O. E. Mosley *et al.*, Nitrogen cycling and microbial cooperation in the terrestrial subsurface. *ISME J.* **16**, 2561-2573 (2022).
169. C. Müller *et al.*, Molecular interplay of an assembly machinery for nitrous oxide reductase. *Nature* **608**, 626-631 (2022).
170. J. C. Chee-Sanford, L. Connor, A. Krichels, W. H. Yang, R. A. Sanford, Hierarchical detection of diverse Clade II (atypical) *nosZ* genes using new primer sets for classical- and multiplex PCR array applications. *J. Microbiol. Methods* **172**, 105908 (2020).
171. C. Bettigole *et al.*, Optimizing sampling strategies for near-surface soil carbon inventory: One size doesn't fit all. *Soil Syst.* **7**, 27 (2023).
172. T. Suenaga, S. Riya, M. Hosomi, A. Terada, Biokinetic characterization and activities of $N_2O$-reducing bacteria in response to various oxygen levels. *Front. Microbiol.* **9** (2018).
173. J. Zhou *et al.*, Effects of acidification on nitrification and associated nitrous oxide emission in estuarine and coastal waters. *Nat. Commun.* **14**, 1380 (2023).
174. T. Suenaga *et al.*, Enrichment, Isolation, and Characterization of High-Affinity N2O-Reducing Bacteria in a Gas-Permeable Membrane Reactor. *Environmental science & technology* **53**, 12101-12112 (2019).
175. S. E. Morales, T. Cosart, W. E. Holben, Bacterial gene abundances as indicators of greenhouse gas emission in soils. *The ISME Journal* **4**, 799-808 (2010).
176. W. G. Zumft, Cell biology and molecular basis of denitrification. *Microbiology and Molecular Biology Reviews* **61**, 533-616 (1997).
177. C. M. Jones, B. Stres, M. Rosenquist, S. Hallin, Phylogenetic analysis of nitrite, nitric oxide, and nitrous oxide respiratory enzymes reveal a complex evolutionary history for denitrification. *Molecular Biology and Evolution* **25**, 1955-1966 (2008).
178. B. Wang, Y.-L. Qiu, Phylogenetic distribution and evolution of mycorrhizas in land plants. *Mycorrhiza* **16**, 299-363 (2006).
179. K. T. Konstantinidis, R. Rosselló-Móra, R. Amann, Uncultivated microbes in need of their own taxonomy. *ISME J.* **11**, 2399-2406 (2017).
180. R. W. Portmann, S. Solomon, Indirect radiative forcing of the ozone layer during the 21st century. *Geophysical Research Letters* **34** (2007).

181. L. R. Bakken, Å. Frostegård, Sources and sinks for $N_2O$, can microbiologist help to mitigate $N_2O$ emissions? *Environ. Microbiol.* **19**, 4801-4805 (2017).
182. S. Buessecker *et al.*, Coupled abiotic-biotic cycling of nitrous oxide in tropical peatlands. *bioRxiv* 10.1101/2022.01.14.475290, 2022.2001.2014.475290 (2022).
183. X.-Y. Xing *et al.*, Warming shapes nirS-and nosZ-type denitrifier communities and stimulates N2O emission in acidic paddy soil. *Applied and Environmental Microbiology* **87**, e02965-02920 (2021).
184. D. D. Kim *et al.*, Identification of nosZ-expressing microorganisms consuming trace N2O in microaerobic chemostat consortia dominated by an uncultured Burkholderiales. *The ISME Journal* 10.1038/s41396-022-01260-5 (2022).
185. W. Shen *et al.*, Effects of copper on nitrous oxide ($N_2O$) reduction in denitrifiers and $N_2O$ emissions from agricultural soils. *Biol. Fertil. Soils* **56**, 39-51 (2020).
186. X. Li, P. Sørensen, J. E. Olesen, S. O. Petersen, Evidence for denitrification as main source of N2O emission from residue-amended soil. *Soil Biology and Biochemistry* **92**, 153-160 (2016).
187. P. M. H. Kroneck, Walking the seven lines: binuclear copper A in cytochrome c oxidase and nitrous oxide reductase. *JBIC Journal of Biological Inorganic Chemistry* **23**, 27-39 (2018).
188. K. Fujita, D. M. Dooley, Insights into the Mechanism of N2O Reduction by Reductively Activated N2O Reductase from Kinetics and Spectroscopic Studies of pH Effects. *Inorganic Chemistry* **46**, 613-615 (2007).
189. A. P. Davis, O. J. Hao, J. M. Chen, Kinetics of heavy metal reactions with ferrous sulfide. *Chemosphere* **28**, 1147-1164 (1994).
190. J. Chang *et al.*, Methanobactin from Methylosinus trichosporium OB3b inhibits N2O reduction in denitrifiers. *The ISME Journal* **12**, 2086-2089 (2018).
191. I. Manconi, P. van der Maas, P. Lens, Effect of copper dosing on sulfide inhibited reduction of nitric and nitrous oxide. *Nitric Oxide* **15**, 400-407 (2006).
192. J. Bartacek, I. Manconi, G. Sansone, R. Murgia, P. N. L. Lens, Divalent metal addition restores sulfide-inhibited N2O reduction in Pseudomonas aeruginosa. *Nitric Oxide* **23**, 101-105 (2010).
193. M. Conthe *et al.*, Denitrification as an N2O sink. *Water Res* **151**, 381-387 (2019).
194. Y. Gao *et al.*, Competition for electrons favours N2O reduction in denitrifying Bradyrhizobium isolates. *Environmental Microbiology* **23**, 2244-2259 (2021).
195. Y. Wang *et al.*, Inhibition by free nitrous acid (FNA) and the electron competition of nitrite in nitrous oxide (N2O) reduction during hydrogenotrophic denitrification. *Chemosphere* **213**, 1-10 (2018).
196. Y. Zhou, M. Pijuan, R. J. Zeng, Z. Yuan, Free Nitrous Acid Inhibition on Nitrous Oxide Reduction by a Denitrifying-Enhanced Biological Phosphorus Removal Sludge. *Environmental science & technology* **42**, 8260-8265 (2008).
197. B. LaSarre, R. Morlen, G. C. Neumann, C. S. Harwood, J. B. McKinlay, Non-catalyzable denitrification intermediates induce nitrous oxide reduction in two purple nonsulfur bacteria. *bioRxiv* 10.1101/2022.06.21.497020, 2022.2006.2021.497020 (2022).

198. S. Yoon, C. Cruz-García, R. Sanford, K. M. Ritalahti, F. E. Löffler, Denitrification versus respiratory ammonification: environmental controls of two competing dissimilatory $NO_3^-/NO_2^-$ reduction pathways in *Shewanella loihica* strain PV-4. *ISME J.* **9**, 1093 (2014).
199. S. Yoon, B. Song, R. L. Phillips, J. Chang, M. J. Song, Ecological and physiological implications of nitrogen oxide reduction pathways on greenhouse gas emissions in agroecosystems. *FEMS Microbiology Ecology* **95** (2019).
200. M. Senbayram *et al.*, Soil $NO_3^-$ level and $O_2$ availability are key factors in controlling $N_2O$ reduction to $N_2$ following long-term liming of an acidic sandy soil. *Soil Biol. Biochem.* **132**, 165-173 (2019).
201. D. Mania, K. Woliy, T. Degefu, å. Frostegård, A common mechanism for efficient N2O reduction in diverse isolates of nodule-forming bradyrhizobia. *Environmental Microbiology* **22**, 17-31 (2020).
202. A. Black, P.-C. L. Hsu, K. E. Hamonts, T. J. Clough, L. M. Condron, Influence of copper on expression of nirS, norB and nosZ and the transcription and activity of NIR, NOR and N2OR in the denitrifying soil bacteria Pseudomonas stutzeri. *Microbial Biotechnology* **9**, 381-388 (2016).
203. Y. Pan, L. Ye, Z. Yuan, Effect of H2S on N2O Reduction and Accumulation during Denitrification by Methanol Utilizing Denitrifiers. *Environmental science & technology* **47**, 8408-8415 (2013).

# Vita

Guang He was born in Guangzhou City, Guangdong Province, China in 1995. He spent his childhood (up to 12 year-old) in Guangzhou City and teenager in Leiyang City, where his parents were born. As such, Guang He does well in both Mandarin and Cantonese. Guang He moved to Changsha City pursuing the bachelor degree in Agricultural Resource and Environment at Hunan Agriculture University. The undergraduate research was more related to large-scale field study (e.g., on-site camping and sampling). He got a good internship opportunity in Chinese Agricultural Academy Science, where he enrolled in a fundamental research project. These experiences inspired Guang He to pursue a master education in the China Agriculture University. He then joined the Junling Zhang's lab researching the tri-party interaction between host-plant, arbuscular mycorrhizal fungi and $N_2O$-cycling bacteria. During his master education, he self-learned versatile molecular techniques (e.g., qPCR and clone sequencing). In addition, Guang He developed great interests in computational analysis (e.g., omics analysis and R visualization). The skills Guang He obtained in master program stand him ready to the Ph.D study in Department of Plant, Soil and Environmental Science at the University of Tennessee, Knoxville, supervised by prestigious Dr. Frank E. Löffler and Dr. Mark Radosevich. In the past five years, Guang He has been researching the microbial reduction of $N_2O$ under acidic conditions, which has been a decade-lasting retard topic. The most impressing intellectual merit achieved by Guang He is that he obtained different enrichment cultures from either agricultural or tropical soils, all of which have the low pH $N_2O$ reduction capacity. More strikingly, he has made it available of an acidophilic $N_2O$ reducing bacterium in pure culture. Guang He is also involved in other collaborative projects including N-PFAS supporting microbial growth, where he contributes to the bioinformatic analyses and data interpretation. After graduation from the University of Tennessee, still driven by the passion, Guang He intends to continue his research career and contribute to resolving the global climate changes induced by $N_2O$ emissions.